The Dissertation Committee for Bing Huang
certifies that this is the approved version of the following dissertation:

Mixed-integer Programming in Power Systems: The Interdiction and Unit Commitment Problems

Committee:

Ross Baldick, Supervisor

Jonathan Bard

Grani Hanasusanto

Surya Santoso

Hao Zhu

Mixed-integer Programming in Power Systems:
The Interdiction and Unit Commitment Problems

by

Bing Huang

DISSERTATION

Presented to the Faculty of the Graduate School of

The University of Texas at Austin

in Partial Fulfillment

of the Requirements

for the Degree of

DOCTOR OF PHILOSOPHY

THE UNIVERSITY OF TEXAS AT AUSTIN

August 2019

Dedicated to my family.

Acknowledgments

I want to express my gratitude to my family, especially, my parents Xiaoqing Zhang and Xin Huang. This dissertation would not possibly be completed without their unconditional love and devoted support. I am thankful for them always being there and backing me, especially in my time of need.

I would like to express my gratitude and admiration to my advisor Dr. Ross Baldick. I sincerely appreciate his dedicating, inspiring and patient advising. Dr. Baldick is no doubt a true intellectual. At the same time, he is also extraordinarily kind and considerate. I am extremely fortunate to have worked with and learned from Dr. Baldick over the past four years. He sets up such a high standard both intellectually and morally that I want to pursue in my future career and life.

My gratitude extends to my committee members who kindly offered their help in a number of ways. I am thankful for their great advice on my dissertation. Especially, I would like to thank Dr. Jonathan Bard for his excellent guidance in the fields of linear programming and mixed integer programming. I am grateful to Dr. Grani Hanasusanto for his fantastic teaching on optimization under uncertainties and stochastic processing. I thank Dr. Santoso for broadening my views to the distribution side of power systems. I thank Dr. Zhu for constructive discussions on several topics in my dissertation.

Apart from my dissertation committee, I want to thank my mentors and colleagues I collaborated with in several internships. I want to thank Dr. Yonghong Chen and Jessica Harrison for their great effort in helping and supporting me in my internship with Midcontinent ISO. I am grateful to Dr. Venkat Krishnan and Dr. Bri-Mathias Hodge for our collaborated work on wind flexible ramping products. I appreciate Dr. Guangyi Liu's creative and open mind attitude in our work on the load characterization.

I am indebted to my colleagues and friends from the energy system track at UT Austin. I am especially grateful to Manuel Garcia, Bowen Hua, Mohammad Majidi, Tong Zhang, Jeff Manning, Hyeongon Park, Wan K Cho, Quan H. Nguyen and Piyapath Siratarnsophon. I am thankful for many interesting discussions and comforting conversations. Their intelligence and perseverance have always being encouraging and motivating. I am fortunate to be with them and I appreciate their friendships and warm support along the way. This journey is special because of them.

I want to thank staff members at ECE department of UT Austin. I appreciate their hard work to maintain the logistics involved with thousands of students and faculty members. Especially, I would like to thank Melanie Gulick. Her kindness and warmhearted attitude made the stress of graduate school easier to handle.

Mixed-integer Programming in Power Systems: The Interdiction and Unit Commitment Problems

Publication No. _____

Bing Huang, Ph.D.
The University of Texas at Austin, 2019

Supervisor: Ross Baldick

Mixed integer programming (MIP) maximizes (or minimizes) a linear objective subject to a set of constraints. In particular, one of the constraints for a MIP is that at least one of the variables can only take integer values. This technique has been widely studied in operations research and a MIP can be solved efficiently by commercial solvers. In this dissertation, two power system problems namely, an interdiction problem and a unit commitment problem, are formulated and solved with MIP techniques. The studies presented in this dissertation focus on extracting the special features embedded in the problems and formulating the problems such that they can be solved using the available MIP techniques.

The objective of an interdiction problem in a power system is to find a set of the most critical or vulnerable components to secure and reliable operation. Before formulating the problem, we need to study the outages and

their impacts in power systems in depth. Once a critical component of a power system fails, the outages including generator and load trips can sequentially spread and frequently lead to large blackouts. The efforts to develop a model to analyze cascading outages is first summarized. Reports about cyber attacks on the Ukraine power grid revealed that one or more malwares were deliberately developed to attack industrial facilities, with power systems as one of the major targets. Another potential cyber threat to secure operation of power transmission grids involves Internet of Things (IoT) demand attacks. Increasingly, Internet connections are available to devices with high energy consumption such as air conditioners and water heaters. However, these new connections expose the control of new electric loads to potential manipulation by attackers. To help assess the effects of cyber attacks, we develop numerical experiments and define different types of cyber attacks to simulate Ukraine-style cyber attacks and IoT demand attacks to study the system responses in a North American regional interconnection system. Based on the studies in cascading outage analysis and cyber attack simulations, an interaction problem between a defender (e.g. system operator) and an attacker (e.g. terrorist) in a power system is formulated as a MIP and a "short-term" impact of an attack is considered using a cascading outage anylsis (COA) tool. A demonstrative case study with an existing method is presented and numeric studies with "short-term" impacts with COA model are ongoing.

The unit commitment (UC) problem in a power system is another MIP problem. UC determines the start-up and shut down schedules of generat-

ing units to meet forecast demand in a short term future (few hours to few days). It is critical to precisely represent the generating units in a UC problem to maximize the social welfare, which is the objective of the problem. The formulation of two types of unit namely, combined-cycle gas units and pumped-storage hydro units in a UC problem are presented in this dissertation.

In recent years, combined-cycle units (CCUs) have been operated as providers of flexibility needed due to the increasing shares of renewables. Consequently, optimization models have been proposed to determine the configuration of CCUs. However, most of the existing models assume that any transition between configurations finishes in a single interval. This assumption is often violated in reality, as a transition might last up to a few hours during which the CCU has limited dispatchability. In this work, a mixed-integer programming formulation that represents the transition ramping of CCUs is summarized and the formulations of ramping constraints are discussed. Numerical studies are performed on an illustrative test system and a Mid-continent Independent System Operator (MISO) system.

As one of the mature technologies for energy storage, pumped-storage hydro is able to provide services in a time range from minutes to days. Particularly, pumped storage hydro units are useful for enhancing the integration of renewable generations that are naturally intermittent. Optimization models have been proposed to determine strategies to dispatch a energy storage unit in the system. However, most of existing work assumes the output from a

energy storage unit is continuous. This assumption is not true for a pumped storage hydro unit. Inspired by the work of modeling a combined cycle unit in the unit commitment problem, this work proposes a configuration based pumped storage hydro model that removes the invalid continuous outputs assumption in order to enhance the use of pumped storage hydro resources in the system. By introducing three "configurations," namely, pumping, generating and "alloff" or off-line, for a pumped storage hydro unit, the proposed model can more accurately reflect the practical operations of pumped storage hydro units in the day-ahead market. A comprehensive review of the existing pumped storage hydro models and industry practices is presented. The definition of configurations of a pumped storage hydro unit and the transitions between the configurations during operation are revealed and discussed in detail to describe the proposed model. A case study is presented to illustrate the proposed model.

Table of Contents

List of Tables

List of Figures

Chapter 1

Introduction

1.1 Outline

This dissertation is organized as follows. The first part of this dissertation is focused on power system interdiction problems. The details of cascading outage analysis (COA) models are discussed in Chapter 2. The framework of the COA model and the designs of different checkers are presented. Examples are demonstrated. Different cyber attacks on power systems are discussed in Chapter 3. The implementation of the COA model and simulation results in the North American regional interconnection case are included. The model and knowledge learned in these two chapters are applied in a power system interdiction problem that is formulated as a mixed-integer programming (MIP) model in Chapter 4.

The second part of the dissertation focuses on a typical mixed-integer programming problem in the operation of a power system – the unit commitment problem. The unit commitment (UC) problem determines the start-up and shut down schedules of generating units to meet forecast demand in a short term future (few hours to few days). It is critical to precisely represent the generating units in a UC problem to maximize the social welfare, which

is the objective of the problem. In Chapter 5, a transition ramping model is summarized based on a configuration-component hybrid combined cycle gas unit model. Ramping constraints are discussed and computational studies are presented with a Mid-continent Independent System Operator (MISO) system. In Chapter 6, a configuration based pumped hydro unit model is formulated. An illustrative case study is shown, while further study on the MISO system will be conducted as future work.

The rest of this chapter is organized as follows. Section 1.2 discusses cascading outages in a power system. Section 1.3 introduces cyber attack simulations on power systems. Section 1.4 presents a formulation and techniques to solve a power system interdiction problem considering "short-term" effects. Section 1.5 and section 1.6 discusses the formulation of two different generation units, namely, a combined-cycle unit and a pumped-storage hydro unit, in the power system unit commitment problem.

1.2   Cascading Outages in Power System

Many large blackouts have occurred across the globe, such as the 2003 Northeastern America Blackout [377] and the 2012 India Blackout [281]. It is noticeable that during the 2003 Northeastern America Blackout, 14 high voltage transmission lines tripped out within 5 minutes. The blackout also caused 61,800 MW of load lost. Over 50 million people were without power in northeast US and Ontario, Canada and an estimated monetary cost of 6-10 billion US dollars is reported. Many of these large blackouts are caused

by a consecutive series of various outages, or cascade, following an initial disturbance. Some major blackouts in North America due to cascading outages are shown in Table 1.1.

The practice in electric system design and operations has considered the N-1 security criterion [91]. The North American Reliability Standards require that the "transmission system is operated so that instability, uncontrolled separation, or cascading outages will not occur as a result of the most severe single contingency and specified multiple contingencies" [90]. However, when multiple, simultaneous or near simultaneous contingencies occur, the outages including transmission line, generator, and load trips can sequentially spread and lead to large blackouts [381].

Nevertheless, it is very difficult to identify critical components that represent weaknesses in the power system and to analyze cascading outages due to the lack of detailed blackout data and complicated electrical-physical interactions. In this work, we propose an improved outage checker based cascading outage analysis (COA) algorithm to simulate the potential cascading outage of the system.

1.3 Cyber Attack on Power System

Based on the further developed cascading outage analysis tool, two types of cyber attacks on power systems are studied in this work. The first type of cyber attack targets power grid control centers. Once the cyber attackers have access to the power grid control system, an attack could blackout

Table 1.1: Examples of Cascading Blackouts in North America (Source: data is from [381], [376], [132])

Date	Location	Customers Affected / MW Lost	Collapse Time
Nov. 9, 1965	Northeast	30 million	13 minutes
July 13, 1977	New York City	1 million	1 hour
Dec. 22, 1982	West Coast	12,350 MW	Few Minutes
Dec. 15, 1994	Western U.S.	9,336 MW	N/A
July 2, 1996	Western U.S.	2 million	36 seconds
Aug. 14, 2003	Northeastern and Mid-western U.S. and Ontario, Canada	55 million	Few Minutes
Sep. 8, 2011	Southwestern U.S.	7 million	Few Minutes

a regional power system and may trigger cascading outages and cause large-scale load losses. The second type of cyber attack targets consumers that have high-energy consumption loads and potentially could interrupt the system operation by manipulating the compromised load. These types of attacks are described in the next two sections.

1.3.1   2015 Ukraine Cyber Attack

On December 23rd 2015, a regional electricity distribution company in Ukraine reported service outages to customers. The outages were due to a third party's illegal access into the company's computer and Supervisory Control and Data Acquisition (SCADA) systems. Forensic investigations re-

vealed that a malware named BlackEnergy had infected the SCADA systems after a successful attack. Seven 110 kV and twenty-three 35 kV substations were disconnected for three hours. Later it was revealed that three different such distribution companies were attacked, resulting in several outages that caused approximately 225,000 customers to lose power across various areas in Ukraine [326]. On December 17th 2016, a second power outage occurred in Ukraine and deprived part of its capital, Kiev, of power for over an hour. Although the official investigation is still ongoing, an assessment was made that a more advanced malware, Industroyer, was used in the second cyber attack against the power grid in Ukraine [1].

On May 11, 2017, President Trump signed an executive order to strengthen the cyber security defenses of federal networks and critical infrastructure. In the executive order, there is a section that specifically addressed the threats from "electricity disruption and prolonged power outages resulting from cyber security incidents." Incident responses have been carefully studied and a substantial set of cyber requirements has been placed on all U.S. grid operators of bulk power grid for several years [284]. On October 19th 2017, the Federal Energy Regulatory Commission (FERC) proposed new mandatory cybersecurity controls to address the risk posed by, for example, smaller grid control centers that are typically less critical than major control centers, but which are nonetheless vulnerable to intrusion software [354].

Power system vulnerability under cyber security threats has also been studied previously in the engineering literature. Ten et al [371] proposed a

vulnerability assessment framework for a systematic analysis incorporating both power and cyber systems of the control networks. Chen et al [73] built a real-time cyber physical test bed that simulates the communication system and power system simultaneously.

A typical assumption in this literature is that the cyber attackers have full or partial control of the SCADA systems. For example, Xuan et al [240] solved a bi-level linear programming problem to study the effects of a cyber attack on the system economic operation cost. These methods only considered partial effects of a cyber attack on power systems. For example, Xi et al [430] proposed a model to investigate the cascading failures in a smart grid consisting of a power grid and a coupled cyber network. In [430], they studied cascading sequences of transmission overloading. However, there are other protection actions such as generator over- and under-frequency that may contribute to the cascade that were not considered in [430].

Thus motivated, for the purpose of developing a tool to assess the effects of cyber attacks, we propose a method to simulate the power system responses under cyber attacks using a cascading outage analysis model that considers generator tripping under rotor angle and system frequency deviations, under-frequency and under-voltage load shedding, and overload protections on branches. The emphasis of this study primarily involves adapting a previously developed cascading outage analysis (COA) tool to simulate the effects of cyber attacks. We implement the tool in a planning case of a North American regional interconnection system. The initial cyber attacks are modeled

6

as simultaneously opening circuit breakers associated with various categories of devices in each transmission and distribution company (owner) in the interconnection system. Our results show different features of system responses under different cyber attacks.

1.3.2   IoT Cyber Attack

The vulnerability of Internet of Things (IoT) devices is a well-known problem [8, 111, 328]. An IoT cyber attack has become a concern to power system operators recently since more and more devices with high-energy consumption such as water heaters and air conditioners can be controlled by consumers through the Internet. Although manipulating the energy consumed in a single household is not enough to cause any major problem to the power grid, a recent paper presented in USENIX Security 2018 [361] proposed the Manipulation of demand via IoT (MadIoT) attacks, and showed an attacker who could coordinate the compromise of hundreds of thousand of high-energy IoT devices to launch several attacks on the power grid, including (i) frequency instabilities, (ii) line failures, and (iii) increase in operating costs.

In this work, we perform an in-depth study of the power grid effects of MadIoT attacks using the COA tool. Our analysis shows that while MadIoT attacks can create negative consequences on the power grid, the negative impact on the grid will not be as serious as originally claimed in [361]. In particular, while some load shedding may be necessary to deal with these attacks, our results show that creating a system blackout–which would a require

black start period of several days to restart the grid—would be very difficult, given the embedded protections that all power systems have throughout their infrastructure.

1.4   Power System Interdiction Problem

Based on our knowledge learned from cascading outage analysis and cyber attacks studies, an interdiction problem between a defender (e.g. system operator) and an attacker (e.g. terrorist) in a power system is formulated as a mixed-integer programming (MIP) problem. A "short-term" impact of an attack is considered and discussed with the cascading outage anylsis (COA) tool.

The electric system is designed to satisfy the $N-1$ security criterion, which means the system could lose any one of its N components (such as generators, transmission lines) and continue operating within emergency limits. However, when multiple, simultaneous contingencies occur, the system might experience various stability problems, which might lead to the large cascading events. Outages are typically caused by storms or other extreme weather conditions but could also be carried out deliberately by knowledgeable attackers with little risk of detection. Furthermore well-planned and coordinated attacks by terrorists could leave the electric power system in a large region of the country at least partially disabled for a very long time [95].

In [338], an interdiction problem is formulated as a bi-level mixed-integer programming problem. A decomposed heuristic algorithm was devel-

oped. Salmeron et al. [339] introduced Global Benders Decomposition (GLBD) to solve the same problem described in [338] and observed improved convergence toward the optimal solution even with a non-linear, non-convex subproblem. The key advantage of GLBD over a single level MILP formulation is that the algorithm's subproblems represent simple, familiar instances of the primal linear program OPF. Thus, the user need not maintain a problem that involves unfamiliar constructs from the dual of the OPF model that are complicated by interactions with binary variables as in Mixed-Integer LP procedure in [276] and as in the KKT method to solve the subproblem described in [428].

To better represent the "short-term" system responses to an attack, the COA model that analyzes both transient and steady state system responses to a contingency is incorporated as a sub-problem in the interdiction framework in [398] in addition to DC-OPF used in [338] and [339]. Because of the non-linearity brought by COA model, the problem in [398] is solved through a heuristic method that is similar to the algorithm in [338]. A key question is whether the GLBD method might also be successful for the problem in [398].

In this dissertation, the efficiency of the application of the GLBD method on the bi-level system interdiction problem with DC-OPF as the sub-problem is first demonstrated. Then the GLBD method is applied in the problem with COA model incorporated as the sub-problem. The test systems are built on a PowerWorld 7 bus OPF case and a PowerWorld 37 bus system with transient stability data and generic costs for OPF.

1.5 Combined Cycle Unit Formulation

Unit commitment (UC) problem in a power system determines the start-up and shut down schedules of generating units to meet forecast demand in a short term future (few hours to few days). The objective of a UC problem is to minimize the total generation costs; that is, to maximize the social welfare. Unit commitment decisions (binary variables) and unit dispatch levels (continuous variables) are determined. Also, a large set of operational constraints has to be satisfied. Therefore, the UC problem is a complex optimization problem that can be formulated as a mixed-integer programming problem.

There are new features in electricity markets that may involve formulation modifications and potentially add computational complexity to the UC problem. One such new feature is the participation of combined cycle gas power plants. A combined cycle power plant has a combination of gas and steam turbine units. The exhaust heat from a gas turbine is used by a steam turbine to generate more electricity. Combined cycle units (CCUs) have higher efficiency, lower CO_2 emission, better flexibility and faster response. Therefore, there is an upward trend of installing combined cycle units [201], [52].

Consequently, optimization models have been proposed to determine the configuration and operation of CCUs in the electricity market. However, there are assumptions made in existing models that are often violated in reality. In this work, we will first address a one interval transition assumption made in the existing models. A mixed-integer programming formulation that represents

the transition ramping of CCUs and removes the invalid assumptions of one interval transitions is proposed in [181]. We build on [181] by incorporating a set of configuration-wise ramping constraints into the transition ramping model. Numerical studies are performed on a MISO system.

1.6 Pumped Storage Hydro Unit Formulation

Pumped hydro plants use power to pump water uphill to an elevated reservoir when the electricity price is low. The water is released to a lower reservoir and drives the turbine to generate electricity when it is needed. There are now about 38 pumped storage plants in the United States. As one of the mature technologies for energy storage, pumped storage hydro is able to provide service in a time range from minutes to days. The services in this time range include spinning reserve and load or generation shifting. Therefore, pumped storage hydro units can be used as a flexible energy management tool and it is particularly useful for enhancing the integration of renewable generations that are naturally intermittent.

Inspired by the work of modeling a combined cycle unit in the unit commitment problem, this work proposes a configuration based pumped storage hydro model for the day-ahead market, in order to enhance the use of pumped storage hydro resources in the system. By introducing three "configurations," namely, pumping, generating and "alloff" or off-line, in a pumped storage hydro unit, the proposed model can more accurately reflect the practical operations of pumped storage hydro units in the day-ahead market. A

comprehensive review of the existing pumped storage hydro models and industry practices is presented. The definition of configurations of a pumped storage hydro unit and the transitions between the configurations during operation are revealed and discussed in details to describe the proposed model.

Part I

Power System Interdiction Problem

Chapter 2

Cascading Outages in Power Systems

2.1 Introduction

[1] Cascading outages is the main mechanism of large blackouts, and the duration of the sequence of cascading events can be very short so that there is little time for operator intervention. In the 2003 North-Eastern America Blackout [377], 14 high voltage transmission lines were tripped out within 5 minutes. In order to evaluate the short term impacts of a particular attack, the amount of short-term load shed should be calculated. Many efforts have been put into research to identify the cause of these events and the methods to mitigate them. Eppstein et al [119] has developed a Random Chemistry algorithm to identify the multiple contingencies that initiate cascading failure. Hazra et al [164] proposes pattern recognition and fuzzy estimation to calculate the cascading sequences of an event. Jie Chen et al [75] introduces a hidden failure model with an embedded DC model to study the cascading dynamics

---

[1]Bing Huang, Mohammad Majidi and Ross Baldick, "Case Study of Power System Cyber Attack Using Cascading Outage Analysis Model," 2018 IEEE Power Energy Society General Meeting, Portland, OR. Mohammad Majidi contributed in advising on the design of Cascading Outage Analysis (COA) Model and the techniques in programming used in this paper. Ross Bladick contributed in advising the design of Cascading Outage Analysis (COA) Model, the simulations using the COA, discussion of results and multiple revisions of the paper.

and mitigation.

These methods are either very computationally expensive, or do not very accurately represent the system behavior after the initial disturbances. In several cases, these methods explicitly model initiating events that are "natural" or caused by equipment failure, rather than initiating events that are deliberately chosen to cause damage, as is the main focus of our research. Thus motivated, we developed an improved outage checker based algorithm to simulate the potential cascading outage of the system. While our approach is also computationally intensive, it is directly aimed at modeling the effects of deliberate large-scale attacks. Some previous work on developing sequential outage checker based Cascading Outage Analysis (COA) is presented in [190] and [396]. In this chapter, we provide an improved COA model, more detailed and accurate preventive equipment modeling, and a case study using a PowerWorld test system.

2.2   Framework of the COA

In previous models [190], [396], the cascading outage analysis is performed with sequential application of the checkers. This sequence is applied based on assumptions about the timing of various system protective actions subject to different criteria. For example, it is assumed in the previous models that the transient stability protection will detect rotor angle instability and trip generators before Under Frequency Load Shedding (UFLS) activates. The frequency relay will deploy UFLS before the over current relays trip the

overloaded components, and over current relays will act before the under voltage relays trip out the loads or generators that experience voltage instability. However, in practice, the time of potential relay actions for the frequency relays, over current relays, and voltage relays could overlap. Once an element is tripped out (i.e., the line tripped out by the fastest relay), the system topology is changed accordingly, which will induce a sudden change of the power flow. The elements that were not tripped out will experience different loading, and could then be tripped by subsequent protective action. Therefore, in the improved COA developed here, simultaneous application of protection is modeled by the checkers and more detailed models of each protection scheme are implemented to provide a better representation of the sequence of the cascade. We ignore the possibility of operator intervention between outages, under the assumption that events occur too rapidly for an operator to handle.

The analysis starts from a specification of the initial disturbances. Then the transient stability or rotor angle stability is checked by the Transient Stability Checker (TSC). If the generator rotor angle is larger than a certain threshold, say, 100 degrees, the generator will be automatically tripped. At the same time, the frequency at each bus is checked by the frequency outage checker (FOC). If the frequency at a bus deviates from from the nominal frequency of 60 Hz to be outside the range (e.g. 57.6 Hz to 62.4 Hz) for longer than a minimum time threshold, then the generator connected to this bus will be tripped. If the frequency at a load bus drops lower than some predefined thresholds for longer than a minimum time threshold then a percentage of the

total loads connected to this bus will be shed. After any of these actions, the analysis goes to the next cascading stage involving analysis with the TSC and FOC. If the system reaches a transiently stable state, the COA activates the two other checkers (overload outage checker or OOC, voltage outage checker or VOC) simultaneously. Each checker is implemented with a relay function to return a potential trip time. Then the COA determines the first element to trip (if any). If the topology changes, the COA will come to the next cascading stage and start the transient stability checker and frequency outage checker again. The workflow diagram is shown in Figure 2.1.

2.3   Design of the Transient Stability Checker (TSC)

Transient stability, or rotor angle stability, is the ability of the power system to remain in synchronism when subjected to large transient disturbances [218]. According to [250], the power system dynamic behavior can be represented as a set of differential equations (2.1) and a set of algebraic equations (2.2).

$$\dot{x} = f(x, y) \tag{2.1}$$

$$0 = g(x, y) \tag{2.2}$$

where x represents electromechanical state of the power system and y represents control inputs. Both x and y are implicitly functions of time.

A disturbance in the network usually requires a change to both the net-
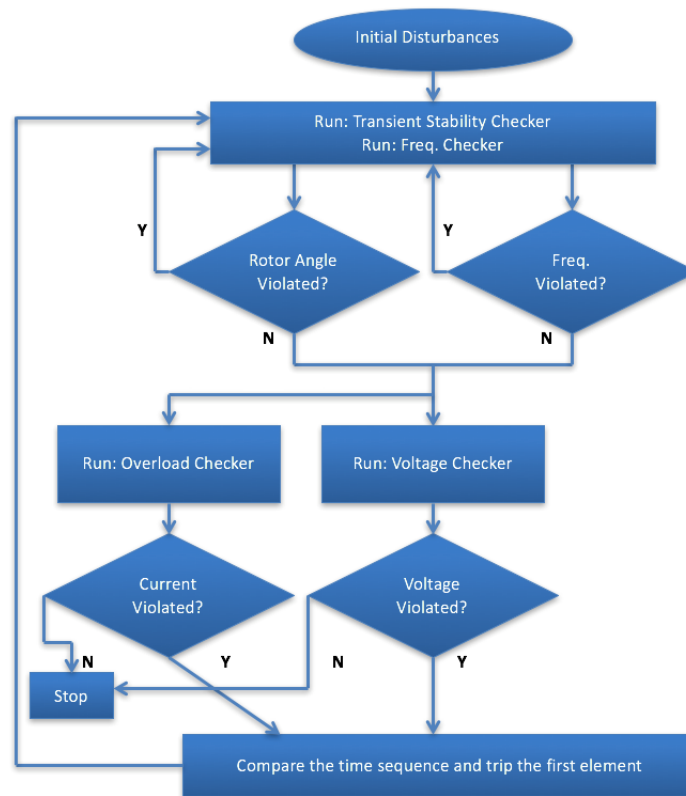
Figure 2.1: Work Flow of the COA

work configuration and boundary conditions. These are modeled by changing the coefficients in the functions appearing on the right-hand side of (2.1) and (2.2).

In the context of transient stability under disturbances, the disturbances may include faults on transmission elements, loss of load or loss of generation. Notice that typical "natural" faults on the transmission elements, which are normally short-circuits, if cleared and re-closed successfully, should not result in physical destruction of the assets [421]. This is very different from

the physical attack aimed at damaging the facilities or cyber attack targeted at taking control of Supervisory Control and Data Acquisition (SCADA) systems, since permanent damage or intended opening of breakers with a denial of service attack, could contribute to long-term impacts on the system.

Transient stability analysis has been performed in power system analysis by many methods. Studies in [422] and [115] use time-domain simulation to calculate the exact system response in time by implicitly numerically integrating the differential equations (2.1) and solving the algebraic equations (2.2) at each time step. The time domain simulation is the most accurate method, but is slow in computation and does not provide any measurement of degree of system stability.

Other approaches include transient energy function (TEF) and potential energy boundary surface (PEBS) [141], [70], [83]. These methods avoid numerical integration by constructing energy functions and comparing the system energy at the time when the fault is cleared to a critical energy value estimated by the energy functions to determine whether or not the system will remain stable. These methods are fast in computation compared to the time simulation, and also able to provide useful information regarding the degree of stability or instability. However, they are only applicable to power system stability models having energy functions, and are not as accurate as numerical integration. Hybrid methods [252] combine the numerical integration and the energy functions method.

We use time-domain simulation to perform the transient stability as-

sessment because of its high accuracy. The time-domain simulation allows taking into account the full system dynamic model and consists in checking that inter-machine rotor angle deviations lie within a specific range of values.

Different models have been used to represent different dynamic characteristics of the generator. In our simulation, a "GENROU" model is selected to represent the round rotor generator. It is noticeable in [320] that the GENROU model provides a very good approximation of the behavior of a synchronous generator. More than two-thirds of the machines in the 2006 North American Eastern Interconnect case are represented by GENROU models. Additionally, standard "IEEE T1" exciter model is used to represent a brushless alternating current (AC) exciter with a rotating rectifier, and "IEEE G1" governor model is used to represent the governor response model. However, we observe that data for these models may not be readily available publicly because of data security issues (see Section 3.2.1).

The transient stability checker uses the PowerWorld transient stability solver to numerically calculate the system response after a fault. If the rotor angle deviation of a generator is bigger than a certain threshold (e.g. 100 degrees), then the generator will automatically be tripped. The implementation of transient stability enables the Cascading Outage Analysis (COA) model to include transient stability assessment (that is, it analyzes the rotor angle stability problem), and hence provides a more accurate representation of the system behavior [421].

2.4   Design of the Frequency Outage Checker (FOC)

If there is a mismatch between the generation mechanical power and the net-load, then a frequency excursion will occur. The frequency excursion may then trigger the over- or under-frequency protection. To represent this possibility, the frequency outage checker (FOC) is designed to model the protection behavior against system over or under-frequency events. In previous work [421], a system frequency response (SFR) model [14] was used as a frequency response model. In the model, nonlinearities and all but the largest time constants in the equations of the generating units of the power system are neglected, with the added assumption that the generation dynamics are dominated by reheat steam turbine generators.[2]

Since the latest PowerWorld transient simulation includes models for generator over- under- frequency relay and under frequency load shedding relays, the frequency checker can be embedded in the transient simulation and use the PowerWorld transient solver to calculate the frequency response of disturbances. It adds two advantages to the model. First, actual frequency response is used by relays instead of system wide approximation while the computational efforts are not significantly increased since we are running the PowerWorld transient simulation for rotor angle stability anyway. Second, as it is part of the transient analysis, if the protection relay takes any action, the

---

[2]With increasing capacities of gas turbine and combined cycle gas turbines, this assumption is not literally true in, e.g. ERCOT. However, the resulting second order model for frequency may still be a reasonably accurate representation if it is calibrated to actual behavior.

Table 2.1: Over/ Under Frequency Generator Tripping (O/UFGT) (Source: data is from [320])

Frequency O/UFGT (Hz)	Time Delays(s)
62.4	2
57.6	2

Table 2.2: Under Frequency Load Shedding (UFLS) (Source: data is from [122])

Frequency UFLS(Hz)	Time Delays(s)	Percentage of Total Load Shed
58.9 - 59.3	270	5 %
58.5 - 58.9	30	15 %
58 - 58.5	2	25 %
below 58	at least 2	Approval of ERCOT

impact of that action on transient analysis is automatically considered.

There are two protections implemented in the frequency checker, namely Over/Under Frequency Generator Tripping (O/UFGT) and Under Frequency Load Shedding (UFLS). If the frequency at a bus deviates from a predefined threshold for more than a threshold time period, the generator connected to that bus would be tripped, and a certain percentage of load connected to the bus will be shed. A default configuration of PowerWorld O/UFGT and a configuration of ERCOT UFLS are shown in Table 2.1 and Table 2.2 respectively.

2.5 Design of the Overload Outage Checker (OOC)

Line overloading for violating thermal limits is an important and common measure to identify the mechanism of cascading outages and to assess vulnerability to cascading outages [397]. In a cascading outage scenario pertinent to line overloading, a line outage can cause increased flows on other lines, potentially leading to overloading of these other lines. As a result, when a line violates the thermal limit, it may be tripped.

It usually takes more than a few seconds for an over-current protection to trip an over-loaded line because of the deliberate time delay built into over-current relays; therefore we use steady-state power flow results to trigger over-current protections. For steady state analysis, we used the PowerWorld Simulator to solve the AC power flow. The status and dispatch set point of units from transient analysis are used as a starting point for AC power flow. Based on the result of AC power flow, we would first consider the transmission over current protection.

A normal inverse-time over-current model described in Siemens SIPRO-TEC 5 Current Relay [355] is implemented in our model. The time when the over current relay trips the element is determined by (2.3):

$$T = \frac{0.14}{(\frac{I}{I_{th}})^{0.02} - 1} T_p[s], \tag{2.3}$$

where I_{th} is the current threshold value of the relay, and T_p is the setting value of the relay. Both values are set by the relay operator. The current I is on

the monitored component such as a transmission line or a transformer. The value of T in (2.3) determines when the protection operates.

The normal inverse current relay characteristic is shown in Figure 2.2. Note that in some cases a sag of a transmission line may result in a short circuit to other objects, e.g. a tree, which would result in a much faster trip due to distance protection actuation. This phenomenon was observed in 2003 North America blackout [377]. We are not modeling this issue in the COA.
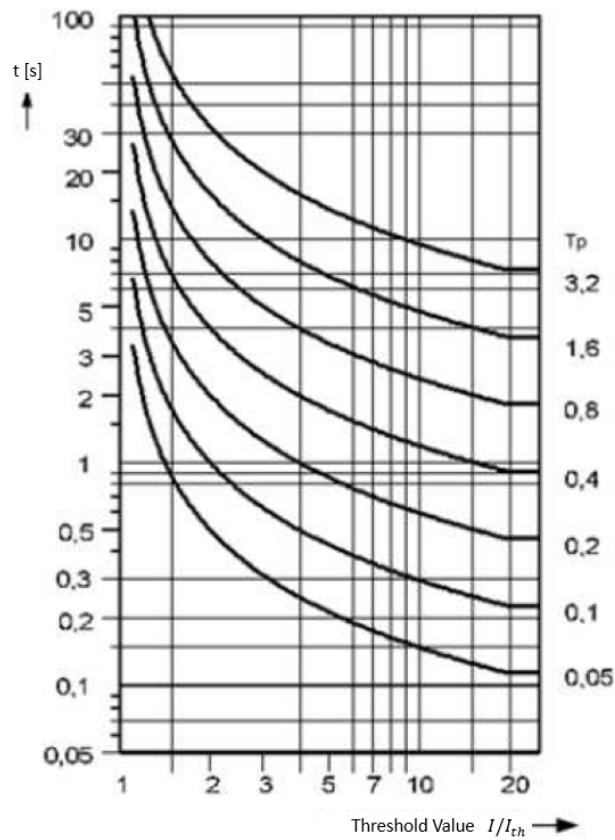
Figure 2.2: Normal Inverse Current Relay Characteristic. [355]

2.6 Design of the Voltage Outage Checker (VOC)

Another typical character of cascading outages includes under (or over) voltages. When the system is highly stressed, the voltage profiles of power systems may decline. Similar to the line outage checker, when a voltage profile for a bus violates a pre-defined threshold chosen to maintain system stability, the voltage outage checker (VOC) may activate. If a bus voltage stays below the lower limit during the VOC process although the power flow calculation converges, load shedding action may be taken to maintain bus voltages within limits [397].

A standard Inverse time characteristic model described in ABB RXEDK 2H Time over/under voltage relay [2] is implemented in voltage relay modeling. The time that under or over voltage relay trips the element is determined in (2.4) and (2.5).

$$T = \frac{k}{\left(\frac{U}{U_{th}^o} - 1\right)}[s], \tag{2.4}$$

$$T = \frac{k}{\left(1 - \frac{U}{U_{th}^u}\right)}[s], \tag{2.5}$$

where k is the inverse time constant, parameters U_{th}^o and U_{th}^u are the over/under voltage relay pick-up values respectively. The voltage U is the monitored bus voltage. The values of T in equation (2.4) and equation (2.5) determine when the protection operates. The inverse voltage relay characteristic curve is shown in Figure 2.3.
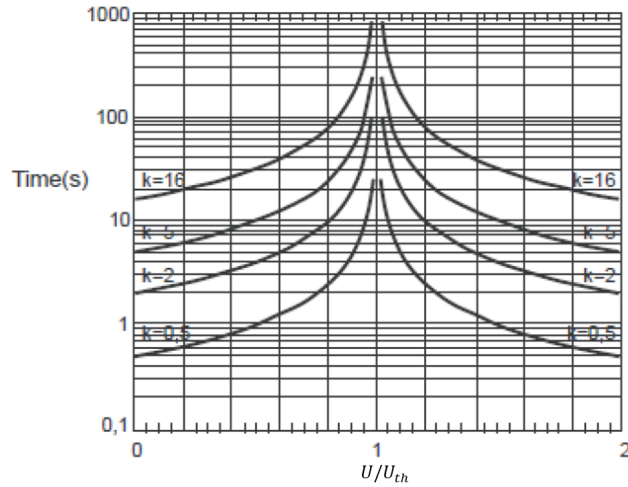
Figure 2.3: Normal Inverse Current Relay Characteristic [2].

2.7 Case Study of COA

Before a detailed discussion of the case studies in this paper, we clarify the terms of Load Shedding and Blackout used in this section and Chapter 3 indicating the results of the simulations.

When some load is disconnected by under frequency load shedding (UFLS), the customer in the relative small load region will experience a temporary loss of electric power that can be quickly corrected once the system is taken to a stable state. For example, load could be restored within 30 minutes or an hour. UFLS is therefore nowhere near as serious as a complete system blackout. When a complete system blackout happens, all the customers in the system will lose their electric power from the system and it typically takes several days to restore the system and the power supply to its customers.

The proposed improved COA model is demonstrated on a PowerWorld

26
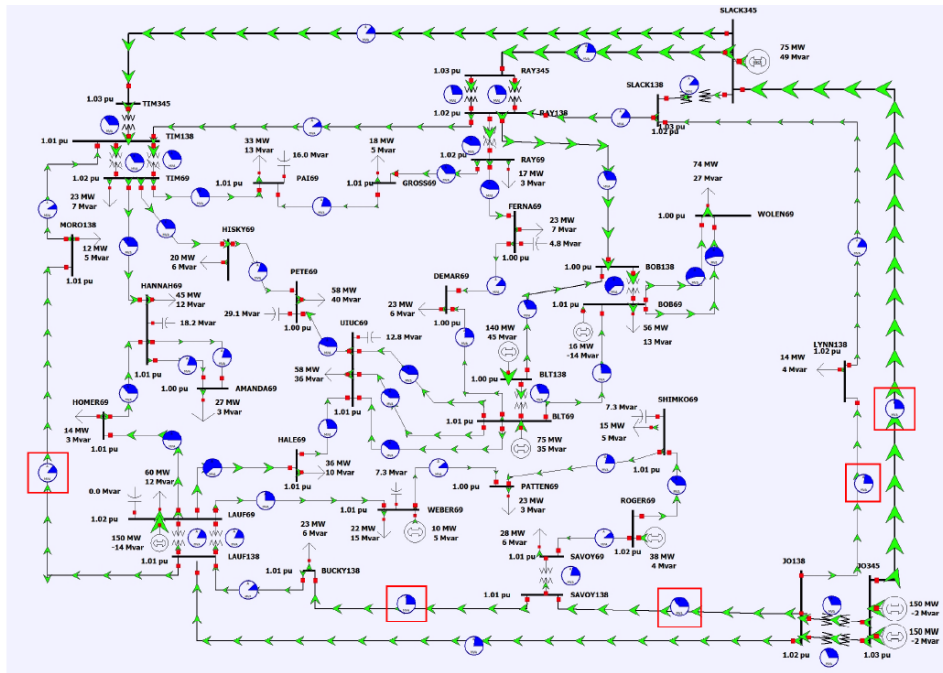
Figure 2.4: 37 Bus System and the Targeted Lines.

37 bus test case [301] for the purpose of illustration. An application of COA to a large system is presented and discussed in Chapter 3. In our simulation, transmission line and transformer MVA limits are set relatively tight in order to illustrate the cascading scenarios. The cascading outage analysis (COA) tool has been built in python 2.7.13 [383] in order to make it easier to connect to other model or software such as PowerWorld simulator [320]. The AC power flow calculations and the numerical integrations of the transient stability checkers are based on the PowerWorld simulator results.

Figure 2.4 shows the topology of the PowerWorld 37 bus test system. The initial disturbances that are highlighted by the red boxes in the figure are

tripping transmission lines MORO138-LAUF138-1, BUCKY138-SAVOY138-1, SLACK345-JO345-1, SAVOY138-JO138-1 and LYNN138-JO138-1.
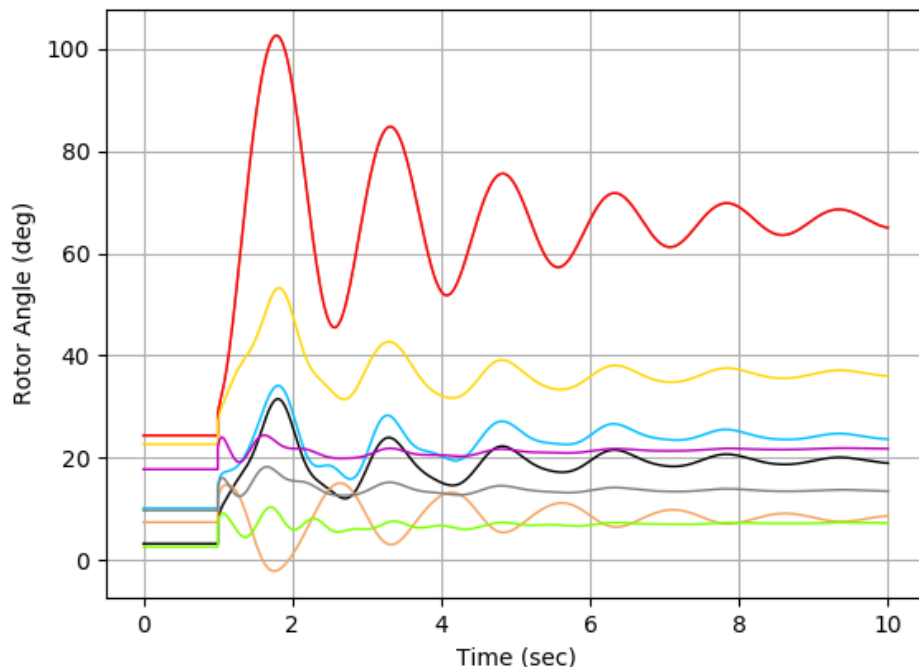
Figure 2.5: Generator Rotor Angle.

Figures 2.5 to 2.8 display simulation results of system responses after the initiating disturbances triggered at 1 second. These four figures present the simulation results of, respectively, generator rotor angle, bus frequency, branch current, and bus voltage corresponding to the four checkers. It can be observed from Figure 2.5 that rotor angle at each generator converges to a new value after some swings caused by the initial disturbances, which occur simultaneously at time equal to 1 second. In Figure 2.6, after the disturbance

at 1 second, the frequencies at all buses deviate from 60 Hz and gradually settle at the end of the simulation. Notice that, since the rotor angle deviations at all generators are within the limits and the frequency at each bus has not reached any thresholds, there are no actions from TSC and FOC. In Figure 2.7 and Figure 2.8, similar to rotor angle, the current and voltage start to settle after a few seconds of fluctuations. The red horizontal line in Figure 2.7 indicates a threshold value for OOC. Therefore, observed from the figure, because of the violation of the OOC threshold, OOC will start to calculate tripping time for two transmission branches.
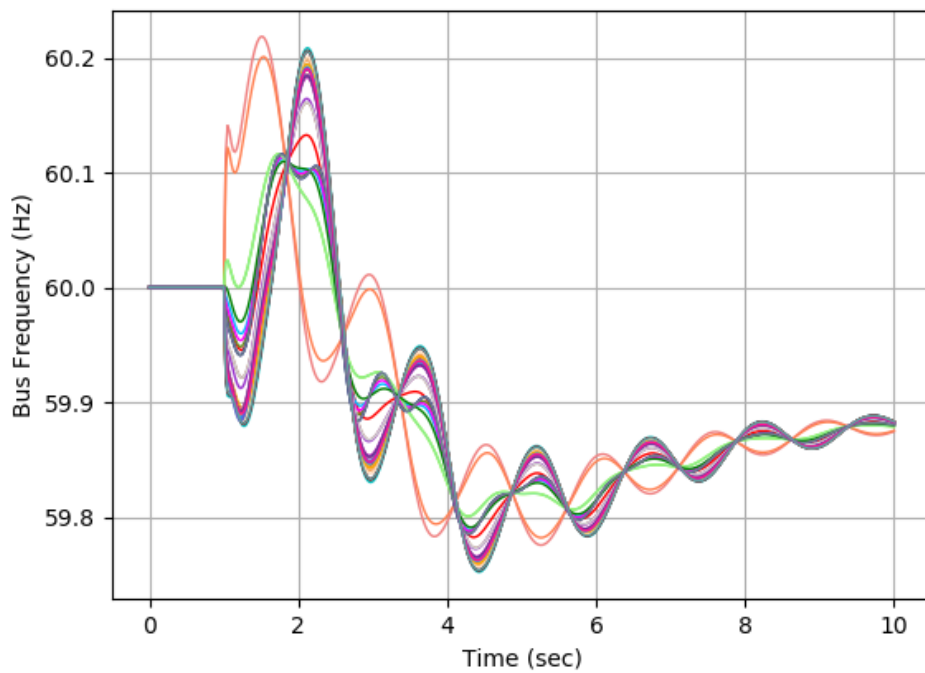
Figure 2.6: Bus Frequency.
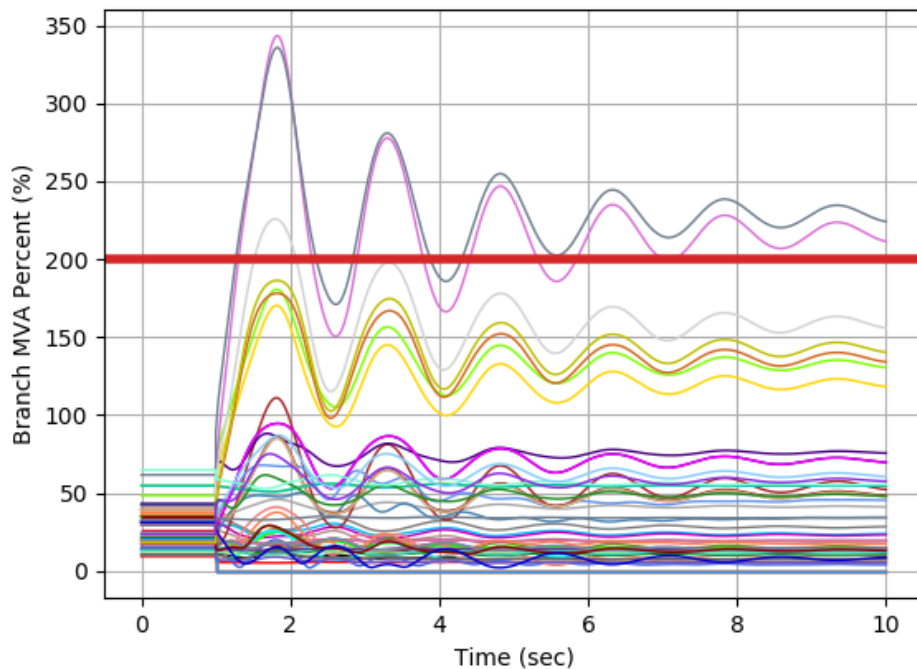
Figure 2.7: Branch Current.

The real power flow on branches calculated by AC Power Flow are shown in Figure 2.9. The green circles with green crosses inside are the tripped lines during the initiating disturbances. The red arrows and red circles indicate the overloaded transmission lines or transformers consistent with Figure 2.7. The number in the red circle tells how much the element is overloaded by a percentage of its MVA limit.

As a result from OOC and VOC, the transmission line highlighted in the red box in Figure 2.9 LAUF69-HALE69-1 has the shortest tripping time (27.8 sec). Therefore, transmission line LAUF69-HALE69-1 will be opened
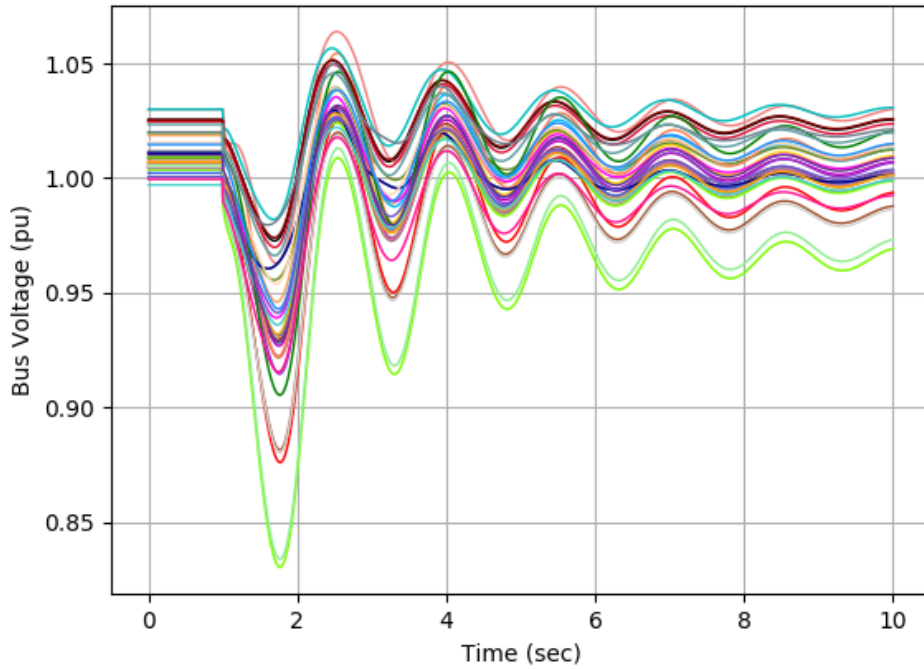
Figure 2.8: Bus Voltage Magnitude.

and thereby this becomes the 2nd disturbance to the system. Notice from Figure 2.5, that by 27.8 seconds, the transient variations will die out and each of the variables will reach a steady state. Hence, the transient simulation with TSC and FOC start to run with the 2nd disturbance and an updated system topology from a steady state again depicted in Figure 2.10. The initial conditions for this transient analyses correspond to the state just before tripping transmission line LAUF69-HALE69-1.

The transient simulation results of rotor angle and frequency are presented in Figure 2.10a and Figure 2.10b. First, in both figures, we can observe
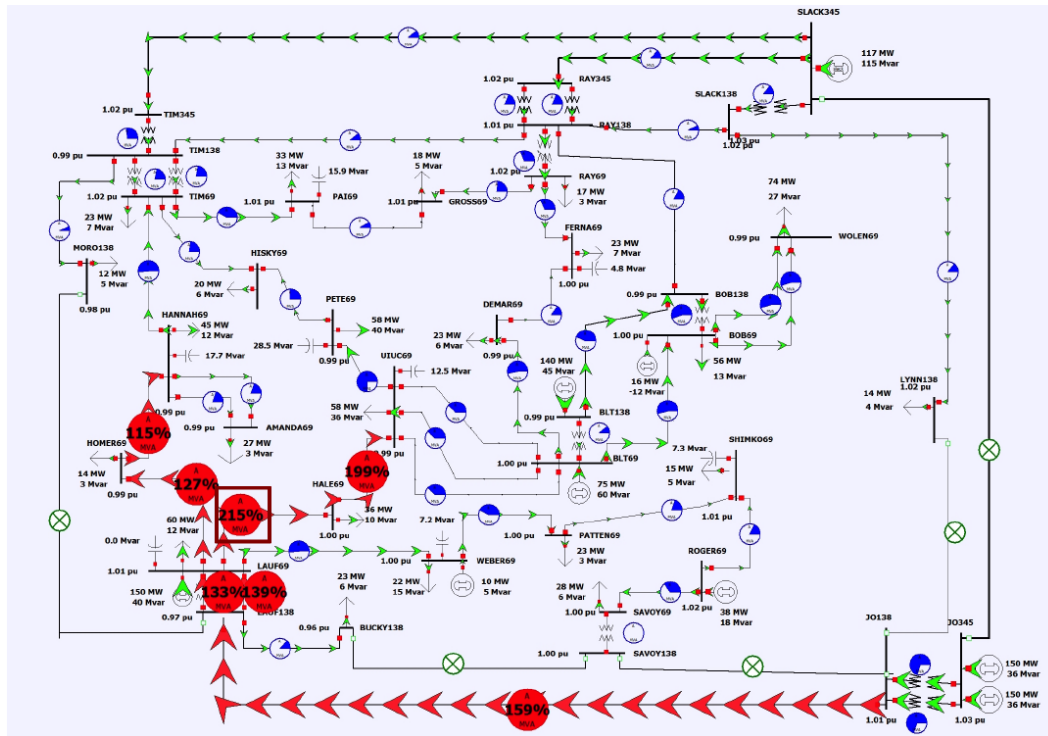
Figure 2.9: Steady State Reached After the Initiating Contingency.

that the 2nd disturbances happens 27.8 sec after the end of the initiating transient simulation. We expect, for large systems, that the shortest tripping time from overload and voltage protections will significantly exceed the transient simulation time. Therefore, the accumulation of overload time that occurs during the transient simulation is ignored. After the lines are tripped, the generator rotor angles and bus frequencies start to deviate from their original values. In Figure 2.10a, after 37.8 sec, rotor angle of five generators indicated by four lines (there are two generators connected to one bus and thereby represented by one line) go up very rapidly. Between 38.97 sec and 38.99 sec, these five generators are tripped by TSC since the magnitudes of their rotor

32

angle deviations are larger than the predefined threshold.
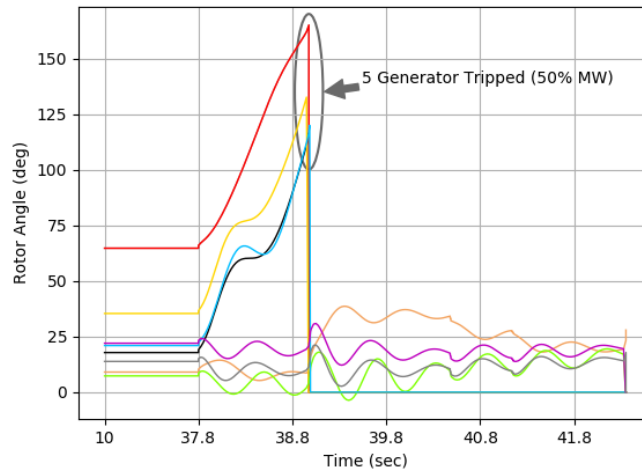
(a) Generator Rotor Angle
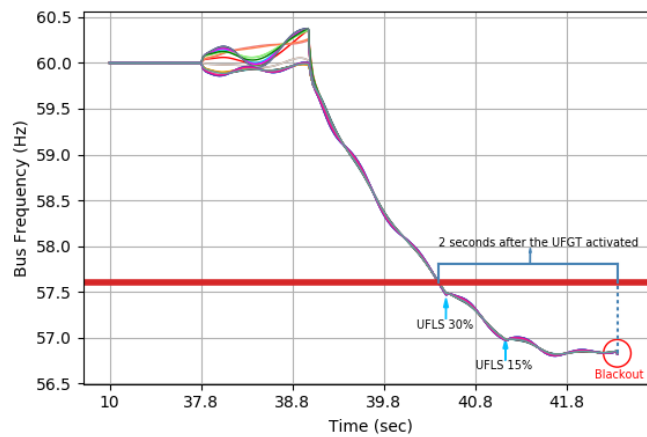
(b) Bus Frequency

Figure 2.10: Simulation Results of the Cascading Contingencies

As a result, in Figure 2.10b, at 38.99 sec, the frequency of buses started

33

to drop quickly as marked by the horizontal red arrow. This frequency drop is due to the sudden loss of generators in the system. The frequencies at buses keep decreasing and at 40.48 sec and 41.12 sec, respectively, the frequencies have dropped below two thresholds for enough time so that the FOC activates the Under Frequency Load Shedding twice. At time 41.12 sec, 45% of the total load in the system is shed. After the second load shedding, the imbalance between generation and load in the system is relieved a little bit and the frequencies stopped decreasing at 41.6 sec. However, before the frequencies reach to a steady state, at 42.35 sec, highlighted by the red circle, 4 more generators are tripped by FOC because the bus frequencies stay below the lower threshold of the generator frequency protection for longer than a predetermined period of time. At the same time, all 9 generators in the system are disconnected which means the system has no power generation, a blackout happens, and the simulation stops.

2.8   Conclusion and Future Work

In this chapter, a cascading outage analysis model (COA) is proposed and illustrated in a case study of a small test system. The model provides a way to evaluate the short term impacts of an attack, e.g. the amount of short-term load shed. The COA model applies four outage checkers, namely Transient Stability Checker, Frequency Outage Checker, Overload Outage Checker, and Voltage Outage Checker to simulate the system behavior after an initial disturbance, i.e. an attack.

Building on previous work [397], we enhance the COA model further. First, we write the cascading outage analysis model with an open source language - Python. After moving to Python, the COA model is easier to connect to other models or other software. Second, the previous model was only semi-automated, needing a human to manually specify outages as a result of an attack. The current COA code is fully automated and can directly read initiating events from a database, modify the case study and run transient and steady state analysis. Third, we add the frequency checker (as under and over frequency protection relays) into the transient analysis. It gives two advantages to the model namely actual frequency response is used by relays instead of system wide approximation, and since it is part of the transient analysis, if the protection relay takes any action, the impact of that action on transient analysis is automatically considered.

The cascading outage analysis has several limitations. Potential improvements include:

- The cascading outage analysis model does not consider breaker failures and back-up protection schemes such as zone-2 and zone-3 protection. The future work may include these models to reflect the real-world scenarios.

- The cascading outage analysis model uses a set of predetermined parameters and settings for protection devices. In the industry applications, different coordinations and settings among various protection schemes may lead to different system behavior.

- There are some control schemes in the power systems, including controlled islanding schemes and automatic tap changers, etc that are not modeled in the cascading outage analysis tool. These sophisticated models could be incorporated and studied to make the simulation results more reflective of reality.

Given the ability to simulate the potential cascades, a natural next step is to develop a tool to analyze the effects of attacks on power systems. Recently, cyber attacks have been a security concern of power systems operations and, potentially, can cause large scale disturbances in the system. In the next chapter, these issues are studied.

Chapter 3

Cyber Attack on Power System

3.1   Introduction

[1] [2] Two types of cyber attacks on power systems are discussed in this chapter. The first type of cyber attack targets power grid control centers. Once the cyber attackers have access to the power grid control system, an attack could blackout a regional power system and may trigger cascading outages and cause large-scale load losses. The second type of cyber attack targets consumers with high-energy consumption and potentially could interrupt the system operation by manipulating the compromised load.

Reports about cyber attacks on the Ukraine power grid revealed that one or more malwares were deliberately developed to attack the industrial facilities, with power systems control centers as the major targets. Such cyber

---

[1] Bing Huang, Mohammad Majidi and Ross Baldick, "Case Study of Power System Cyber Attack Using Cascading Outage Analysis Model," 2018 IEEE Power Energy Society General Meeting, Portland, OR. Mohammad Majidi contributed in advising on the design of Cascading Outage Analysis (COA) Model and the techniques in programming used in this paper. Ross Bladick contributed in advising the design of Cascading Outage Analysis (COA) Model, the simulations using the COA, discussion of results and multiple revisions of the paper.

[2] Bing Huang, Alvaro Cardenas and Ross Baldick, "A Study of the Impacts of IoT Demand Attacks on Power Grids," 28th USENIX Security Symposium, Santa Clara, CA, 2019. Alvaro Cardenas and Ross Baldick contributed in advising and discussion of IoT simulations, polishing and revising the paper in multiple rounds.

security threats have been considered and studied by the North American Electric Reliability Corporation (NERC) since at least 2012. Thus, the purpose of the work described in this chapter is to develop a tool, of potential use to government entities, to assess the effects of specific types of cyber attacks that are modeled on the Ukraine attacks. The previous chapter described the previous work on a sequential outage checker based cascading outage analysis (COA) model. In this chapter, we first apply this COA model to a North American regional interconnection system model and perform case studies to simulate analogous system interdictions assuming the cyber attackers gained full control of the system. During the cyber attacks in Ukraine in 2015, attackers opened breakers using Supervisory Control and Data Acquisition (SCADA) systems in three distribution companies that they previously compromised. This is the most intuitive way for cyber attackers to create power outages once they have access to SCADA. To help assess the effects of such attacks, we further develop the COA model and study the impacts of opening different types of devices of each transmission and distribution company (owner) in the studied North American regional interconnection system.

The vulnerability of Internet of Things (IoT) devices is a well-known problem [8, 111, 328]. Previous work has demonstrated that various of IoT devices from cameras to door locks can be compromised directly or through their designated smart phone applications [135, 282]. Vulnerabilities of IoT devices go beyond personal privacy and information security. For example, the Distributed Denial of Service (DDoS) attack by the Mirai botnet compro-

mised over six hundred thousand IoT devices and was able to affect multiple websites and network infrastructures [15]. Recently, more and more devices with high-energy consumption such as water heaters and air conditioners are also enabling consumers to interact with them through the Internet. Although manipulating the energy consumed in a single household is not enough to cause any major problem to the power grid, a recent paper presented in USENIX Security 2018 [361] proposed the Manipulation of demand via IoT (MadIoT) attacks, and showed an attacker who could coordinate the compromise of hundreds of thousand of high-energy IoT devices to launch several attacks on the power grid, including (i) frequency instabilities, (ii) line failures, and (iii) increase in operating costs. These attacks paint a dire picture of the security of the power grid as they show that a 30% increase in demand trips all the generators in the US Western interconnection and a 1% increase of demand in the Polish grid results in a cascading failure with 263 line failures and affecting 86% of the load in the system.

In this chapter, using the COA model, we perform an in-depth study of the power grid effects of MadIoT attacks. Our analysis shows that while MadIoT attacks can create negative consequences on the power grid, the negative impact on the grid will not be as serious as originally claimed in [361]. In particular, while some load shedding will be necessary to deal with these attacks, our results show that creating a system blackout–which would require black start period of several days to restart the grid—will be very difficult, given the embedded protections that all power systems have throughout their

infrastructure.

3.2   The Design of Cyber Attack Experiments

There are certain limitations of the studies on power system cyber attacks: first, the absence of accurate transient simulation data; second, the lack of perfect fidelity of power flow model; third, the imperfect models of protection. The first limitation will be elaborated in section 3.2.1. For reasons of confidentiality, the power flow model of the North American regional interconnection system is not the real system case. As discussed in detail in section 3.2.2, we model the system protections in a way that approximates the system response to the contingencies but do not try to replicate the real protection configurations.

Because of these limitations, our results are indicative of the types of outcomes that might result from attacks by terrorists but are not specific predictions for a real system. The assumptions would reflect the sort of limited information that might be gathered by a terrorist.

3.2.1   Transient Data

The power flow case available for investigation does not include transient data. Therefore, in order to implement the COA model, we assemble the transient data (machine, exciter, governor) from IEEE standard 300 Bus case. The generators in the IEEE 300 Bus system have 6 levels of real power outputs, so we create a range of generation level with 7 intervals. Then, we

considered each generator in the interconnection case in our study and locate which interval its power capacity falls into and use the IEEE 300 Bus system transient data of that interval to configure the generator in the interconnection case.

For reasons of confidentiality, we were not able to obtain the actual generator transient data, so we apply the above method to approximate the system transient behaviors. With the approximated transient data, the generator rotor angles in the system are very sensitive to even single contingencies indicating that the model is not reflecting how an actual system would behave. However, some of these results still display some interesting insights that will be shown and discussed in section 3.3.1.3.

3.2.2 Protection Configurations

There are two protections implemented in the transient simulation, namely Over/Under Frequency Generator Tripping (O/UFGT) and Under Frequency Load Shedding (UFLS). If the frequency at a bus deviates from a predefined threshold for more than a specific time period, the generator connected to that bus would be tripped, and a certain percentage of load connected to the bus will be shed. The details of the protections are shown in Tables 2.1 and 2.2. As discussed in Sections 2.5 and 2.6, since the current and voltage responses in the system are normally slower than frequency feedbacks, the Time Inverse Overload, Time Inverse Under Voltage Load Shedding, and Time Inverse Over Voltage Generator Tripping are modeled in the

steady state simulation. Both protections will calculate tripping times once the current flow on branches or the voltage at buses exceed the thresholds. The element (branch, generator, or load) with the shortest tripping time will be tripped as the initial conditions for the next iteration of transient simulation. The parameters of the steady state protection models described in equations (2.3),(2.4) and (2.5) are shown in Table 3.1.

Table 3.1: Steady State Protections

	Over Load	Over Voltage	Under Voltage
Threshold	$I_{th} = 2 \times$ line limit [amps]	$U_{th}^o = 1.3$ [pu]	$U_{th}^u = 0.8$ [pu]
Parameters	$T_p = 0.05$	$k = 0.5$	$k = 0.5$

3.2.3 Cyber Attacks Target on Grid Control Centers

Based on the experience in Ukraine power system hacking events, we present three types of experiments that simulate analogous attacks on each transmission and distribution system provider (TDSP) in the system in turn:

1. Open all devices of that TDSP;

2. Separately open all branches in each of three different voltage levels of that TDSP;

3. Open all generators and loads connected to the lines of that TDSP.

Although experiment 1 is the closest scenario to the Ukraine attack, experiment 2 creates examples that apply when companies only own branches at specific voltage levels or otherwise have control systems that are partitioned

across voltage levels, while experiment 3 creates examples where the attack targets the creation of supply/demand imbalance as well as removing transmission and distribution capability.

Before detailed discussion of the case studies, we state two main assumptions that we make about a cyber attack:

- Cyber attackers already have full and unlimited ability to control the tripping of breakers, and
- Cyber attackers actions of tripping of breakers of a TDSP are simultaneous.

In this study, an "Algorithmic non-convergence" is deemed to occur if the PowerWorld transient solver could not find a solution. This could happen either after the initial contingency or in subsequent transient runs. In contrast, "Convergence" case means PowerWorld was able to obtain a transient solution after the initial contingency, and also that any subsequent runs of the transient solver were completed.

Algorithmic Non-convergence is a proxy to a complete blackout occurring; however, it should be recognized that the correspondence between Algorithmic Non-convergence and blackout is not perfect. Convergence is a proxy to the system staying energized, although some generation and load could be lost.

3.2.4   IoT Demand Attack

We state three main assumptions (in line with previous work) about an IoT demand attack:

1. IoT attackers already have full and unlimited ability to control the compromised portion of loads;

2. IoT attackers' actions of increasing or decreasing of compromised loads are simultaneous;

3. The portion of the system demand compromised by the cyber attackers are evenly distributed at each demand connection point in the transmission system.

The third assumption is a speculation about the scalability of an IoT attack. For example, if the adversary is able to compromise one brand of AC, they can systematically apply the attack to as many ACs as possible in the target system. Thus, if the total energy capacity of all such ACs is 10% of the system demand, this 10% of demand is likely to be spread to every demand connection point in the transmission system.

3.3   Simulation Results of Cyber Attacks on Grid Control Centers

In this section, we present the simulation results and discussions of experiments described in section 3.2.3. First, we would like to investigate what types of initial attacks are prone to cause an algorithmic non-convergence to

the system in section 3.2.3. Although convergence means that a complete algorithmic non-convergence does not happen, there is still load shed in the system. Therefore, we display the results of load shedding in the convergence cases and discuss relations between the amount of lost load and the voltage levels of the attacked lines in section 3.3.2.

3.3.1 Algorithmic Non-convergence Cases

A brief summary of the number of algorithmic non-convergence cases in the experiments is shown in Table 3.2.

Table 3.2: Number of Algorithmic Non-convergence Cases

Initiating Contingency	All Devices	All Branches			All Loads and Generators
		EHV	HV	MV	
Results	9/231	6/66	9/99	0/55	3/214

The results in Table 3.2 show the number of algorithmic non-convergence cases as a fraction of the total number of cases of each type. For example, in the experiment to open all extra-high-voltage (EHV) branches, the results 6/66 indicates that in total there are 66 TDSPs with EHV lines, and if all of the EHV lines of a given TDSP are opened, 6 cases of TDSPs would result in algorithmic non-convergence. The ratio of algorithmic non-convergence cases to total cases is the same for opening EHV lines and high-voltage (HV) lines. It is zero in the experiment on medium voltage (MV) lines. Since EHV and HV lines carry heavy power flow in the system, opening those high voltage lines will result in very large changes in power flow, which has a greater poten-

tial to overload other lines and precipitate a cascade. Similarly, opening such high voltage lines would also tend to cause power imbalance locally or globally and stress the system the most. Therefore, opening the lines of TDSPs that have high voltage lines is more prone to cause algorithmic non-convergence. In contrast, while opening MV lines may interrupt load, there is a smaller effect on overloading other lines.

3.3.1.1 Open All Devices of a TDSP
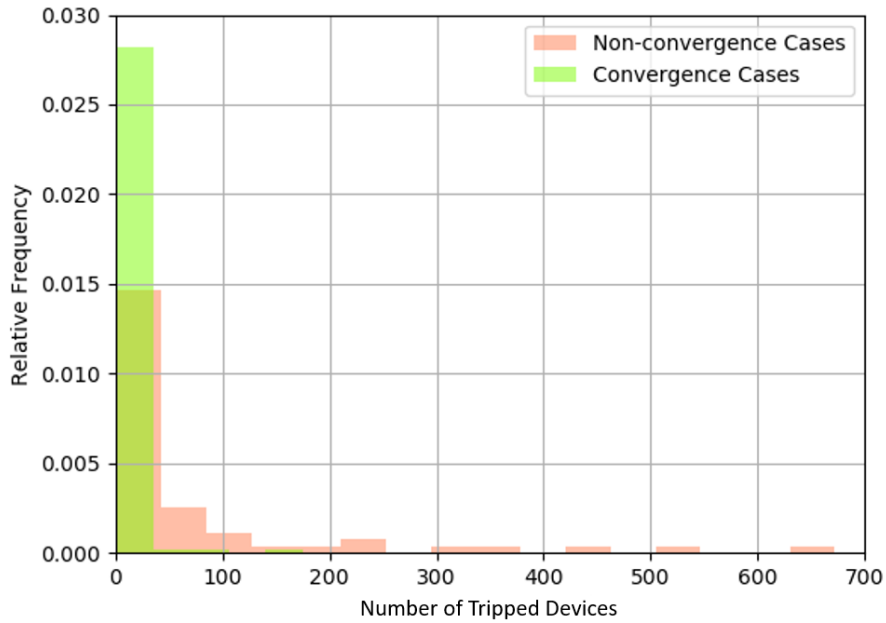
Figure 3.1: Histogram of Algorithmic Non-convergence and Convergence Cases

Figure 3.1 shows the distribution of the number of tripped devices for both the algorithmic non-convergence and convergence cases. Here, "devices" include generators, loads, lines, transformers, and capacitors. The comparison between the distribution of the number of devices in algorithmic non-

convergence cases versus convergence cases suggests the intuitive result that algorithmic non-convergences are more likely to occur when TDSPs with large numbers of devices have their devices removed from the system. Nevertheless, algorithmic non-convergences occur even for some TDSPs that have a small number of devices.

3.3.1.2 Open All Branches at a Particular Voltage Level of a TDSP
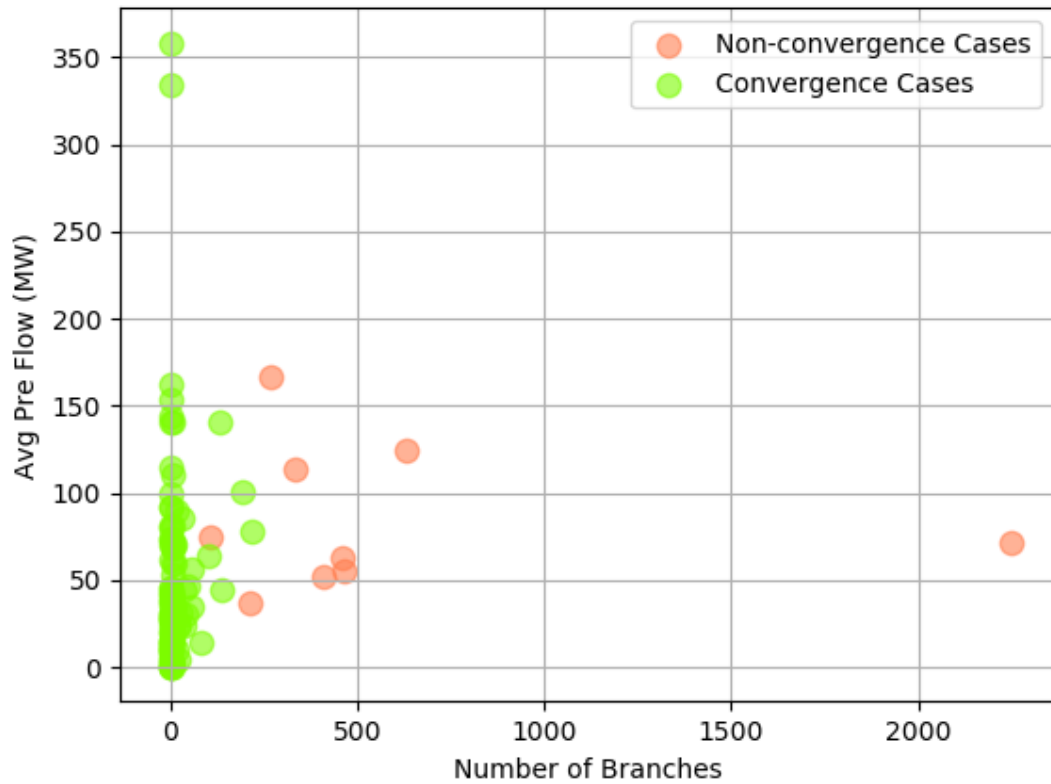
Figure 3.2: Average Pre-attack Flow vs Number of HV Branches Scatter Plots

Figures 3.2 and 3.3 show the scatter plots of the average pre-attack flow (vertical-axis) and number of branches (horizontal-axis) in each case. In

the plot, each dot represents a simulation result from opening all the lines at a particular voltage level for a particular TDSP. Algorithmic non-convergence cases are the red dots, convergence cases are the green dots. The average pre-attack flow is the average power flow on the branches before they are opened in the contingency. These figures show the results of simulation without rotor angle checker.

Figure 3.3: Average Pre-attack Flow vs Number of EHV Branches Scatter Plots

At both HV and EHV, it can be observed that there are thresholds in the number of branches. This is consistent with the conclusion drawn from Figure 3.1. In particular, an algorithmic non-convergence will happen if the
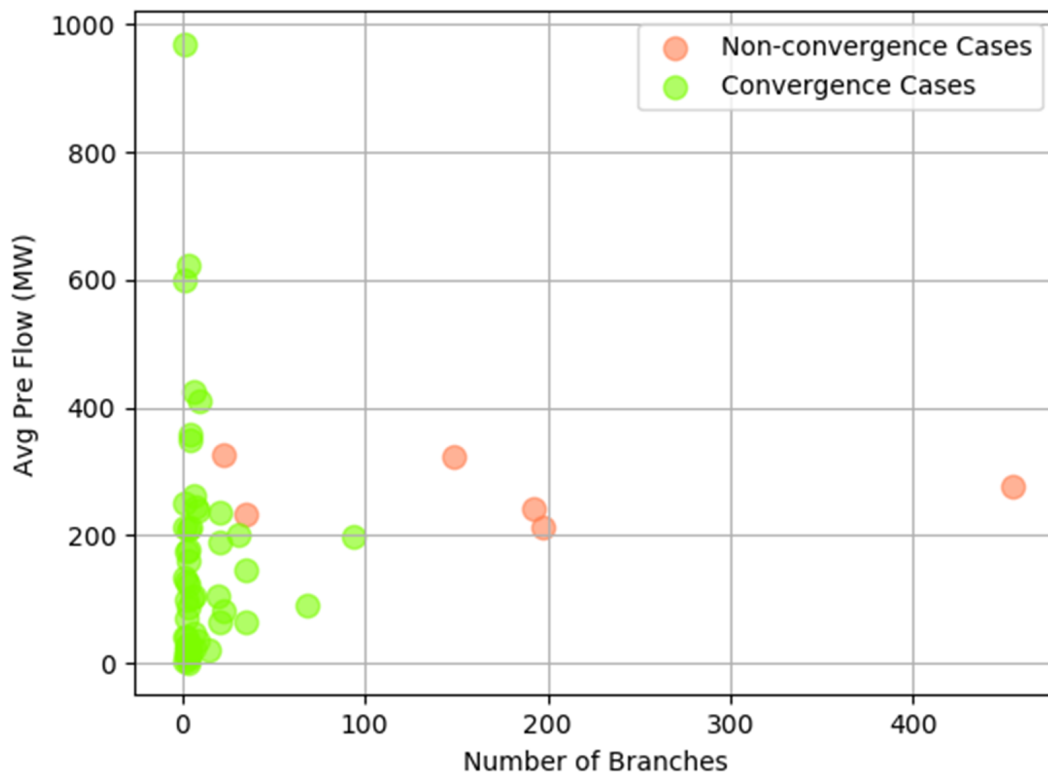
number of branches in an initiating event is greater than the threshold.

When we include the rotor angle checker in the same experiment, in addition to the similar thresholds in Figures 3.2 and 3.3, the results show thresholds on average pre-attack flow that result in algorithmic non-convergence. This result indicates the importance of loading on branches before the attack. Intuitively, the observation from the simulation with rotor angle is reasonable. The more power flow is disturbed, the higher the probability that local power imbalance would happen, and the more generators would be tripped because of rotor angle deviation. Therefore, we would expect a qualitatively similar result if more accurate transient data were available, although the details of the number of tripped devices would be different.

3.3.1.3   Trip All Generators and Loads of a TDSP

In the experiment of tripping all generators and loads of a TDSP, there are only three algorithmic non-convergences in the simulation results with no rotor angle checker. The TDSPs in these three cases either have very large amounts of generation relative to load, or vice versa. The algorithmic non-convergence is primarily caused by the significant supply-demand imbalance due to the initial contingency.

Figures 3.4 and 3.5 show the results of tripping all generations and loads of a TDSP when the rotor angle checker is included in the simulation. It can be observed that the difference between generation and load lost is important. In Figure 3.4, the vertical axis indicates how much load is lost in the initial
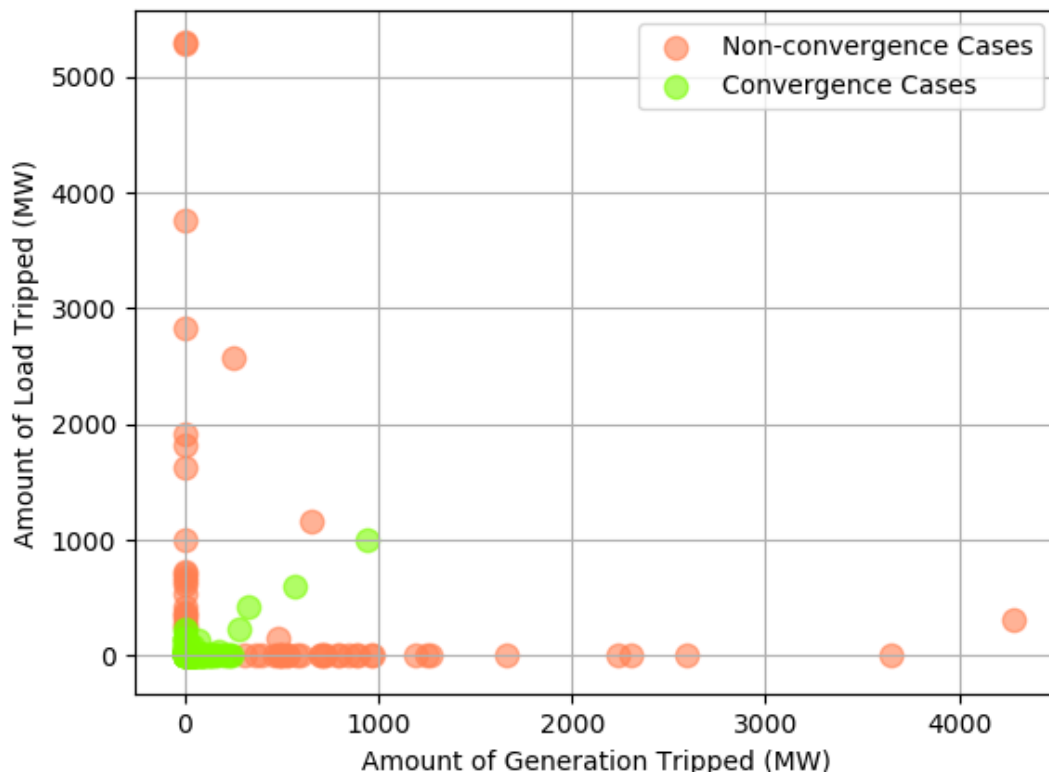
Figure 3.4: Tripping All Generation and Loads Scatter (Include Generator Rotor Angle Checker)

contingency and the horizontal axis indicates how much generation is lost in the initial contingency. In this case, we can see that above a certain level of load and generation, all the convergence cases (green points) involve roughly equal amounts of generation and load tripped. This result clearly shows that the power imbalance caused by the initial contingency is critical to algorithmic non-convergence in the system. The extreme case shown in the figure is that the system converged when around 1000 MW of both loads and generations are lost in the initial contingency.
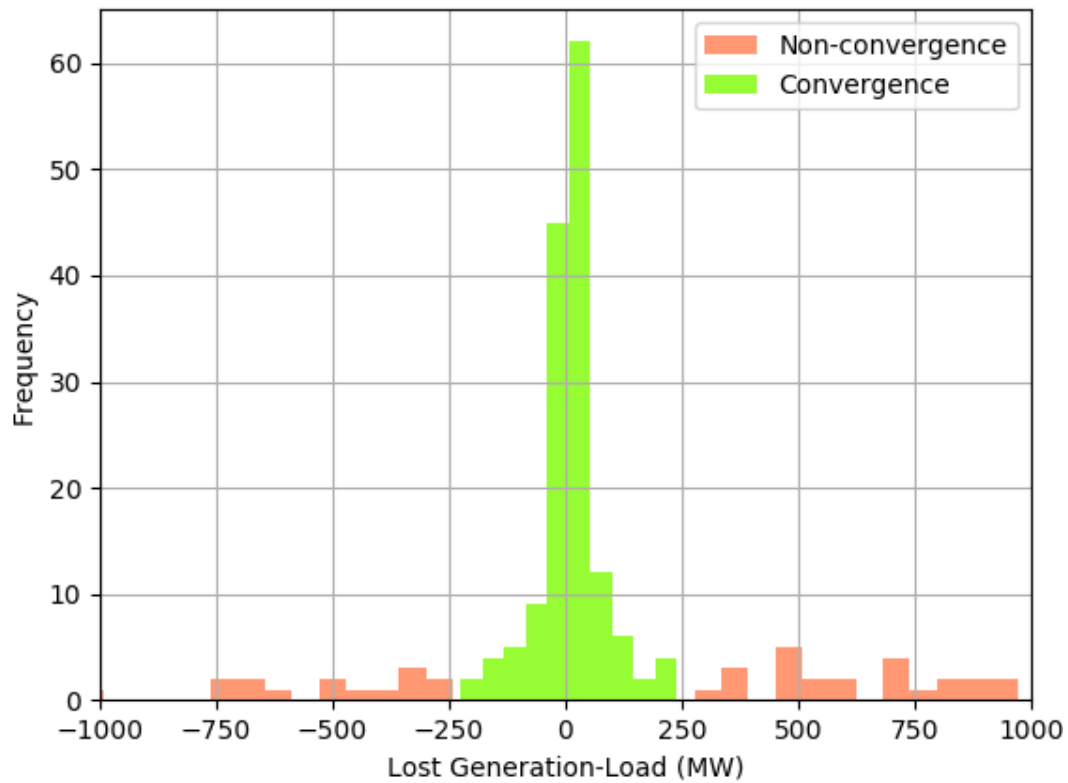
Figure 3.5: Tripping All Generation and Loads Histogram (Include Generator Rotor Angle Checker)

In Figure 3.5, the horizontal-axis is the power imbalance caused by the initial contingency calculated as the amount of generation minus the amount of loads. The vertical-axis is the frequency occurrence. This histogram shows how the algorithmic non-convergence and convergence cases distribute for different levels of power imbalance. The results show that the convergence cases mostly occur when the differences between generation and load lost is small. In addition, the frequency of algorithmic non-convergence (the red bars) on the right is greater than the left. That is, in the case of creating energy imbal-

51

ances in the system by tripping generations and loads, given the same level of imbalance, tripping more generations are more likely to cause an algorithmic non-convergence than tripping more loads.

3.3.2 Load Lost in Convergence Cases

Convergence cases are the cases in which both transient and steady state simulation would have a feasible solution at the end of COA. As mentioned above, although convergence means that a complete algorithmic non-convergence did not happen, there is still load shed in the system.

Figure 3.6 shows the lost load for the case of opening lines at a particular voltage level of a TDSP. The vertical axis shows the amount of load shedding at the end of simulation, and the horizontal axis is the sum of real pre-attack flow on the branches that are attacked. We can observe that, at each of the three voltage levels, the amount of load lost caused by opening the breakers of a TDSP at a particular voltage level has a relatively linear relationship with total pre-attack flow on the branches for that TDSP. In addition, the slope of MV cases is higher than HV cases, and EHV case has the lowest slope.

This result suggests that the more pre-attack flow on the lines that are attacked, the more load would be lost. In addition, attacks on MV and HV lines are more effective than attacks on EHV lines in terms of creating load lost. In many cases, because the lower voltage lines are close to the load, the loss of those low voltage lines would directly disconnect loads, or lead to overloads on lines that disconnect loads. In addition, since EHV lines are
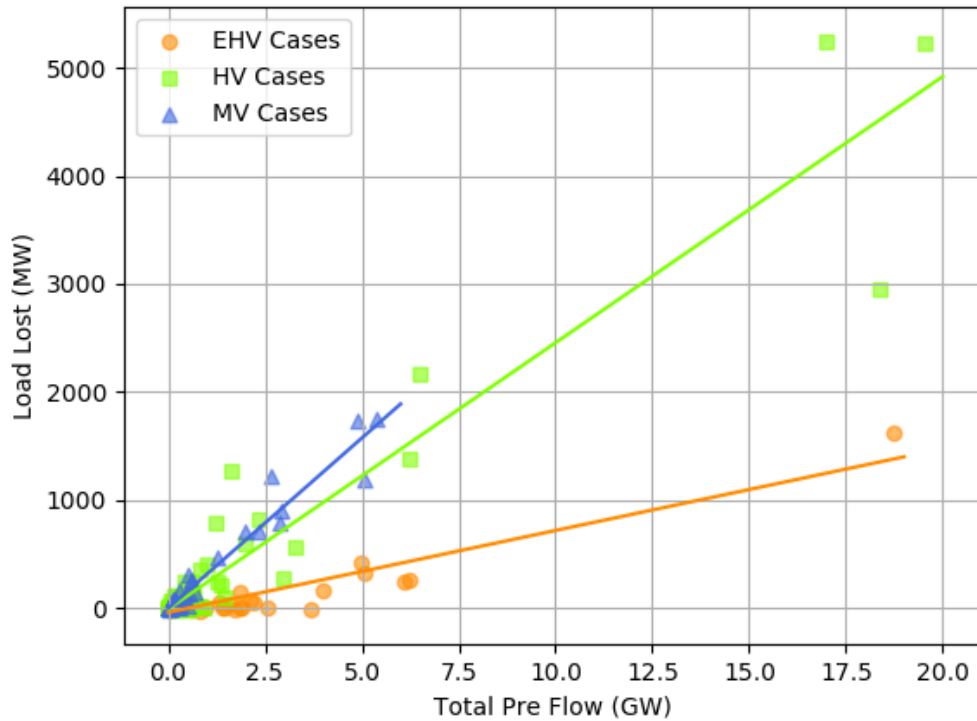
Figure 3.6: Load Lost of Open Branches in Different Voltage Levels

highly meshed, if the system does not face algorithmic non-convergence, the loss of EHV pre-attack flow is easier to be handled by the remaining network. Therefore, the loss of EHV lines is less likely to result in further load lost.

3.4 Simulation Results of IoT Demand Attacks

This section will first demonstrate the contribution of applying the cascading outage analyzer to the study of IoT demand attacks with a relatively simple but standard Western System Coordinating Council (WSCC) model with 9 buses and 9 lines to compare our results with previous work. Then, a

detailed study of IoT demand attack described in Section 3.2.4 on the large study case described in Section 3.2 is presented. The settings for the frequency protections are updated according to ERCOT operation guide [123] for the study in this section:

Table 3.3: Over/Under Frequency Generator Tripping. Source: data is from Section 2.6.1 of [123].

Over Frequency Threshold	Time Delay	Under Frequency Threshold	Time Delay
60.6 Hz	9 min	59.4 Hz	9 min
61.6 Hz	30 sec	58.4 Hz	30 sec
61.8 Hz or above	0 sec	58.0 Hz	2 sec
		57.5 Hz	0 sec

Table 3.4: Under Frequency Load Shedding. Source: data is from Section 2.6.2 of [123].

Frequency Threshold	System Load Relief	Time Delay
59.3 Hz	5 %	0 sec
58.9 Hz	15 %	0 sec
58.3 Hz	25 %	0 sec

3.4.1 Demonstration of IoT Demand Attacks Simulations with a Cascading Outage Analyzer

In order to understand the effect of an IoT attack on the grid, it is important simulate the response of power systems to disturbances, and in

particular, to include the existing power system protections. The Cascading Outage Analyzer described in Chapter 2 is designed to provide such a simulation. This tool is used to update analyses in [361] using a higher fidelity model.

3.4.1.1 The Need for Closed Loop Transient and Steady-State Simulations

Since the operation of a power system after a disturbance is a continuous process from seconds to minutes and even a longer time frame, a closed loop structure of the cascading outage analyzer can better approximate the operations of the power system over those various time scales after a disturbance. As previously discussed, the results and states of the system after the transient simulation are stored and set as the starting point of the steady state simulations. The cascading outage generated from steady state simulations, if there is any, will be used as the initial condition in the transient simulation for the next loop.

Previous work in [361] considered transient and steady state simulation as separate, and as a result, the transient impacts on generators and system frequencies are not present in the power flow simulations. Therefore the predictions of cascading outages can differ between the two simulations. Let us look at an example to see a possible inconsistency between the prediction in [361] and the COA model prediction, while emphasizing the significance of a closed loop simulation to the analysis of cascading outages and IoT demand attacks.
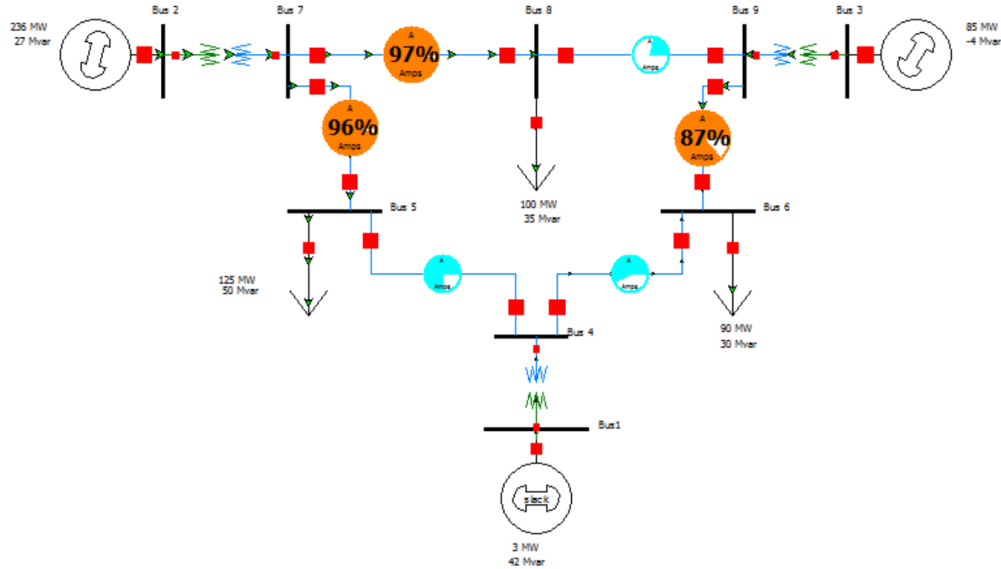
Figure 3.7: PowerWorld 9-bus system.

Figure 3.7 shows the WSCC 9-bus system considered by Soltan et al. [361]. Consider an IoT demand attack that increases all loads by 15% in the system. Assume an outage would happen on a line if the power flow is over its rated capacity [68]. If the transient impacts of this attack are not considered, the results from the steady-state power flow would indicate a line outage between bus 7 and bus 8. The resulting line considered to be in outage is highlighted with a red circle (with the number showing the percentage of the rated capacity) in the top left corner in Figure 3.8.

However, because of the sudden load increase caused by the MadIoT attack, load and generation are not balanced and the frequency of the system will be affected. A frequency protection relay would disconnect a generator from the system if the frequency of the system stays lower or higher than the
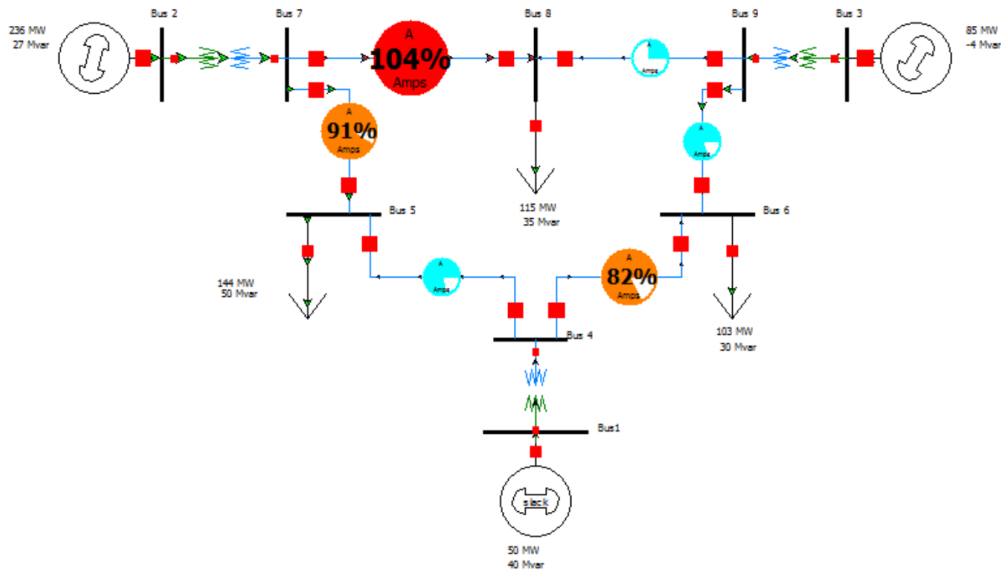
Figure 3.8: Power flow results of 15% of load increase.

generator's threshold values for too long in order to prevent permanent damage to the generator. Figure 3.9 shows the frequency responses to the 15% load increase by considering frequency protection relays on generators [361]. We can see that the system frequency starts to decline after the attack starts (at time equal to one second of the simulation). The frequency relays then disconnect all the generators in the system two seconds after the frequency drops below the threshold of 58 Hz. Therefore, the system is completely blacked out in the transient simulation of the IoT demand attack. These transient stability results are different from the steady state stability study, which identified only one cascading line outage as discussed in the previous paragraph.

This is a motivating reason to include transient and steady state analysis together in a single simulation. Because transient and steady-state simula-
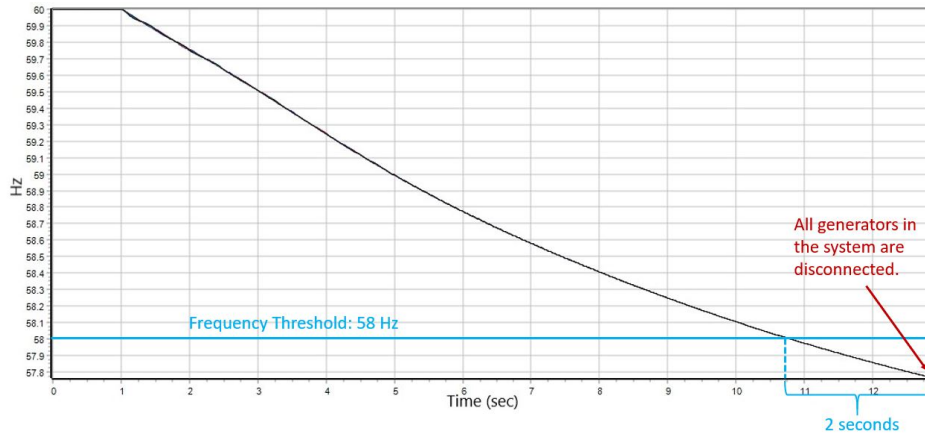
Figure 3.9: Frequency responses to the 15% of load increase in the transient simulation.

tions are connected in a closed loop in our model, the transient solution at the end of the simulation time will be used as initial condition for the steady-state power flow simulation. In this example, if the under frequency load shedding is not considered, which will be discussed in subsection 3.4.1.2, the transient solution would include the fact that all three generators were disconnected from the system. Thus, the power flow solution would indicate a system blackout.

3.4.1.2 Under Frequency Load Shedding

Under Frequency Load Shedding (UFLS) is a countermeasure applied by bulk power system operators [123] to reduce the incidence of generator under-frequency tripping, which is a great danger to the reliable operation of the power systems. UFLS is a coordinated disconnection of small and non-critical loads (e.g., no Hospitals are ever disconnected) to prevent a large blackout.

58

To illustrate why it is important to consider UFLS in the simulation of IoT demand attacks, let us first take a second look at Figure 3.9. As observed, after the 15% load increase attack, the system frequency starts to decrease. Because there is no action that could relieve the imbalance between the increased load and unchanged generation, the system frequency declines fast until it drops below the thresholds of frequency protections at generators. Because the frequency stays below the thresholds for longer than the delay time set at the frequency protections, the generators are disconnected and there is a system blackout.

Now, let us compare the simulation results when we incorporate UFLS. Figure 3.10 shows the frequency response to the 15% system demand increase attack on the WSCC 9-bus system. The system frequency declines after the IoT load increase attack starts at one second of the simulation time. The frequency of the system then reaches the first UFLS threshold at 59.3 Hz, and as a result, 5% of the system load is disconnected. However, this is not enough and the system frequency keeps declining until it reaches the second threshold: 58.9 Hz, and at that time a total of 15% of the system demand is disconnected and the frequency stops decreasing and starts to stabilize. The system frequency reaches a new stable state and there are no generator disconnections from the system.

What is more, because of UFLS, the system load is reduced to a level that no transmission line is overloaded as defined to be a line carrying power flow that is greater than its rated capacity. Therefore, there are no cascading

59
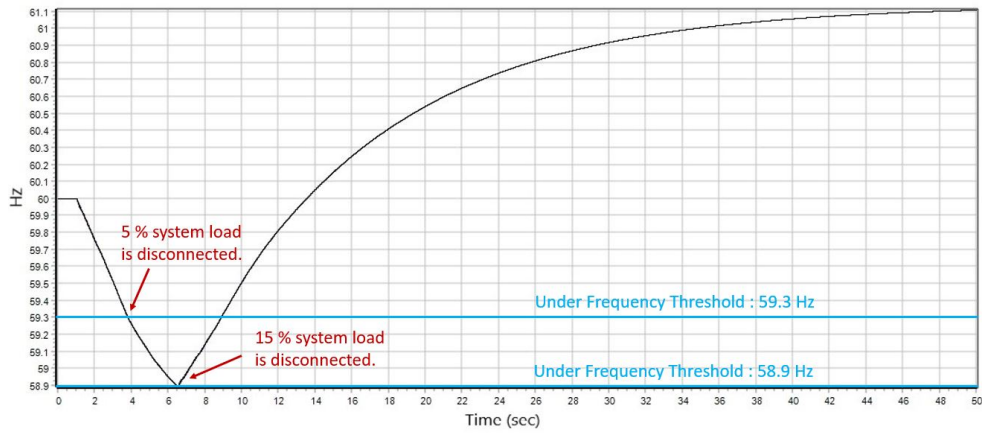
Figure 3.10: Frequency responses with Under Frequency Load Shedding to the 15% of load increase in the transient simulation.
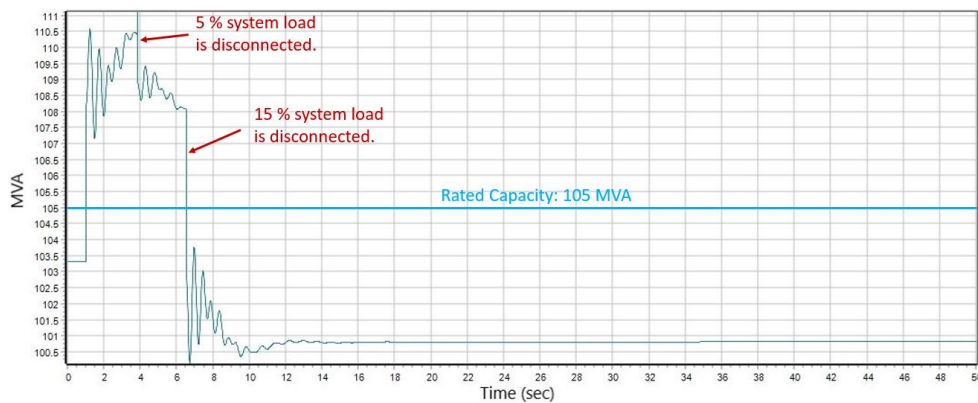
Figure 3.11: Power flow on the transmission line connected between bus 7 and bus 8 in the transient simulation

outages. In Figure 3.11, we can observe that the transmission line between bus 7 and bus 8 in Figure 3.7 is overloaded after the IoT demand increase attack begins at one second. However, the power flow on the line soon decreases following the load shedding event caused by UFLS and remains below its rated capacity at the end of the transient simulation. As discussed in Section

60

3.4.1.1, a power flow steady state simulation starts based on the solution of the transient simulation; the results of this new steady state stability analysis are shown in Figure 3.12. As seen in Figure 3.12, no line is overloaded and the closed loop transient and steady state simulation ends.
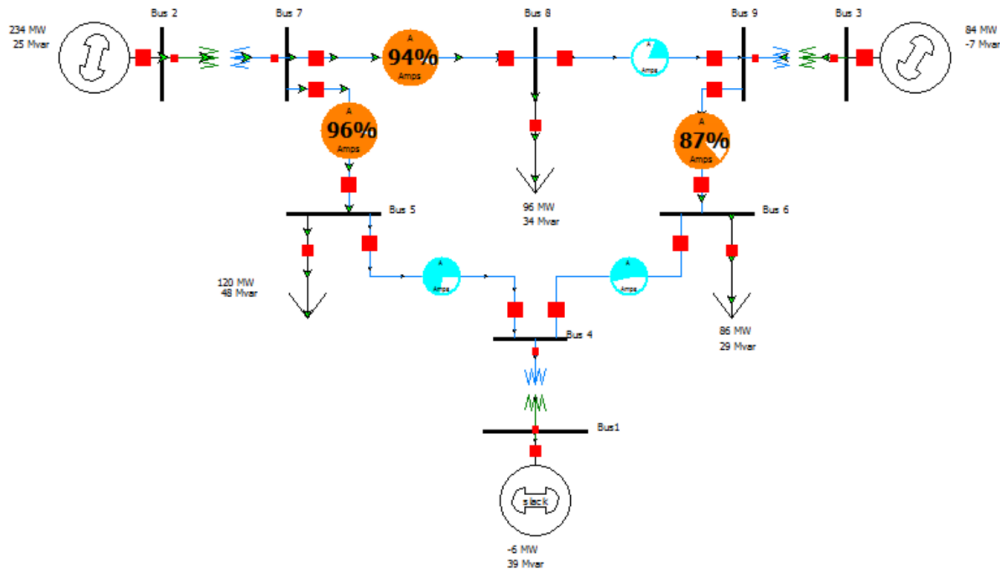
Figure 3.12: Power flow results after the transient simulation with UFLS.

The example in this section shows that the simulation results will be significantly affected if UFLS protections are considered. In fact, by including UFLS, the closed-loop transient and steady state simulations used in this work generates a result suggesting that the system would shed some demand, but all the system transmission lines and generators will remain in operation. This result is different from the cascading line outage suggested by our earlier steady state simulation and the complete system blackout suggested by previous work [361]. This example shows the importance of detailed modeling of

transient response and protection.

3.4.1.3 Frequency Response Model

UFLS protections have been considered in previous work in [97] on load attacks in power systems. However, the simplified frequency response model in [97] does not fit well with the analysis of IoT demand attacks. The system frequency responses in the study are modeled as a single large machine that represented an "aggregation" of all the synchronous generators in the system. Under this simplification, each of the generators in the system will respond to a disturbance exactly the same as described by the model in [97]. The assumption implicitly made by this simplification is that all the generators in the system will always keep synchronism and respond identically. However, when the system is under a significant disturbance, generators will respond differently to the disturbance and the system will risk losing synchronism in a short time after the disturbance. In some scenarios, the frequencies at different buses will diverge from synchronism. This frequency diversity can not be reflected in the single machine model studied by Dabrowski et al. [97]. A detailed discussion of these phenomenon will be demonstrated with examples in Section 3.4.2.5.

3.4.1.4 Power Flow, Line Overload Outage and Bus Voltage Outage

Power flow have been solved in previous work in [361]. Although not directly specified, it is very likely the previous work [361] uses DC power flow

for the cascading outage analyses. In contrast, we use PowerWorld [320] to solve an AC power flow for each of the steady state simulations.

The computation of AC power flow gives voltage magnitude, phase angles, and power flow on transmission lines. However, DC power flow is a linearized calculation based on several assumptions ignoring variation in voltage magnitudes. First, using a DC power flow model for cascade prediction may result in a misrepresentation of the gravity of a cascade. Secondly, the voltage changes in the cascading outages will not be captured in a DC power flow. DC power flow is a simplification to obtain fast simulation results, but it is not adequate in a study of a major disturbance like an IoT demand attack.

The line overload outage models also play an important role in understanding the impact of MadIoT attacks. Previous work in [361] relied on the criteria described by Cetinay et al. [68], where a line will be removed from the system if the steady-state results indicate that the power flow on the line is greater than its rated capacity. When a transmission line is overloaded, the heat generated from the extra power flow on the line will sag the transmission line. Although it exposes the line to a possible outage from faults associated with ground elements or vegetation, it does not necessarily cause any immediate real danger to the system. In fact, under an emergency, the system operator is allowed to use overloaded transmission lines for additional transmission capacity [124]. Therefore, instead of immediately removing the overloaded lines, we utilize an Overload Outage Checker (OOC) that will calculate the time of tripping given the overload level. The details are described

in Section 2.5. The time inverse calculation in the OOC will result in a quick tripping time for the lines that are heavily overloaded. In this way, we approximate the different actions taken at different levels of overload on transmission lines.

Finally, the voltage profile of the system may decline when the system is under extreme conditions and voltage collapse is a typical pattern seen in cascading outages. Therefore, a Voltage Outage Checker is defined and discussed in Section 2.6. To the best of our knowledge, we haven't found a specific model of voltage failures in the previous work of IoT demand attacks.

Based on the above discussions, we believe that, with a more detailed and realistic model, our results of IoT demand attack simulations can provide a different set of insights for similar studies.

3.4.2 Simulation Results in a Large Power System

In addition to the demand increase attacks, we also consider attacks that increase and then subsequently decrease the load. The intuition for this attack is that the demand increase attack may trigger system automatic responses such as UFLS and therefore cause the system to drop loads, for example, to reverse the frequency decline. Then, a successive demand decrease attack can potentially drive the system to an unstable state, because there is less UFLS available after the first attack.

First, because of the features of an IoT attack, it is easy to increase and decrease the demand in a short period time once the demand is compro-

mised. In addition, if the attackers have some knowledge of the power system operation, it would not be hard for them to figure out that there are some system frequency protections that are designed to stop and reverse the frequency drop caused by a sudden demand increase. The attackers will decrease the demand when they think the system frequency reverses due to UFLS and by doing so intend to overshoot the system frequency to be above the thresholds of generator over-frequency protections in the hopes of causing a generator disconnection.

This demand increase and decrease attack was studied by Dabrowski et al. [97]. However, our results will differ because the simplification of the frequency model in [361] as discussed in Section 3.4.1.3. In addition, if the attacker can cyclically increase and decrease then decrease demand, it is also reasonable to assume that the attacker is capable to achieve a repetition of this cycle of attacks. This extends the attack in [361]. The simulation results and detailed discussions of the experiments are shown in Section 3.4.2.4.

3.4.2.1 Terminology

First, as mentioned in Section 2.7, the loss of electric power caused by load shedding from UFLS is temporary and can be quickly corrected within an hour. However, a complete system blackout will result in all customers in the system losing their electric power for several days before the system is restored. Therefore, limited UFLS is nowhere as serious as a complete system blackout.

Second, as mentioned in Section 3.4.1.4, a transmission line is overloaded when the power flow on the line is over 100% of its rated capacity. As discussed in Section 2.5, overloaded transmission lines are potential causes for cascading failures but they do not necessarily lead to immediate disconnections of the lines.

3.4.2.2 Cascading Failures on Transmission Lines after an IoT Demand Increase Attack

One outcome the attackers can attempt to achieve is to overload the transmission lines and potentially cause cascading failures. Those severely overloaded transmission lines will be disconnected by protection relays. The trip time of the overload relay on the transmission lines is approximated by equation (2.3). Then, the attack of load increase may cause cascading failures on the transmission lines as discussed in Section 2.5. In the following sections, we consider protection system responses to load increases of 1% and 10% as suggested by previous work, together with some variations.

1% System Demand Increase Attack

One percent of the system load in this case study is equivalent to 822.7 MW. Figure 3.13 shows the bus frequency responses after 1% of load increase occurring at second 1 and Figure 3.14 shows the power flow on branches as a percent of the branch rated capacity.

From Figure 3.13, we can observe that the bus frequencies decline after the attack at second 1 except for very few buses that are connected to the

66
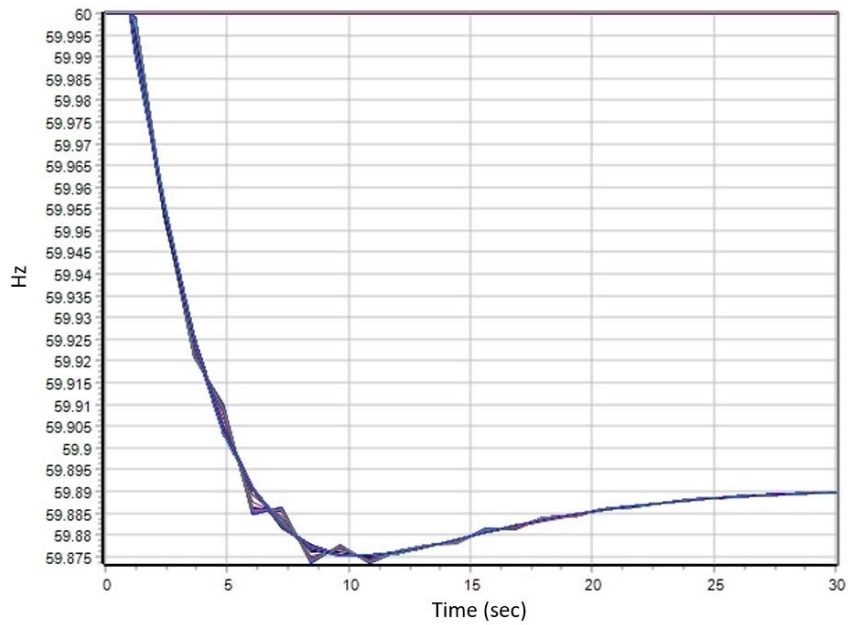
Figure 3.13: Frequency Response to 1% System Load Increase

region outside of the system with DC tie lines and thereby remain less affected. The system frequency declines from 60 Hz to 59.875 Hz in about 9 seconds and is settling towards a new stable state towards the end of the transient simulation. As indicated in Table 3.3 and Table 3.4, the system frequency doesn't violate any thresholds of frequency protections on generators and loads. Notice that we focus our study in a short time window, since 30 seconds of transient simulation is enough to display the moving trends of the frequency in this case. In Figure 3.13 we can see the how the frequency is affected after the attack; however, as long as the bus frequency converges to a stable level, driving the frequency back to 60Hz can be accomplished either automatically or manually over a longer time scale.

67
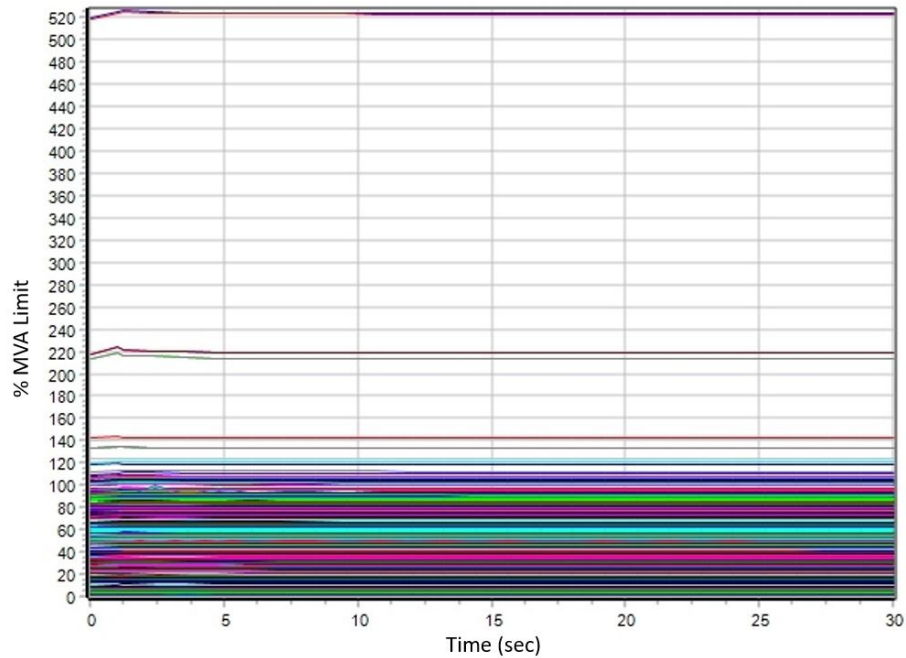
Figure 3.14: Branch Flow after 1% System Load Increase

In Figure 3.14, we can see that the power flow of some branches slightly increases after the attack at second 1. However, no transmission line is overloaded due to the IoT 1% load increase attack alone. Note that some branches are initially overloaded before the simulation and remain unchanged during the simulation and the overload outage checker is not activated on those lines under the assumption that protection in the actual system would not have been activated under these conditions.

The results show that 1% of load increase attack does not interrupt any generator or load in the system. In addition, in the end of the simulation, there is no transmission line that is overloaded above its initial loading due to this load increase attack.

68

In contrast to our results showing fairly small changes to our system, Soltan et al. [361] find that with a 1% increase in load there could be cascading outages in the summer peak of the Polish grid. We are surprised that a sudden 1% increase is load can lead to cascades in a power system. The reason for our surprise is the N-1 security criterion.

The N-1 criterion requires that electricity systems be operated to be able to withstand sudden step changes in the supply-demand balance due to outages of generation. The NERC disturbance control performance standard [285] requires any system to be able to withstand "the most severe single contingency" which may include certain common-model double outages. For ERCOT, for example, (the Power Grid of Texas) this amounts to always having 2700 MW or more of reserves to cope with a simultaneous outage of nuclear units having total production of around 2700 MW. To put that in perspective, peak load in ERCOT is around 70GW, and 1% of 70GW is 700MW, which is much smaller than the 2700MW of reserves carried in ERCOT.

While an increase by 700MW in load due to an IoT attack (and the reaction by generation reserves) would result in somewhat different changes in transmission flows compared to the effect of a 700MW decrease in generation (and the reaction by generation reserves), it is unlikely that an increase in load of 1% would result in any unacceptably adverse conditions on the transmission system. This is because load is geographically distributed around the system, so that it is unlikely for there to be a more than a 1% increase in most transmission flows, and it is unlikely that the system is operating such that a

1% increase in current would immediately trigger the overload protection.

In the Eastern and Western Interconnections of North America, the total load is much larger (several hundred GW) but even 1% of this would only amount to slightly more than the double outage of a nuclear unit. To summarize, the results of the Polish power grid reported by Soltan et al. [361] imply that the system being modeled is not N-1 secure. Since this is not an allowable operating condition sunder NERC standards, we believe that a result analogous to that in [361] is not credible for a North American System.

IoT Demand 10% System Demand Increase Attack

Ten percent of system load in our case study is equivalent to 8,227.3 MW, which would be equivalent to an adversary controlling approximately over 8 million air conditioners. Figure 3.15 shows the bus frequency responses after 10% of a load increase attack at $1s$ and Figure 3.16 shows the power flow on branches as a percent of the branch rated capacity.

To better understand the variations of power flow depicted in Figure 3.16, consider Figure 3.15. From Figure 3.15, we can observe that the bus frequencies plummet after the attack begins ($1s$). The only lines that are not affected are the few buses that connect the power grid to another region outside the system with DC tie lines. UFLSs are then activated at second 3.5 and reverse the system frequency decline by shedding 5% of the system load. Again, as long as the bus frequency converges to a stable level, the differences between the converged value and its initial value of 60 Hz can be made up
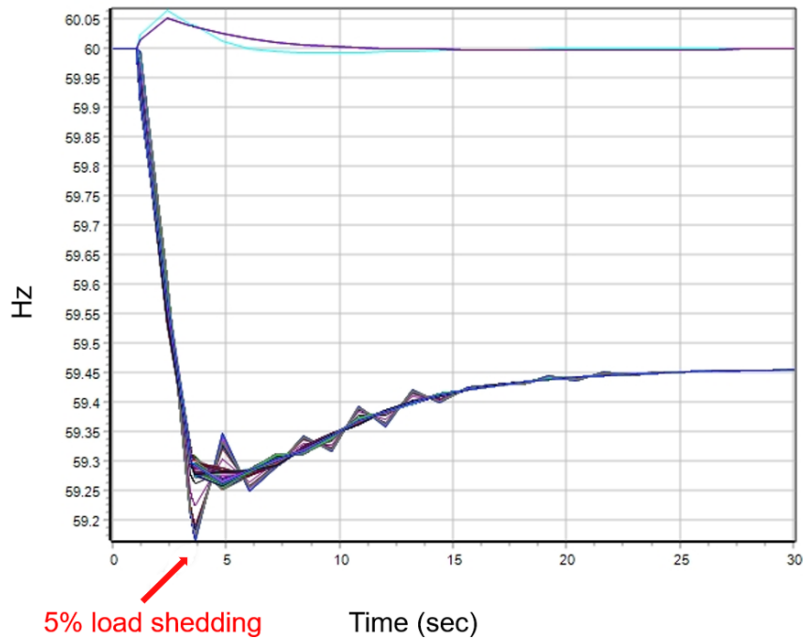
Figure 3.15: Frequency Response to 10% System Load Increase

either automatically or manually over a longer time scale. Although the under frequency shedding has no deliberate time delay as indicated in Table 3.4, a 0.02 second of relay operation time is included in the simulation. Therefore, the load shedding occurs 0.02 second after the time frequency falls below the first UFLS threshold of 59.3 Hz.

In Figure 3.16, we can find the power flows of some branches increase after the attack at second 1. However, the power flows of those branches drop to or gradually decrease to roughly their initial values after the action of under frequency load shedding at 3.5 second. Therefore, at the end of the simulation, there is no additional transmission line overloaded due to the IoT load increase attack. Note that some branches are initially overloaded

71
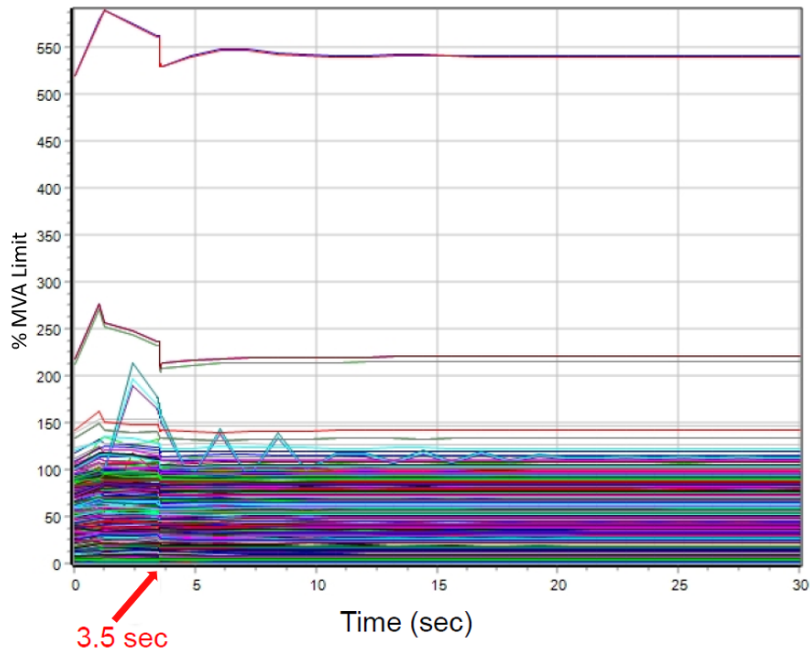
Figure 3.16: Branch Flow after 10% System Load Increase

before the simulation and remain unchanged during the simulation and so ,as previously, the overload outage checker is not activated for those lines.

Thus, even with an assumption of 10% of load compromised and increased by adversaries, our case study doesn't suggest a major threat of cascading failure on transmission lines. The simulation results show that the quick action of under frequency load shedding after the load increase plays a critical role in relieving the negative effects of the attack. The amount of UFLS is intended to reflect ERCOT standards. The Eastern and Western Interconnections may have overall lower levels of UFLS than ERCOT; however, they have much larger levels of inertia than ERCOT. We have not investigated the situation in detail for the Eastern and Western Interconnections.

3.4.2.3   IoT Demand Increase and Decrease Attack

One of the characteristics of an IoT attack is that the attack is highly distributed and it is hard to detect. Once the load is compromised, it is difficult to clear the threats in a short time after the adversaries launch their first attack.

From the study in section 3.4.2.2, under frequency load shedding successfully prevents cascading failures of transmission lines from a single load increase attack. However, under an IoT demand attack, the adversary may be able to reduce the compromised load again after the system under frequency load shedding reverses the frequency decline in order to cause a frequency overshoot that may trigger over frequency relays on the generators and disconnect generators.

Based on the simulation shown in Figure 3.15 and Figure 3.16, we create an experiment of an IoT demand increase and then decrease attack. The bus frequency responses are displayed in Figure 3.17. To make the highest frequency overshoot from the load decrease, we choose to decrease the load at second 20 where the bus frequencies roughly reaches to and stabilizes at the maximum observed from Figure 3.15.

A straightforward approach in this experiment is to increase the load in the first attack and decrease the same amount of load in the second attack. However, we investigate a worse scenario where in the second attack, we decrease by twice the amount of the load increase in the first attack. A
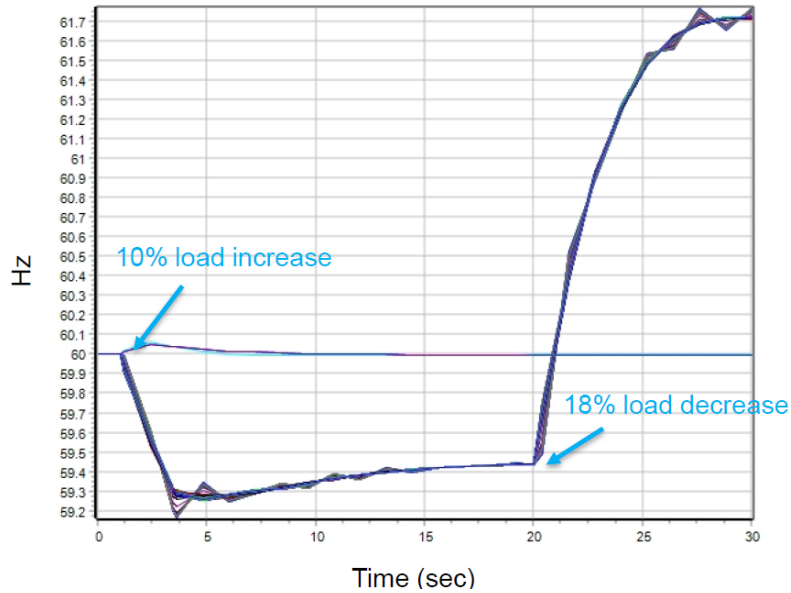
Figure 3.17: Frequency Response to a Cycle of Load Increase and Decrease

scenario for this experiment is the attackers have control of some AC loads, they may decide to run half of the AC loads until peak hour and then suddenly increase to full capacity. The reason attackers might not want to keep the load at zero before increasing to maximum capacity can be interpreted as follows: First, the attacker may pick the peak hour when the system has the least spare generation capacity in a day to launch this attack to stress the system the most with a given amount of compromised load. Second, holding the AC load at zero means keeping the AC off, and this would expose the attackers to discovery. Therefore, holding the compromised load capacity at 50% before increasing them into the maximum during the peak hours is a proxy to something the attackers may want to do to create larger impacts.

The result in Fig. 3.17 shows that the frequency does overshoot af-

74

ter the loads decrease at second 20, however the system frequency tends to stabilize at 61.7 Hz, which happens about 10 seconds later. From Table 3.3, we can observe that 61.7 Hz will not cause an immediate generation trip by the generators' frequency protections. Again, it should be emphasized that these protection parameters are intended to reflect ERCOT. The Eastern and Western Interconnection may perform differently.

As mentioned in Section 3.4.2.2, 10% system load compromised by the adversary is already a significant assumption. We take this even further to 20% of the system load in this simulation to see if the IoT attack can cause a worse result. However, we still do not observe an immediate generation trip after this demand increase and decrease attack in a system that is intended to reflect ERCOT standards for UFLS.

3.4.2.4   Under Frequency Load Shedding in a Repeated IoT Attack

In section 3.4.2.3, we explored the attack of a "cycle" of load increase and decrease. The adversary could repeat the attack cycle of increasing and reducing the compromised load as long as their capabilities are not disabled. The under frequency load shedding would disconnect some amount of demand each time when the IoT attack causes the frequency drop below any thresholds. Once the load is disconnected by Under-Frequency Load Shedding (UFLS) systems, the restoration of shed load is coordinated between the Independent System Operator (ISO), Transmission Service Providers (TSPs) and Distribution Service Providers (DSPs) [123]. As discussed in Section 2.7, such

restoration associated with coordinations between different entities may take 30 minutes to an hour to complete. Therefore, a potential negative effect of such repeated attacks is that it can deplete the under frequency load shedding resources before they are restored, which might eventually lead to a system frequency failure.

However, it may take many cycles of IoT demand increase and decrease attacks to deplete the UFLS resources. Therefore, the efficiency, even the feasibility of the approach of using up the UFLS by such repeated IoT demand attack remains unclear. The result in Fig. 3.15 shows that although the system frequency needs additional measures to be brought back to its initial frequency of 60 Hz, the frequency decline caused by 10% of system load increase can be stopped by only 5% of system load shedding. From Table 3.4, in ERCOT 25% of the system load is contracted with the ISO as UFLS and this level is modeled in this study. Under this condition, the adversary needs to apply the attack at least five times to deplete the UFLS resources. What is more, additional under-frequency relays may be installed on transmission facilities with the approval of the ISO provided the relays are set at 58.0 Hz or below [123]. That means, in reality, the adversary may need to apply the attack even more times to deplete the UFLS and cause a possible system failure.

3.4.2.5   Over/Under Frequency Generator Tripping

In Section 3.4.2.3, we briefly discussed the potential threats of generator disconnections caused by over frequency protections. In this section, we extend

this discussion to IoT attacks that specifically target disturbing frequency and causing generator disconnections by frequency protection. In order to observe the response of frequency protection at generators, we studied the IoT attack of load increase or decrease by 30% as suggested in [361].
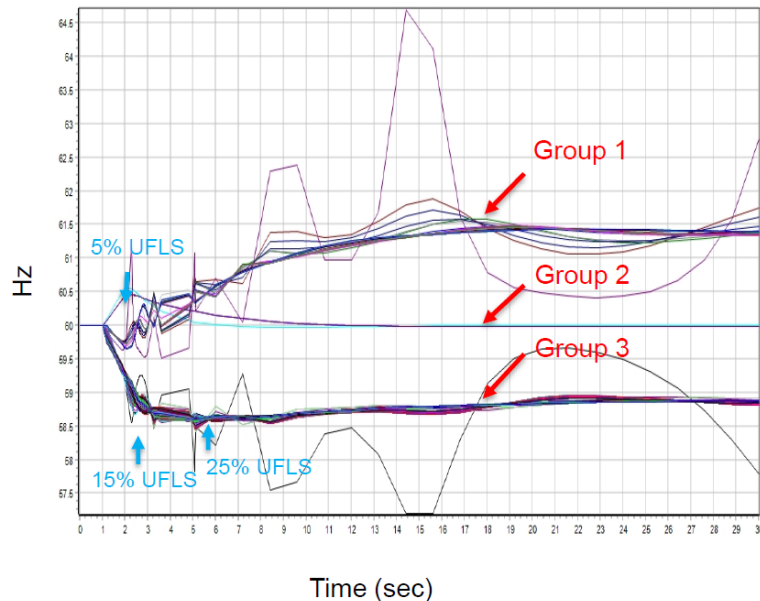
Figure 3.18: Frequency Response to 30% System Load Increase

Fig. 3.18 shows the system frequency response to an IoT attack that increase the system load by 30% at second 1. First, we can observe that due to the sudden load increase, the bus frequencies decline dramatically and some of them drop quickly below the first UFLS threshold of 59.3 Hz. Then 5% of system load are disconnected by UFLS. We notice that the frequency at some buses decline slower at the instant of the attack (potentially with no direct connection of load before the attack) and haven't reached any UFLS thresholds. For convenience, we name this group of buses as Group 1. The

buses with DC tie lines that are less affected as mentioned in section 3.4.2.2 is Group 2. The group of buses such that their frequencies decline faster and drop below UFLS thresholds are named Group 3. The group names are indicated in Fig. 3.18. Notice that, even within a group, the frequency responses are not exactly the same. Because of the first UFLS action, the frequency deviation between buses increases. After 5% of system load shed, the frequency at Group 1 potentially with more generation in the region starts to increase while the frequency at Group 3 with insufficient generation keeps declining.

Shortly afterwards, the frequency at Group 3 declines to be below the second and third UFLS thresholds - 58.9 Hz and 58.3 Hz at around second 2.6 and second 5.6, respectively. An additional 10% of system load is disconnected on each occasion. The frequency deviation between Group 1 and Group 3 gets larger after the two UFLSs. What is more, the frequency deviation between buses in a group, especially in Group 1, increases after the actions of UFLS. After the three UFLSs that disconnect a total 25% of system load, the frequency decline at Group 3 is stopped. Because there is no additional load shedding, the frequency at Group 1 stops increasing as well. Thus, although the bus frequencies haven't converged at the end of the simulation, they stop further diverging and prevent frequency protections disconnecting generators.

Fig. 3.19 shows the system frequency response to an IoT attack that decreases the system load by 30% at second 1. We can find the bus frequencies increase fast after the attack and few of them go above the threshold of immediate over frequency protections at generators - 61.8 Hz within 5 seconds.

78
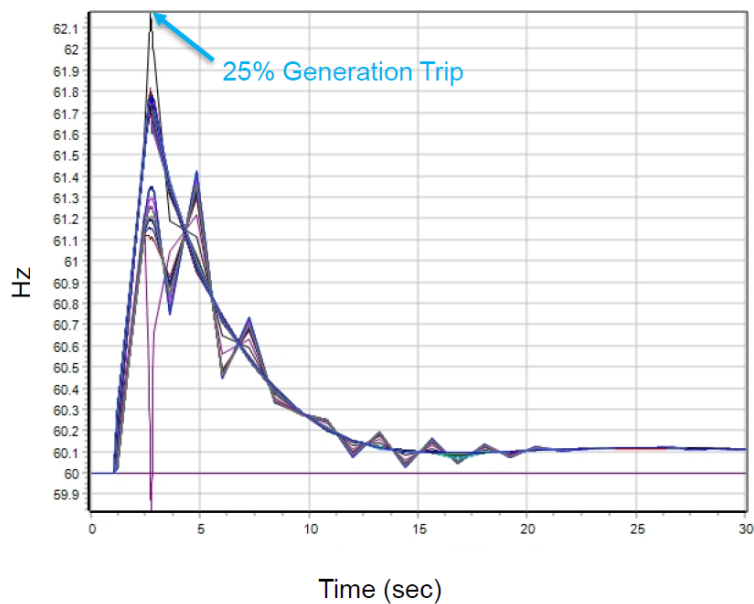
Figure 3.19: Frequency Response to 30% Load Decrease

The over frequency protections then disconnect generators that result in 25% reduction of system generation. After the tripping of generators, the bus frequencies reduce and converge to a value close to 60 Hz and no more protection actions or failures are observed.

Compared to the system frequency response to an IoT attack that increases the system load, we find that the bus frequencies react differently to the IoT attack that decreases the system load. In Fig. 3.19, although the frequencies of some buses increase faster than those in some other buses, the frequencies gradually converge after 25% of the system generation is tripped. One of the conclusions we can draw from this comparison is that a quick protection reaction in big scales like the generation tripping in Fig. 3.19 performs

better than the gradual protection actions like the load shedding in Fig. 3.18 in terms of the system frequency restoration.

We also find that the tripped generations in this simulation consist of a significant amount of wind generation. The benefit of disconnecting the wind generation or any generation that doesn't provide inertia in this condition is that the system loses less inertia after the over frequency protection action. Therefore, the system doesn't become weaker in terms of maintaining frequency stability. This phenomenon suggests that generation that doesn't provide inertia could be included in the over frequency protection to protect the system against any following attacks targeting at disturbing the system frequency after an IoT attack.

3.5   Conclusion and Future Work

By implementing the COA model into a North American regional interconnection system, we demonstrate that this method can be used to assess the effects of different types of cyber attacks.

3.5.1   Conclusion

From the simulation results of cyber attacks target on grid control centers, we find that the number of transmission lines outaged at a given voltage level in the attacked TDSP is critical as a predictor of an algorithmic non-convergence. There exists a threshold at each voltage level such that an algorithmic non-convergence will happen when the attacked TDSP has

more branches tripped than the threshold. We also observe that if the system survived from the contingency, then an attack on a TDSP with more branches at the lower voltage levels would cause more load lost.

From the simulation results of IoT demand attacks, we show that, 1% of load increase attack does not interrupt any generator, load, or transmission line in the system. We also find that, thanks to under frequency load shedding protections, a 10% of sudden IoT load increase does not cause a cascading failure on the transmission lines. In addition, a "frequency swing attack" is defined as a cycle of load increase and decrease IoT attack that aims to push the frequency swing to violate the frequency protection thresholds in the system. However, the frequency swing attack doesn't show an ability to cause an immediate disconnection of generators. A possible repeated frequency swing attack has been discussed. The impacts of depleting the UFLS resources are discussed. The analysis shows the effectiveness of such attack would be impacted by any additional frequency protection measures in the system.

Last but not the least, a single IoT attack targeted at disturbing the system frequency is presented. The simulation results show that, load shedding by UFLS would split the frequencies at buses under a sudden IoT attack increasing 30% of the system demand. The same amount of IoT load decrease attack would cause swift frequency increases and make some bus frequencies pass the thresholds of the over frequency protections that result in generator disconnections. The simulation shows the actions of UFLS and over frequency protection are sufficient to prevent an immediate system failure over a short

time after the attack. Additional actions may be needed over a longer time scale to restore the stable operation of the system, but the main point is that a system blackout will likely not occur in this situation. In addition, we discover that including generations that are not providing inertia in the over-frequency protections would benefit the system in case of following IoT attacks targeting at disturbing the system frequency.

3.5.2 Future Work

The results from simulation with rotor angle checker cannot be validated since the data is generic and not specific to the real system generators. However, for the cyber attacks targets on grid control center, we expect that with accurate transient data, the intensity (number or amount) of algorithmic non-convergence cases and load lost may be changed, but the general observation, for example, that tripping equal amount of generations and loads would not cause an algorithmic non-convergence, may still be valid. Therefore, results qualitatively similar to the outcomes in this study are expected if accurate transient data were available. We hope to be able to utilize more accurate transient data in the future.

The model developed to simulate the IoT demand attack is not perfect. As discussed in 3.2 and above, there are certain limitations in the studies. Particularly, the results from transient simulations can be more precise if a detailed transient data for a large system becomes available. We believe the type of protections considered in this study is the subset of the protections

in power systems that would contribute to a cascading outage the most after a disturbance in the system. However, future work can be done to explore the impacts from other protections that are commonly equipped in the power systems e.g. different protections on buses [149]. In addition, in this study, we considered only an IoT demand attack that is evenly distributed across all the load points in the system. However, in the future work, we will consider IoT demand attacks targeting only a part of the system.

Chapter 4

Power System Interdiction Problem

4.1 Introduction

In this chapter, an interaction problem between a defender (e.g. system operator) and an attacker (e.g. terrorist) in a power system is presented. The electric system is designed to satisfy the N-1 security criterion, which means the system could lose any one of its N components (such as generators, transmission lines) and continue operating within emergency limits. However, when multiple, simultaneous contingencies occur, the system might experience various stability problems, which might lead to the large cascading events described in Chapter 2. Outages are typically caused by storms or other extreme weather conditions but could also be carried out deliberately by knowledgeable attackers with little risk of detection. The cyber attacks on power systems studied in chapter 3 are good examples. Further well-planned and coordinated attacks by terrorists could leave the electric power system in a large region of the country at least partially disabled for a very long time [95].

In [338], an interdiction problem is formulated as a bi-level mixed-integer programming problem. A decomposed heuristic algorithm was developed. The algorithm starts with the defender solving a DC-OPF problem

84

(with no attack), the "sub-problem." The result is an optimal power flow and generation dispatch that minimize generation costs without any load shedding. A "value" is assigned to each interdictable asset based on, for example, the power flow on it. Based on the result of the "sub-problem," the attacker solves a "master problem" to identify an interdiction plan that maximizes the estimated value of interdicted assets while not exceeding available interdiction resources. With this plan, the constraints of the DC-OPF problem are modified and the new "sub-problem" is solved. Given the interdictions, the result of the DC-OPF problem minimizes generation costs and the penalty associated with load shedding. Typically, some load will be shed in the new solution since valuable assets have been removed from the grid. The process continues by finding alternative interdiction plans and by evaluating load shedding and system operation cost for each of them. The heuristic algorithm has the drawback that it can require many iterations to obtain a close-to-optimal solution.

Salmeron et al. [339] introduced Global Benders Decomposition (GLBD) to solve the same problem described in [338] and observed convergence toward the optimal solution even with a non-linear sub-problem. Like Benders Decomposition(BD) [39], the algorithm does build a concave piecewise-linear approximating function to the function being maximized. Unlike BD, However, the function being approximated need not be concave. The key advantage of GLBD over a single level MILP formulation is that the algorithm's subproblems represent simple, familiar instances of the primal linear program OPF. Thus, the user need not maintain a problem that involves unfamiliar con-

structs from the dual of the OPF model that are complicated by interactions with binary variables as in Mixed-Integer LP procedure in [276] and as in the KKT method to solve the subproblem described in [428].

The Cascading Outage Analysis (COA) model analyzes both transient and steady state system responses to contingencies. These are "short-term" effects of an attack, but may have various implications. Therefore, to better represent the system responses to an attack, the COA model is incorporated as a sub-problem in the interdiction framework in [398] in addition to DC-OPF used in [338] and [339]. Because of the non-linearity brought by COA model, the problem in [398] is solved through a heuristic method that is similar to the algorithm in [338].

In this chapter, the efficiency of the application of the GLBD method on the bi-level system interdiction problem with DC-OPF as the sub-problem is first presented. Then work will be proposed to use the same method to solve the problem with COA model incorporated in the sub-problem. The test systems are built on a PowerWorld 7 bus OPF case and a PowerWorld 37 bus system with transient stability model and generic costs for OPF.

4.2   Problem Formulation

The problem is first formulated as a bi-level model to maximize the load shedding and medium-term system operational costs as in [339]. The DC Optimal Power Flow (DC-OPF) problem is included as a "sub-problem." The DC-OPF problem is a linear optimization problem run by the system operator

to economically dispatch the system generations. The objective of DC-OPF is to minimize the total system generation costs. The cost of any unserved load is also included as a penalty in the DC-OPF problem. Based on the DC-OPF solution, the integer interdiction problem is formulated as the "master problem." The objective of the master problem is to maximize the minimum objective value of the sub-problem over choices of interdiction plan.

4.2.1 Sub-problem

Indices:

$i \in I$ set of buses;

$g \in G$ set of generating units connected to bus i;

$l \in L$ set of transmission lines;

$o(l)$ origin bus of line l;

$d(l)$ destination bus of line l.

Data [units]:

H_g generation cost of unit g [\$/MWh];

Q_i load shedding cost at bus i [\$/MWh];

$\bar{P}_g^G$ maximum output from generating unit g [MW];

$\bar{P}_l^L$ transmission capacity for line l [MW];

B_l series susceptance of line l [ohm^{-1}];

D_l load at bus i [MW];

δ_l^L attack on transmission line l provided by the master problem;

δ_g^G attack on generator g provided by the master problem;

δ_l^L attack on transmission line l provided by the master problem;

δ_i^I attack on bus i provided by the master problem;

Variables [units]:

θ_i phase angle at bus i [radians];

p_l^L power flow on line l [MW];

p_g^G generation from unit g [MW];

s_i load shed at bus i [MW];

Formulation: $OPF(L, G, I; D)$.

$$\min_{p^G, p^L, s, \theta} \sum_{g \in G} H_g p_g^G + \sum_{i \in I} Q_i s_i. \tag{OPF.1}$$

$$p_l^L = B_l(\theta_{o(l)} - \theta_{d(l)}), \quad \forall l \in L. \tag{OPF.2}$$

$$\sum_{g \in G_i} p_g^G - \sum_{l \in L | o(l) = i} p_l^L + \sum_{l \in L | d(l) = i} p_l^L = D_i - s_i, \ \forall i \in I. \tag{OPF.3}$$

$$-\bar{P}_l^L(1 - \delta_l^L)(1 - \delta_{o(l)}^I)(1 - \delta_{d(l)}^I) \le p_l^L \le \bar{P}_l^L(1 - \delta_l^L)(1 - \delta_{o(l)}^I)(1 - \delta_{d(l)}^I), \quad \forall l \in L. \tag{OPF.4}$$

$$0 \leq p_g^G \leq \bar{P}_g^G (1 - \delta_g^G)(1 - \delta_i^I), \quad \forall g \in G. \tag{OPF.5}$$

$$0 \leq s_i \leq D_i, \quad \forall i \in I. \tag{OPF.6}$$

$$\theta_{|I|} = 0. \tag{OPF.7}$$

The objective function (OPF.1) minimizes generation costs and load-shedding costs in \$/h. Constraints (OPF.2) are linearized admittance constraints that approximate active power flows on AC lines. Constraints (OPF.3) maintain power-balance at the buses. Constraints (OPF.4) and constraints (OPF.5) set maximum power flows for lines and maximum generating-unit outputs, respectively. Constraints (OPF.4) represents that when line l or the bus at either end of line l is attacked given by the master problem ($\delta_l^L = 1$, $\delta_{o(l)}^I = 1$ or $\delta_{d(l)}^I = 1$), power flow on line l (p_l^L) has to be zero. The same for constraints (OPF.5), it forces the power output of a generator g to be zero when the generator is attacked or the bus the generator connected to is attacked. Constraints (OPF.6) ensure that load-shedding does not exceed demand. Equation (OPF.7) sets the phase angle at the reference bus to 0.

4.2.2 Master Problem

Formulation : IPF.

$$\max_{\delta^K \in \triangle} \min_{p \in \mathcal{P}(\delta^K; D)} \bar{f}(p). \tag{IPF.1}$$

89

$$\delta^K \in \triangle \subseteq \{0,1\}^{|K|}. \tag{IPF.2}$$

$$K = I \cup L \cup G. \tag{IPF.3}$$

In (IPF.1) $\min_{p \in \mathcal{P}(\delta^K; D)} \bar{f}(p)$ denotes OPF in shorthand, with the vector p incorporating all decision variables in the sub-problem, with $\mathcal{P}(\delta^K; D)$ representing (OPF.2)-(OPF.7), and with $\bar{f}(.)$ representing (OPF.1). Constraint (IPF.2) represents resource-limited, binary interdiction plans defined on generic components $k \in K$, and $p \in \mathcal{P}(\delta^K; D)$ represents feasible operation of the power grid with demand vector D and with operating components that are dictated by δ^K. More precisely, for $\delta_k^K \in \triangle$, $\delta_k^K = 1$ if component k (i.e. a line, a bus or a generator) is attacked and disabled, and $\delta_k^K = 0$, otherwise.

4.3 Methods and Algorithms to Solve the Problem

4.3.1 Mixed-Integer-Programming

The difficulty of formulating this problem as a standard mixed-integer program (MIP) comes from the non-convex, max-min nature of the problem [341]. If we combine two problems into a standard MIP, then the original sets L, I and G in the sub-problem are modified to $L(\delta^L)$, $I(\delta^I)$ and $G(\delta^G)$ respectively. Therefore, in constraints (OPF.4) and (OPF.5), $\delta_k^K \ \forall k \in K$ are no longer given data but decision variables.

Therefore, these non-linear terms make MIP even harder to solve. Previous researches have tried to solve the MIP by linearizing those terms. However, empirical results suggest that it is not an efficient way to solve the problem. For a 48-bus scenario, the method takes up to three minutes to solve on a personal computer [341].

4.3.2 Bi-level Optimization and Heuristic Method

The optimal solution of the bi-level problem can be reached through a heuristic method by solving series of sub-problems and master problems. The master-problem introduced in section 4.2.2 is reformulated to [339]:

Formulation : $IPF(K; \bar{M})$.

Data [units]:

α_k^n index or value of each element k at iteration n [MW];

$\bar{M}$ limit of attacks on elements [NA];

Variable:

δ_k^K binary interdiction decision variables on element k.

$$\max_{\delta^K} \sum_{k \in K} \alpha_k^n \delta_k^K. \tag{IPF.1'}$$

$$s.t. : \sum_{k \in K} \delta_k^K \leq \bar{M}. \tag{IPF.2'}$$

$$\delta^K \in \{0,1\}^{|K|}. \tag{IPF.3'}$$

The index vector α_k^n is calculated based on the operation solution from sub-problem as coefficients of elements in the system. The calculation of coefficients aims to capture the attackers' "interest" in each element or the "importance" of each element. For example, the coefficients for transmission lines can be the power flow on the lines. Then, the objective function (IPF.1') maximize the "importance" of selected elements. Constraint (IPF.2') indicates the maximum number of elements can be attacked due to the resource limits.

The heuristic method is straightforward. Starting with $\delta^K = 0$, the product terms introduced in section 4.3.1 become constants. Then, the sub-problem described in section 4.2.1 will provide a feasible operation solution $p \in \mathcal{P}(\delta^K; D)$. Using p, a index vector α_k^n is calculated. The master problem (IPF.1') is solved and provides a new interdiction plan. These attacked elements are disconnected in the system topology and the sub-problem is solved under the new attacking plan. The system cost (including cost of load shedding) gained at each iteration is recorded. The heuristic procedure continues for a fixed number of iterations or until a time limit is reached. Then the interdiction plan associated with the maximum system cost is the optimal solution of the problem. The heuristic procedure can handle large-scale models because both the DC-OPF sub-problem and MIP master problem can be solved quickly, even at large scale.

One thing we need to handle in the heuristic method is that we need to prevent the master problem from repeating the same interdiction solutions that appeared in any previous iteration in order to speed up the convergence.

Therefore, logical constraints are added:

$$\sum_{k \in K | \hat{\delta}_k^K = 1} \delta_k^K + \sum_{k \in K | \hat{\delta}_k^K = 0} (1 - \delta_k^K) \leq |K| - 1. \qquad \text{(IPF.4')}$$

where $\hat{\delta}_k^K$ is any interdiction solution that has already been evaluated. This constraint forces any new solution δ^K to differ from $\hat{\delta}^K$ in at least one component; such a "super-valid inequality" [194] guarantees not to eliminate any optimal solution unless the incumbent solution is already optimal.

4.3.3   Global Benders Decomposition

The heuristic procedures need to go through all solutions to guarantee convergence. It normally takes a very large number of iterations to reach the optimal in a big system. Reference [260] proposed a new method called Global Benders Decomposition (GLBD). The algorithm alternates between an integer-programming master problem and one or more linear-programming sub-problems. Like Benders Decomposition and Generalized Benders Decomposition [9], the GLBD does build a concave, piecewise-linear approximating function to the function being maximized [260]. The decomposition relies on a sequence of upper-bounding piecewise-linear functions for the interdictor's objective. The maximum of those functions must converge to the optimal solution of the master problem IPF since only a finite number of interdiction plans exist; however, practical use of the decomposition is more interested in finding verifiable close-to-optimal solutions quickly.

GLBD Algorithm

Initialization : $\epsilon \geq 0$ optimality tolerance;

$\hat{\delta}^K = 0$ initial interdiction plan;

$\hat{\triangle} \leftarrow \{\hat{\delta}^K\}$ initial subset of feasible interdiction plans;

$\hat{\delta}^{K*} \leftarrow \hat{\delta}^K$ current best plan for the interdictor;

$z^* \leftarrow 0$ lower bound on cost of the best plan;

$\bar{z} \leftarrow \infty$ upper bound on cost of the best plan;

Sub − problem :

Solve the problem with current iteration plan $\hat{\delta}^K$, $OPF(\hat{\delta}^K)$, receive solution $p(\hat{\delta}^K)$ and objective value $f(\hat{\delta}^K)$.

If $f(\hat{\delta}^K) \geq z^*$, then $z^* \leftarrow f(\hat{\delta}^K)$ and $\hat{\delta}^{K*} \leftarrow \hat{\delta}^K$;

If $\bar{z} - z^* \leq \epsilon z^*$, then report $(\hat{\delta}^{K*}, z^*)$ as the ϵ-optimal solution and halt;

Otherwise $\hat{\triangle} \leftarrow \hat{\triangle} \cup \{\hat{\delta}^K\}$ and go to Master Problem;

Master Problem :

Add following generalized Benders cuts and formulate $MP(\hat{\triangle})$ as:

$$MP(\hat{\triangle}) : z(\hat{\triangle}) = \max_{\delta^K \in \triangle, z} z. \tag{MP.1}$$

$$S.t. \ z \leq f(\hat{\delta}^K) + \sum_{k \in K} \alpha_k(\hat{\delta}^K)(\delta_k^K - \hat{\delta}_k^K), \ \forall \hat{\delta}^K \in \hat{\triangle}. \tag{MP.2}$$

Solve $MP(\hat{\triangle})$ for new interdiction plan $\hat{\delta}^K$ and for objective value $z(\hat{\triangle})$, and set $\bar{z} \leftarrow z(\hat{\triangle})$;

If $\bar{z} - z^* \leq \epsilon z^*$, then report $(\hat{\delta}^{K*}, z^*)$ as the ϵ-optimal solution and halt;

Otherwise, return to Sub-problem step.

4.3.4 Short-term Effects and Cascading Outage Analysis

While the DC-OPF problem used in the interdiction models represents the economical operation (medium-term) of the power system and maximizes the amount of load that can be served, it is a steady-state optimization framework that does not consider short-term cascading outage effects. "Short-term" means the time window of seconds to minutes while "medium-term" indicates minutes to hours or even days.

Many large blackouts are caused by a consecutive series of various outages following an initial disturbance as described in Chapter 2. Therefore, the amount of short-term load shed should be calculated to evaluate the short-term impacts of an attack. The details of the COA model is shown in Chapter 2. Then, the DC-OPF model can be replaced by the COA model as the sub-problem in the GLBD method to consider the short term effects of an attack in the interdiction problem. In the GLBD algorithm, the COA model will take the current interdiction plan $\hat{\delta}^K$ and give system operation solutions under the attack $p(\hat{\delta}^K)$ and system operating cost $f(\hat{\delta}^K)_{COA}$ at each iteration. After the COA model is implemented, as expected, the load shedding due to an attack is more intense than the medium term effects. In a 37 bus test system with

total of 57 transmission lines, tripping 10 of them would easily cause half of the total load to be shed in the short term. However, it should be recognized that in the medium term, some of this load can be restored since only some of the lines may have been damaged. The medium term model can be interpreted as evaluating how much of the load can be restored after any initial cascade.

In the GLBD algorithm, a valid Bender's cut (IPF.4') at each iteration in the Master Problem is easier to determine when the sub-problem is a convex problem such as the DC-OPF problem. Because the cost of load lost is usually larger than the system operation cost, we can use this information to generate a usually valid upper bound for the master problem for an attack on a transmission line. However, this is not always true with the COA model. The line outages in the transient simulation would cause variations on both system frequency and generator rotor angles. It is possible that the cascading outages after the initial line outages cause more load shedding than the power flow on the tripped lines.

Although the Bender's cuts generated by COA may not be valid due to the cascading effects, it is still plausible to find a close to optimal solution for the interdiction problem. From our previous study of cyber attacks in the power systems, we discovered some approximate linear correlations between the total disrupted power flows in an attack and the load lost post the attack under the simulation with COA model. For example, this is shown in Fig. 3.6. A similar correlation is observed from the simulation results of attacks on 69 kV transmission lines in the 37 Bus system as shown Fig. 4.1. Given the
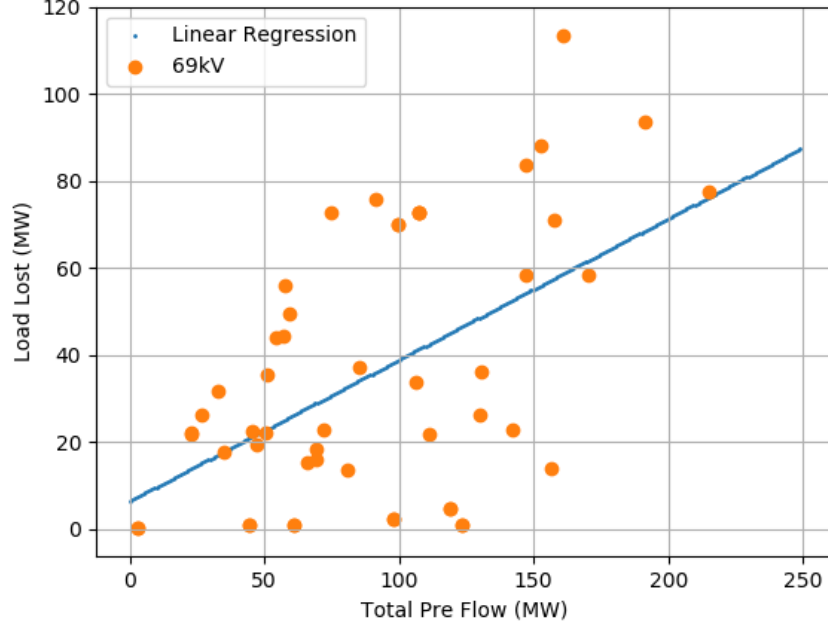
Figure 4.1: Load Lost of Attacks on 69kV Lines.

power flow of attacked transmission lines, we can approximate the load lost using the experimental linear regression results that can be generated before the GLBD algorithm starts. Then, the "importance" index for each attack can be calculated as $\alpha_k(\hat{\delta}^K)_{COA}$. With the system operating cost updated from the COA simulation $f(\hat{\delta}^K)_{COA}$, the benders cut generated at each iteration in a master problem is shown in (MP.2') and the structure of the GLBD algorithm remains unchanged.

$$z \leq f(\hat{\delta}^K)_{COA} + \sum_{k \in K} \alpha_k(\hat{\delta}^K)_{COA}(\delta_k^K - \hat{\delta}_k^K), \ \forall \hat{\delta}^K \in \hat{\triangle}. \qquad \text{(MP.2')}$$

4.4   Numerical Results

In this section, we first show the results of a case study of interdiction problem considering only the medium-term effects with the optimal power flow problem (OPF) as the sub-problem.

4.4.1   Medium-term Effects

To generate an illustrative example, we limit the attack to only transmission lines. The Medium-term effects of attacks on transmission lines of a 7 bus test system are evaluated. The Heuristic method is implemented first and then the Global Benders Decomposition (GLBD) is applied. The results show the effectiveness of GLBD on finding the optimal or close to optimal interdiction plans on transmission lines.

Table 4.1: Results of Transmission Line Attacks on a 7 Buses System

Attack Limit	GLBD		Heuristic	
$\bar{M}$	Iteration	Cost	Iteration	Cost
2	12	17,597	45	17,930
3	42	20,134	120	20,919
4	46	21,073	210	21,073

Table 4.1 shows the performance details of both methods. $\bar{M}$ denotes the limit on the number of lines can be attacked. There are total 10 lines in the test system. Given the attack limit, the number of iterations in Heuristic is the number of possible attack combinations. Therefore, the optimal objective value provided by the Heuristic is chosen to be the global optimal value in the

98

problem. Given $\epsilon = 0.8$, it can be observed that the ϵ-optimal solution from GLBD are close to or even equal to the global optimal solution from Heuristic methods. However, the number of iterations in GLBD is much less than for the Heuristics method.

Table 4.2: Contrast Between GLBD and Heuristics

Attack Limit	Iteration Increase	Obj Improvement
$\bar{M}$=2	375 %	1.9 %
$\bar{M}$=3	286 %	3.8 %
$\bar{M}$=4	456 %	0.0 %

Using the results from Table 4.1, the number of iterations and the objectives are further compared in Table 4.2. Results in Table 4.2 indicate that applying GLBD to the problem will save two to four times of iterations by sacrificing only less than 4% on the optimal objective values. It should be understood that, for practical problems, the computational time for checking all combinations with the heuristic is impractical.

4.4.2 Short-term Effects

Then, we show the results of a case study of interdiction problem considering short-term effects with the cascading outage analysis (COA) as the sub-problem. The correlations between the power flow on transmission lines and load shedding shown in Fig. 4.1 are included in the global benders decomposition (GLBD) method to generate benders cut at each iteration as described in Section 4.3.4.

The short-term effects of attacks on 69 kV transmission lines are studied in a 37 bus system. To test the intuition of GLBD method in an interdiction problem with COA, we limit the size of the attacks to two and three.

The Heuristic method is applied to be a benchmark. The results show the effectiveness of GLBD on finding the optimal or a close to optimal interdiction plan.

Table 4.3: Results of Transmission Line Attacks on a 37 Buses System

Attack Limit	GLBD		Heuristic	
$\bar{M}$	Iteration	Cost	Iteration	Cost
2	26	3,877	378	3,877
3	329	3,914	3276	3,914

Table 4.3 shows the performance details of both methods. $\bar{M}$ denotes the limit on the number of 69 kV transmission lines can be attacked. There are total 28 of 69 kV transmission lines in the test system. Given the attack limit, the number of iterations in Heuristic is the number of possible attack combinations. Therefore, the optimal objective value received in Heuristic is the global optimal value in the problem. Given $\epsilon = 2$, it can be observed that the ϵ-optimal solution from GLBD are equal to the global optimal solution from Heuristic methods. However, the number of iterations in GLBD is much less than the Heuristics method.

The number of iterations and the objectives are further compared in Table 4.4. Results in Table 4.4 indicate the proposed method in the interdic-

Table 4.4: Contrast Between GLBD and Heuristics

Attack Limit	Iteration Increase	Obj Improvement
$\bar{M}=2$	14.53	0 %
$\bar{M}=3$	9	0 %

tion problem considering short-term effects can save more than ten times of iterations.

4.4.3 Discussion of Computation Effects

To the best of our knowledge, there is no general theory about the size of system effects on the computations for Benders' Decomposition or Global Benders' Decomposition method. However, Benders' Decomposition has been applied in a wide range of problems in the literature and the efficiency of Benders' Decomposition has been demonstrated.

In the interdiction problem discussed in this chapter, the majority computation efforts of the proposed method are from the sub-problem which is the simulation of cascading outage analysis (COA) which involved with the solver, PowerWorld, solving differential equations for the system dynamic in the studied time window. However, the size of the sub-problem remains unchanged in each iteration. Compare to the sub-problem, the master problem can be solved much faster. The master problem starts with only few constraints as described in Section 4.3.3. The number of constraints in the master problem grows along with iterations due to one benders cut is added each time. However, we expect the algorithm converge before it reaches too many iterations. Therefore, we

are expecting a close to linear growth on computational efforts with number of iterations. For a small system shown in Section 4.4.2 , in Table 4.3, the computation time when $\bar{M} = 2$ with GLBD is 520 seconds and 8844 seconds with Heuristic.

4.5   Summary

In this chapter, the Global Benders Decomposition method is discussed and implemented. First, the efficiency of the GLBD method in solving the bi-level system interdiction problem with DC-OPF sub-problem is confirmed and presented with a 7 bus illustrative system.

The work is extended to include the COA model to consider the short-term impacts of attacks. The GLBD algorithm with the COA model as the sub-problem is implemented in a 37 bus test system. Because of the cascading effects, it is difficult to find valid Bender's cuts. However, with a good "importance" measurement for elements in the master problem, it is still feasible to find a close to optimal solution. From our previous study on the cyber attacks in the power systems, we discovered some approximate linear correlations between the total disrupted power flows in an attack and the load lost post attack under the simulation with COA model. A similar correlation is observed in the 37 Bus system. This correlation is used for generating Bender's cuts in the GLBD algorithm. Case studies and tests in the 37 Bus system shown the efficiency of the proposed method and the computational effects of the proposed method is discussed. Case studies on a large system is ongoing.

Part II

Power System Unit Commitment Problem

Chapter 5

Combined Cycle Unit Formulation

5.1 Introduction

In the first part of this dissertation, we introduced cascading outage analysis and cyber attacks on power systems in Chapter 2 and Chapter 3. The model and knowledge learned in the two chapters are applied in a power system interdiction problem as described and discussed in Chapter 4. The interdiction problem is formulated as a mixed-integer programming (MIP) in Chapter 4.

In the second part of this dissertation, we focus on another typical mixed-integer programming problem in power systems – the unit commitment problem. The unit commitment (UC) problem in a power system determines the start-up and shut down schedules of generating units to meet forecast demand in a short term future (few hours to few days). The objective of a UC problem is to minimize the total generation costs; that, is to maximize the social welfare assuming demand is fixed in each time interval. Unit commitment decisions (binary variables) and unit dispatch levels (continuous variables) are determined for each future time interval considered. A large set of operational constraints also has to be met in the problem. Therefore, the UC problem

is a complex optimization problem that can be formulated as a mixed-integer programming problem.

There are new features in electricity markets that may involve formulation modifications and potentially add computational complexity to the UC problem. One such new feature is the participation of combined cycle gas power plants. A combined cycle power plant has a combination of gas and steam turbine units. The exhaust heat from a gas turbine is utilized in a steam turbine to generate more electricity. Combined cycle units (CCUs) have higher efficiency, lower CO_2 emission, better flexibility, and faster response than many other more traditional thermal generators. Therefore, there is an increasing trend of installing combined cycle units [201], [52].

Consequently, optimization models have been proposed to determine the configuration and operation of CCUs in the electricity market. However, there are assumptions made in existing models that are often violated in practice. In this chapter, we will first address a one interval transition assumption made in the existing models. A mixed-integer programming formulation that represents the transition ramping of CCUs and removes the invalid assumptions of one interval transitions is proposed in [181]. A set of configuration-wise ramping constraints are formulated with the transition ramping model. Numerical studies are performed on a MISO system. The work in this chapter builds on the work in [181].

5.2 Background and Motivation

CCUs have many advantages compared to traditional thermal units including shorter installation time, lower levelized cost of electricity, faster response time, less CO_2 emissions, as well as higher operation efficiency and reliability [201] and [238]. In addition, because of the new horizontal drilling and hydraulic fracturing techniques, huge shale gas reserves have been discovered in the U.S. and natural gas has become available with a price comparable to that of coal [98]. Therefore, CCUs have made up the majority of the new generation capacities in the last decade, and an even higher share of CCUs is expected in the near future [300].

The operation of a CCUs is different compared to a traditional thermal unit. There is at least one combustion turbine (CT) and one steam turbine (ST) in a CCU. The exhaust gas from CTs can be used by a heat recovery steam generator to produce steam and drive STs to achieve an overall higher efficiency in the plant compared to a pure combustion gas plant. A CCU can work on different configurations incurring various on/off status combinations of CTs and STs, which have different physical and economic features, e.g., ramp rates, operation cost, feasible transitions between configurations, etc. These complicated operation characteristics in CCUs lead to major challenges to the market modeling and clearing processes. Currently, six CCUs models exist in academic research and industry practice, namely aggregate model, pseudo unit model, component-based model, configuration-based model, edge-based model and configuration-component hybrid model. In [98], Dai et al. provide

a summary of the first five models and discuss the configuration-component based model in detail.

For example, in a configuration based CCU model, each specific combination of turbines in a CCU is a *configuration* and the CCU is committed to operate in exactly one of these configurations in any given time interval. Certain rules have to be followed in the operations due to the physical limits. For instance, a ST has to be dependent on at least one CT and cannot be operated independently. Fig. 5.1 shows an example of feasible configurations and transitions between different configurations for a CCU with one CT and one ST, known as a 1-on-1 CCU. Also, at any given time only one configuration in a CCU can be committed, where we recognize that the "alloff" configuration corresponds to the CCU being out of service.
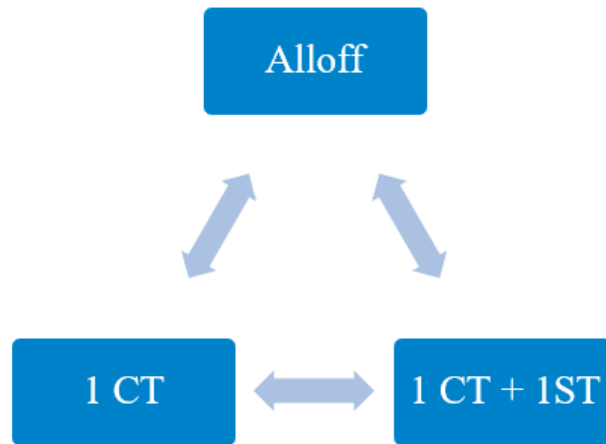
Figure 5.1: Configurations and feasible transitions of a 1-on-1 CCU.

With high shares of variable renewable energy sources and increasing

supply variability, thermal power plants have seen more frequent start-ups and shut-downs [344]. In particular, many combined cycle units (CCUs) have been operated to provide flexibility to the power systems. In the past, CCUs might run for lengthy periods of time and serve as base load generation. However, they now increasingly are being required to respond quickly to variations caused by intermittent supply and demand. The fast output response from a CCU would result in more frequent transitions between configurations in the CCU.

Therefore, it becomes more important to solve the UC problem and optimize the social welfare considering the operation of CCUs with different configurations. Some system operators have already implemented the optimization of CCU configurations in day-ahead unit commitment. In addition, optimizing their configurations in real time (e.g., through "look-ahead" commitment) can pre-position CCUs to cope with the variability in the system.

However, most existing CCU models assume that the transition between any configurations can be completed within one time interval. This assumption is invalid. First, some transitions, especially the transition that involves starting a new turbine, that can take several hours. It is invalid to assume transitions occur within one interval in look-ahead commitment and dispatch models where the length of the time interval is fifteen minutes or even as short as five minutes. To accurately model the transitions, a mixed-integer programming model for the transition ramping processes in a CCU is proposed in [181].

5.3 Contribution

Our contributions to the CCU transition ramping model compared to the formulation in [181] are:

1. A set of configuration-wise ramping constraints are formulated and compared to the plant-wise ramping constraints in [181].

2. The CCU transition ramping formulation [181] along with different ramping constraints is implemented in a MISO prototype UC model.

3. Numerical tests on a MISO system is presented. The results show that there is a moderate increase in computational complexity when transition ramping modeling.

4. Computational impacts of different ramping constraints in the transition ramping model is discussed and presented in the case study.

5.4 Literature Review

The literature review of existing modeling approaches for combined cycle units and the discussion of the issues with the existing models for CCU transitions are presented in [181, Section 5.2], thereby is summarized here.

Currently, many ISOs in the US (e.g., MISO, PJM, and ISO-NE) use an aggregated modeling approach for CCUs in their UC model [128]. The aggregated approach assumes that at each time interval each CCU may either be on or off, which is only a rough approximation for CCUs that have multiple configurations. Besides the aggregated approach, there are mainly two types

of modeling approaches of CCUs in the unit commitment problem. The first approach is the component-based (or physical-unit-based) modeling [86]: each of the physical units of a CCU is represented by a set of commitment and dispatch variables. This approach has been recognized as more suitable for security analysis than for market-clearing [189], in part because many technical parameters would have to be submitted to the ISO had this approach been adopted. Another approach is the configuration-based modeling in which each configuration of a CCU is represented by a set of commitment and dispatch variables [69, 230]. This approach is viewed as suitable for market clearing and bid/offer processing [11, 189], and is adopted by CAISO and ERCOT [272]. However, as pointed out by [128], the standard configuration-based approach cannot describe the minimum up/down time constraints of each individual CT and ST in a CCU. To this end, an edge-based formulation is proposed in [128] and [129] in which the minimum run time constraints of each individual turbine are captured, at the cost of introducing more variables into the formulation. In addition, a new configuration-based model is proposed in [98] where the minimum run time constraints of individual turbines are formulated in the configuration-based variables via projection.

Most of the existing CCU models make a hidden assumption that all transitions are completed within a single interval. As a result, the CCU is modeled as dispatchable during any interval. This assumption may lead to a discrepancy between the model and the reality, as well as suboptimal commitment and dispatch decisions.

110

A CCU's electrical output is reasonably predictable during the non-dispatchable startup and transition process [13]. Therefore, the transition ramping can be modeled as a fixed power trajectory. The start-up and shut-down trajectories of simple-cycle units have been studied in [271]. A mixed-integer programming model for CCUs where the invalid assumption is removed and the power output of CCUs in transition is modeled as a fixed trajectory is proposed in [181].

5.5 Mathematical Formulation of Transition Ramping Model

In this section, we first introduce a standard configuration-based formulation for CCU that has appeared in previous literature and which assumes the completion of any transition within a single interval. Next, a transition ramping model is built upon the standard formulation [181] and the aforementioned assumption is removed. For brevity, we only show the constraints that define the feasible region of a single CCU. Embedding these equations into a complete MIP formulation of unit commitment problem is straightforward.

5.5.1 Standard Configuration-Based Formulation

We show a standard configuration-based formulation from [272]. Let y index the set of configurations $\mathcal{Y}$. Let $t \in \{1, \ldots, T\}$ index the time intervals.

Decision Variables In configuration-based modeling, each configuration has a set of binary variables x, and each feasible transition has a set of binary variables v. The decision variables are:

x_t^y Binary variable for whether configuration $y \in \mathcal{Y}$ is *on* at t;

$v_t^{y,y'}$ Binary variable for transition between $y \in \mathcal{Y}$ and $y' \in \mathcal{Y}$ from $t-1$ to t;

p_t^y Continuous variable for power output from configuration $y \in \mathcal{Y}$ at t;

p_t Continuous variable for power output of the CCU at t.

Constraints

- Bounds on the power output of each configuration:

$$\underline{p}^y x_t^y \leq p_t^y \leq \overline{p}^y x_t^y, \ \forall t, \forall y \in \mathcal{Y}, \tag{5.1}$$

  where $\underline{p}^y$ and $\overline{p}^y$ are, respectively, the lower and upper bound of power output from configuration y.

- Total power output of the CCU:

$$p_t = \sum_{y \in \mathcal{Y}} p_t^y, \ \forall t. \tag{5.2}$$

- Configurations are mutually exclusive:

$$\sum_{y \in \mathcal{Y}} x_t^y = 1, \ \forall t. \tag{5.3}$$

112

- Logical relationship between configuration and transition variables:

$$x_t^y - x_{t-1}^y = \sum_{y' \in \mathcal{M}^{T,y}} v_t^{y'y} - \sum_{y' \in \mathcal{M}^{F,y}} v_t^{yy'}, \; \forall t, \forall y \in \mathcal{Y}. \qquad (5.4)$$

where $\mathcal{M}^{F,y}$ is the set of reachable configurations from $y \in \mathcal{Y}$, and $\mathcal{M}^{T,y}$ is the set of configurations that can reach $y \in \mathcal{Y}$.

- At most one transition in each interval:

$$\sum_{yy' \in \mathcal{M}} v_t^{yy'} \leq 1, \; \forall t, \qquad (5.5)$$

where $\mathcal{M}$ is the set of all feasible transitions.

We note that there might be additional constraints characterizing the feasible set of a CCU, including ramping and minimum run time of each configuration or turbine. However, since these constraints are irrelevant to the representation of the transition between configurations, we omit them here. The feasible set of a CCU under the single-interval transition assumption is defined by constraints (5.1)–(5.5).

5.5.2 Transition Ramping Formulation

The CCU transition model that removes the assumption of single time interval transition is summarized in this section and a full representation with details can be found in [181, Section 5.3.2].

Nomenclature

Additional Data:

$TP_i^{yy'}$ the total power output from the CCU in transition at the end of the i-th interval of the transition process between y and y'.

$TD^{yy'}$ the duration (number of intervals) of the transition process between y and y'.

Where $(TP_1^{yy'}, TP_2^{yy'}, \ldots, TP_{TD^{yy'}}^{yy'})$ is a vector that describes the transition power-trajectory.

Decision Variables:

w_t^y Binary variable for whether configuration y is *dispatchable* at t;

x_t^y Binary variable for whether configuration y is either 1) dispatchable or 2) in an ongoing transition to other configurations at t;

$v_t^{y,y'}$ Binary variable for transition from y at $t-1$ to y' at t. The transition variable becomes one when a new configuration *becomes dispatchable*;

p_t^y Continuous variable for power output from configuration $y \in \mathcal{Y}$ at t;

p_t Continuous variable for power output of the CCU at t.

Constraints Constraints (5.3)–(5.5) are kept from the standard formulation. In addition, the following are included:

- Bounds on the power output of each configuration:

$$\underline{p}^y w_t^y \leq p_t^y \leq \overline{p}^y w_t^y, \ \forall t, \forall y. \tag{5.6}$$

- Constraints that define w_t^y:

$$w_t^y = x_t^y - \sum_{yy' \in \mathcal{M}} \sum_{i=1}^{TD^{yy'}} v_{t-i+1+TD^{yy'}}^{yy'}, \ \forall t, \forall y. \tag{5.7}$$

  – The last term forces w_t^y to zero when CCU is transitioning away from configuration y.

- Total power output of CCU:

$$p_t = \sum_{y \in \mathcal{Y}} p_t^y + \sum_{yy' \in \mathcal{M}} \sum_{i=1}^{TD^{yy'}} TP_i^{yy'} v_{t-i+1+TD^{yy'}}^{yy'}, \ \forall t. \tag{5.8}$$

  – The last term represents the output from the transition power-trajectory.

Minimum up/down time constraints are omitted in this section. The feasible set of a CCU with representation of transition ramping is defined by constraints (5.3)–(5.8). The discussion of the tightness and compactness of this formulation can be found in [181, Section 5.3.3].

5.6 Different Ramping Constraints

In the existing literature such as [272], both intra-configuration and inter-configuration ramp rates are defined. However, the inter-configuration ramp rate is only a rough proxy to the transition trajectories.

5.6.1 Plant-wise Ramping Constraints

A set of plant-wise ramping constraints is proposed in [181, Section 5.3.3.3]:

$$p_t - p_{t-1} \leq \sum_{y \in \mathcal{Y}} R_U^y x_t^y, \ \forall t, \tag{5.9}$$

$$p_{t-1} - p_t \leq \sum_{y \in \mathcal{Y}} R_D^y x_t^y, \ \forall t, \tag{5.10}$$

where R_U^y and R_D^y are respectively the ramp-up and ramp-down rate limits of configuration y when the CCU is dispatchable.

Constraints (5.9) and (5.10) assume that the ramp rate of the power-trajectories are within the limit on the ramp rates when the CCU is dispatchable. If this assumption is not satisfied, additional terms are needed on the right hand side that relax these constraints when the CCU is in transition.

5.6.2 Configuration-wise Ramping Constraints

The plant-wise ramping constraint is straightforward and easy to implement. However, we notice from empirical experiences that the plant-wise ramping constraints involve some limitations.

First, the ALLOFF configuration (the configuration indicating that the CCU is turned off) should not be limited by ramping constraints. Under the transition ramping model, the ALLOFF configuration would not have a positive output except for when it is involved in transitions. However, the output during transitions are fixed in the transition ramping. Thus, it is better to remove the ramping constraints on the ALLOFF configurations to reduce

116

the size of the problem and prevent potential conflicts in data. However, it is not trivial to achieve this in the plant-wise ramping constraints presented in (5.9) and (5.10).

Secondly, the power output variable and unit commitment variable of each of the configurations in the CCU are involved in the plant-wise ramping constraints of the CCU. This would result in more non-zeros in the constraint matrix and increase the computational expense.

We propose additional and optional configuration-wise ramping constraints:

$$p_t^y - p_{t-1}^y \leq R_U^y x_t^y + \sum_{y' \in M^{T,y}} v_t^{y'y} A(y', y) \ \forall t, \forall y. \tag{5.11}$$

$$
\begin{aligned}
-p_t^y + p_{t-1}^y \leq & (R_D^y - H^y)x_t^y + H^y x_{t-1}^y \\
& - \sum_{y' \in M^{T,y}} v_t^{y'y}[A(y', y) - H^y] \ \forall t, \forall y,
\end{aligned}
\tag{5.12}
$$

where each entry (y', y) in the matrix A is the power output in the last time step in the transition curve from configuration y' to configuration y in the CC unit. H^y is picked as the largest output of configuration y in a time interval during transitions to the other reachable configurations in the CC unit.

Notice that, for each configuration y, ramping constraints (5.11) and (5.12) are equivalent to (5.9) and (5.10), respectively, when there is no transition but the terms in the summation change the ramp whenever there is a transition.

When configuration y starts up at t, constraints (5.11) and (5.12) become:

$$p_t^y \le R_U^y + \sum_{y' \in M^{T,y}} v_t^{y'y} A(y', y). \tag{5.11'}$$

$$p_t^y \ge \sum_{y' \in M^{T,y}} v_t^{y'y} A(y', y) - R_D^y. \tag{5.12'}$$

Constraint (5.11') indicates the maximum power output of configuration y at the start up time t is its ramp rate plus the power output in the last time step of the transition. Constraint (5.11') is relevant if the CCU is ramping up in the transition. An example is the output of configuration 2 in the transition from configuration 1 to configuration 2 between $t = 5$ and $t = 6$ as described in Fig. 5.2.

Constraint (5.12') requires that the minimum power output of configuration y at the start up time t is the power output in the last time step of the transition minus a ramp down rate. Constraint (5.12') is relevant if the CCU is ramping down in the transition. An example is the output of configuration 1 at $t = 13$ has to be greater than or equal to the fixed output of configuration 2 at $t = 12$ minus the ramp down rate of configuration y as described in Fig. 5.2.

When configuration y shuts down at t, constraints (5.11) and (5.12) become:
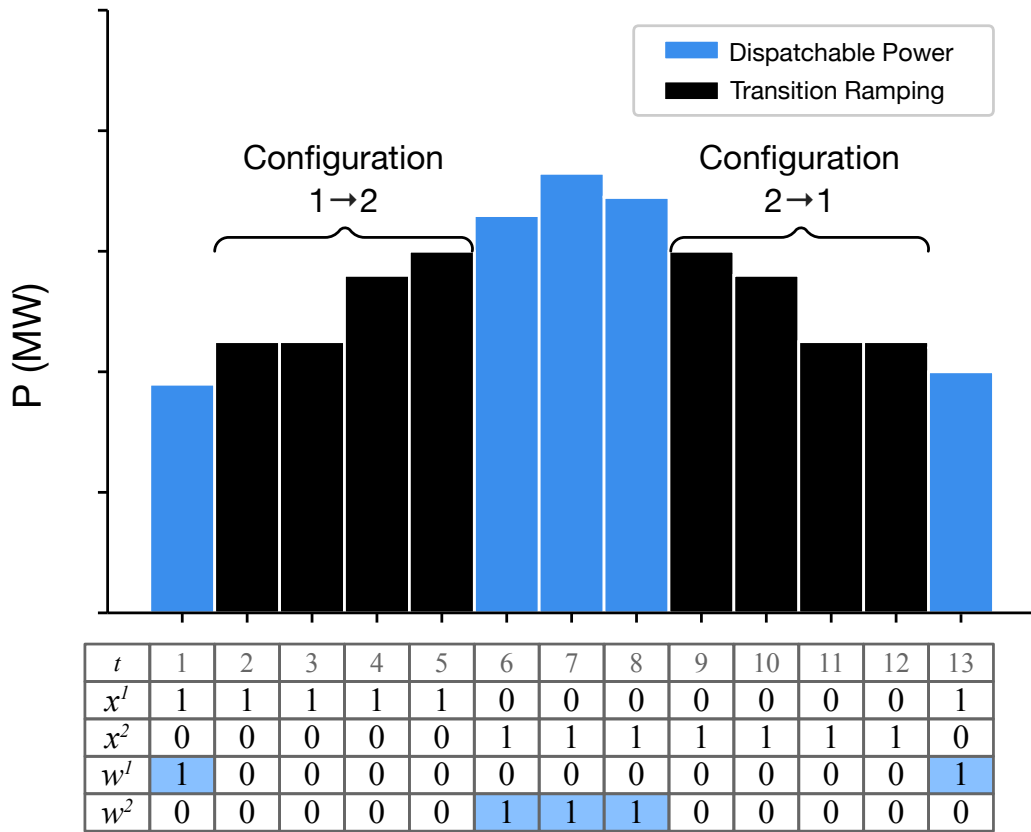
Figure 5.2: Illustration of the ramping constraints with commitment variable x and dispatchable variable w [181].

$$p^y_{t-1} \geq 0. \qquad (5.11")$$

$$p^y_{t-1} \leq H^y. \qquad (5.12")$$

With the transition ramping model, there shouldn't be an active constraint when a configuration shuts down since the configuration is always in a transition curve when it shuts down and the outputs in the transition curve are fixed. Ideally, in order to have a tight formulation, H^y can be picked as

119

the output of the last time step in the transition curve of the configuration y. However, since the transition curve varies with different configurations, the transition variables $v_t^{yy'}$ for each the transition to each configuration y' will be involved in the selection of H^y and it will bring nonlinearity to constraint (5.12).

Compared to a plant-wise ramping constraint, one of the benefits of the proposed configuration-wise ramping constraint is it creates less non-zeros in each of the constraints. However, since the configuration-wise ramping constraint is applied at each CCU configuration, it generates more constraints in total. The impacts of this trade off on the problem size are presented and further discussed in the computation results in section 5.7.

5.7 Numerical Results

An illustrative two units test case is presented in [181, Section 5.4] to demonstrate the CCU transition ramping model. In this section, the CCU transition ramping model described in Section 5.5.2 with two different ramping constraints described in Section 5.6 is implemented with a configuration-component hybrid combined cycle model [98] of CCUs in the MISO system. The computational performance of the proposed model is presented and compared with the configuration-component hybrid CCU model.

MISO has collected combined cycle data from market participants since 2012 for the study of an enhanced combined cycle model [80]. These data has been used for the study of configuration based CC model [79] and configuration-

120

component hybrid CC models [98]. In total, 31 configuration based combined cycle units are modeled using the data and there are 122 configurations under the 31 CC units. Because of the lack of transition ramping data, a transition ramping curve is approximated as a piece wise linear ramping curve given the transition time and the minimum and maximum outputs of the two configurations in each of the transitions. An example of the approximated transition curve between two configurations is shown in Table 5.1. A 36-hour-ahead load profile is randomly selected from historical load data. All test cases are performed on a 2.2-GHz quad-core Intel Xeon CPU E5-2699 with 32-GB RAM; all optimization problems are solved with Gurobi 8.0.

Table 5.1: An Example of Approximated Transition Curves

Configuration	$\underline{p}^y$ (MW)	$\overline{p}^y$ (MW)
1CT+1ST	20	50
2CT+1ST	70	80
Transition	Duration (Interval)	Trajectory (MW)
1CT+1ST to 2CT+1ST	3	$[50, 60, 70]$
2CT+1ST to 1CT+1ST	3	$[70, 60, 50]$

A configuration-component hybrid combined cycle model [98] is adopted and tested with the MISO system [80]. Therefore, this hybrid combined cycle model is used as benchmark to present the computation results of the proposed formulations. Two transition ramping models with different ramping constraints are implemented in the MISO prototype day-ahead security-

constrained unit commitment tool [133]. The computational results are compared in Table 5.2.

- CCH: A configuration-component hybrid CCU model that ignores transition rampings [98];

- CCH+TRP: CCH with transition ramping modeling and plant-wise ramping constraints (5.9)–(5.10);

- CCH+TRC: CCH with transition ramping modeling and configuration-wise ramping constraints (5.11)–(5.12).

In the CCU data, the transition time between configurations in some CCUs are given zero values indicating the starting up configuration is "instantly" dispatchable at the transition hour. A substitution of constants in the ramping constraints of CCH+TRC in (5.11)–(5.12) is needed to keep the formulation valid when the transition time is zero. While this situation is likely to occur in practice, since the formulation is the same after the substitution and it doesn't affect the computations, the discussion of this issue is included in Appendix B.

5.7.1 Computational Performance of CCU Transition Ramping Model

The objective value increases when we consider transition ramping. This is expected because the combined cycle units are modeled as being more flexible than they actually are if we ignore transition ramping. We assume the energy costs during transition ramping are not included as part of the transition costs in the current data. Therefore, we consider both energy costs

Table 5.2: Computational Performance

Model	MIP Gap at 1200s	MIP Gap at 1800s	Root Relaxation Time(s)	Best Objective
CCH	0.17 %	0.10 %	122.5	12,709,826
CCH+TRP	0.28 %	0.15 %	153.4	13,012,604
CCH+TRC	0.28 %	0.15 %	169.6	13,011,413

and transition costs in the objective when a transition occurs in a combined cycle. Since the transition cost was collected from market data without the explicit consideration of transition ramping, it may include some incremental energy costs during the transitions. Therefore, the objective with the transition ramping model may be less than what is shown in Table 5.2 when accurate data is obtained.

In addition, the "root relaxation" [163] time increases when transition ramping is included. This is because the problem size grows when we introduce the variables and constraints related to transition ramping. As a result, the integer relaxation of the UC problem becomes harder to solve.

Despite the increased problem size, computational performance of the models with transition ramping are close to the model without transition ramping. As shown in Table 5.2, the MIP gaps of the two models with transition ramping are only slightly higher than the benchmark model. According to the MISO operating guide, the day-ahead optimization will be stopped at 1200 second if the MIP gap is below 1%; if the MIP gap is above 1%, the optimization will continue for another 600 seconds. From Table 5.2, we find that the

MIP gaps of CCH+TRP and CCH+TRC are very close to the MIP gap of CCH at 1800 seconds and all three models have MIP gaps below 0.2%; that is, the results of all three models can be considered acceptable. This suggests that introducing transition ramping modeling in [181] does not significantly increase the computational complexity.

5.7.2 Problem Sizes with Different Ramping Constraints

Table 5.3: Problem Size

Problem Size	CCH	CCH+TRP	CCH+TRC
Original Problem			
# of nonzero	4,622,554	4,656,582	4,668,482
After Pre-solve			
# of nonzeros	2,704,544	2,789,274	2,769,778
# of continuous variables.	297,451	298,140	298,093
# of integer variables	74,251	75,074	74,499

Next, we compare two formulations of ramping constraints. Table 5.2 shows that the MIP gaps of CCH+TRC and CCH+TRP at both 1200s and 1800s are very close (below 0.01%). Table 5.3 shows that CCH+TRC results in more non-zeros before pre-solving. As mentioned in Section 5.6.2, configuration-wise ramping constraints lead to an increased number of constraints. For this test system, we observe that the configuration-wise ramping constraints (CCH+TRC) lead to more nonzeros than the plant-wise ramping constraints.

After pre-solving, however, the number of nonzeros in CCH+TRC be-

124

comes less than that in CCH+TRP; the number of variables in CCH+TRC also becomes smaller than CCH+TRP. Although it is difficult to identify the cause of such differences, it is reasonable to speculate that, since each configuration-wise ramping constraint involves less variables and parameters, this alternative formulation enables the pre-solving process to identify more redundancy. Although more test cases are needed to have a comprehensive conclusion, results from this study show that modeling the ramping constraints on the configurations in a CCU transition ramping model will potentially provide a smaller problem.

5.8   Summary

Most existing combined-cycle unit (CCU) models assume that any transition completes within a single interval. This assumption is not satisfied by the operating characteristics of most CCUs, and may lead to suboptimal commitment and dispatch solutions. This chapter first summarizes a mixed-integer programming formulation that represents the transition ramping of CCUs [181]. Configuration-wise ramping constraints are formulated and compared with the plant-wise ramping constraints in [181]. The transition ramping model is implemented with configuration-component hybrid CC model in a MISO prototype UC tool. Computational results on a MISO system show a moderate increase in computational complexity when transition ramping modeling is considered. The problem sizes of the transition ramping model with different ramping constraints are presented and discussed.

Chapter 6

Pumped-Storage Hydro Unit Formulation

6.1 Introduction

Inspired by the work on modeling the configurations of combined cycle units in the unit commitment problem, this chapter proposes a configuration based pumped-storage hydro (PSH) model for the day-ahead market, in order to enhance the use of pumped-storage hydro resources in the system. By introducing three "configurations," namely, pumping, generating and "alloff" or off-line, in a pumped-storage hydro unit, the proposed model can more accurately reflect the practical operations of pumped-storage hydro units in the day-ahead market. A comprehensive review of the existing pumped-storage hydro models and industry practices is presented. The definition of configurations of a pumped-storage hydro unit and the transitions between the configurations during operation are revealed and discussed in detail to describe the proposed model.

6.2 Background and Motivation

Pumped-storage hydro plants use power to pump water uphill to an elevated reservoir when the electricity price is low. The water is released

to a lower reservoir and drives the turbine to generate electricity when it is needed. There are now 22.8 GW of pumped-storage capacities in the United States [404]. However, it becomes harder to obtain significant land area with suitable topography for reservoirs not only because many of the best sites are taken, but also due to the opposition from environmental groups. Significant investment and long lead times are important factors limiting further deployment of conventional pumped-storage hydro plants [343].

In the traditional operation of a power system, energy storage has been treated as a way to shave peaks and improve the capacity factor of base-load generation. However, there are a range of energy storage technologies that have been developed that can also provide value by supplying ancillary services such as reserves and frequency control. Therefore, the energy storage unit is not only playing the role of shifting load and generation but also playing a much broader role as an extended and flexible energy management tool.

The effects of stockpiling excess electricity in energy storage has historically been used to avoid the need for some of the peaking generation capacity and also enables more base-load generators to stay on line and generate electricity in the time when demand is low, thereby lowering the system overall operation cost. For example, with energy storage, more base-load generators are able to keep generating in the night with their low cost and avoid the costs of shutting down and starting up. The costs of peaking generation is thereby also avoided.

This load/generation-shifting effects is also particularly useful for en-

Table 6.1: Storage Technologies and Applications (Source: data is from [36])

Full Power Duration of Storage	Applications of Storage	Compressed Air Energy Storage (CAES)	Pumped -Storage Hydro	Battery	Flywheel
3 Days	Weekly smoothing of loads and most weather variations	Y	Y		
8 Hours	Daily load cycle PV, Wind, transmission line repair	Y	Y	Y	
2 Hours	Peak load lopping, standing reserve, wind power smoothing	Y	Y	Y	
20 Minutes	Spinning reserve, wind power smoothing, clouds on PV	Y	Y	Y	Y
3 Minutes	Spinning reserve, wind power smoothing of gusts		Y	Y	Y
20 Seconds	Line or local faults, voltage and frequency control, governor controlled generation			Y	Y

hancing the integration of renewable generation plants. In the past two decades, because of the concerns about the environmental impacts of generating electricity by burning fossil fuels, there are enormous interests and ambitious targets for integrating renewable energy to supply the electricity demand. The

function of energy stockpiling provided by energy storage units would allow renewable resources to get more value in daily operation.

As shown in Table 6.1, as one of the mature technologies for energy storage, pumped-storage hydro is able to provide service in a time range from minutes to days. The services in this time range include spinning reserve and load or generation shifting.

On the one hand, pumped-storage hydro can, in principle, provide a wide range of important and valuable services to the system which, nowadays, is exposed to a greater scale of uncertainties on both generation and demand sides. On the other hand, however, the pumped-storage hydro units have not deeply participated in the market. Currently, many of the pumped-storage hydro units in the footprint of the Midcontinent Independent System Operator (MISO) do not participate in the day-ahead market clearing process. Therefore, their decisions of whether to pump or generate and how much to pump or generate are made under their own forecast of market prices.

This practice of pumped-storage hydro technology is not efficient in two aspects: First, as a market participant with limited information about the market, the forecast of market prices can deviate significantly from the realization. Therefore, the decisions made based on the forecast would impair profits for the pumped-storage hydro units in long-term and this would discourage the further development and investment in the pumped-storage hydro technology; Secondly, the decisions made by pumped-storage hydro unit is also suboptimal to the system welfare. That is, the benefits and the flexibility

129

provided by pumped-storage hydro technology is not fully exploited under the current practice.

To overcome the drawbacks of the current practice, introducing the pumped-storage hydro units into MISO's day-ahead unit commitment model is a first step. Therefore, a suitable model for pumped-storage hydro units in the UC model is studied in this chapter.

6.3 Literature Review

6.3.1 Pumped-storage Hydro Units

Because of the benefits of renewable power smoothing provided by pumped-storage units introduced in Table 6.1, the model of a pumped-storage unit has been explicitly developed in the operation of a renewable plus pumped-storage power plant. For example, in [66] and [118], a profit maximization problem is formulated for a single wind farm together with a pumped-storage hydro plant. A wind plus storage plant model is presented in [213]. This general energy storage model is similar to [66]. In these works, a pumped-storage plant is modeled as two individual units: a pump and a generator. Both pumping and generating have upper and lower limits for every time slot. In addition, generation at every time slot is upper bounded by the total energy stored in the system. The energy stored in the pumped-storage hydro system is modeled as an energy balance constraint with efficiencies for pumping and generating. The total energy stored in the first hour and the last hour is specified. The energy stored in the system is greater than or equal to zero and less

than or equal to its upper limit in all hours. This upper limit represents the maximum energy stored in the system and is derived from the water stored in the reservoir.

The impact of energy storage sizing on wind-hydro system operation and economics has been studied in [67], [213] and [56]. A general energy storage model is defined by its energy capacity, charging efficiency, discharging efficiency, charging power capacity, and discharging power capacity.

In [56], the pumped-storage plant is modeled in a similar way as to [66] but considers the constraints of meeting spinning reserve requirements or frequency regulation unit commitment requirements. Consequently, the model allows the possibility of spilling water without using it to generate electricity by including a variable for spilled energy in the pumped-storage hydro energy balance constraints.

The bidding and scheduling of a pumped-storage unit is studied as part of a generating company with hydro, thermal, and pumped-storage units in [288]. The quantity of pumping and generating is modeled in a single variable representing water discharged (positive) from or pumped (negative) to the upper reservoir assuming one hundred percent efficiency in both processes.

The robust unit commitment problem with wind power and pumped-storage hydro is studied in [196]. A binary variable is introduced to indicate whether the unit absorbs (pumping) or generates electricity. The big-M method is used to prevent the unit from generating and pumping at the same

time.

In [145], stochastic joint optimization is used to maximize the profit of wind generation and pumped-storage units in an electricity market. In [145], each pumped-storage unit is modeled as N identical turbines and each of them can function as either a generator or a pump. An integer variable is introduced to indicate the total number of turbines that are in pumping mode among the N identical turbines in the pumped-storage hydro unit. The generating / pumping mutually exclusive constraint is well handled with the integer variables without using the big-M method. In addition, the start up and shut down costs are considered in this study.

The feasibility of combined solar pumped-storage hydro and solar wind pumped-storage hydro is studied in [249] and [248]. Because the studies focus on the standalone island condition, they provide a way to model the energy stored in the system with a consideration of the available static head in the studied island and how much water volume is used for pumping or generating. Also, the water evaporation and leakage loss are considered in their work.

Although the model of a pumped-storage hydro unit has been studied in the operation of a renewable plus pumped-storage hydro plant explicitly, the model of a pumped-storage hydro unit in the day-ahead unit commitment problem remained obscure. In [66], [118], [213], [67], [56] and [288], the market prices are taken as an input for the plants' profit maximization problem and the generating/pumping level of each unit is defined as a continuous variable. A binary variable is introduced in [196] to represent the generating/pumping

status of a pumped-storage hydro unit in the system. The binary variables for a pumped-storage hydro unit is split into N pairs for each pumped-storage hydro turbine in [145]. References [248] and [249] focused on the study in an island mode, therefore the dispatching of pumped-storage hydro unit in the power system is not their major concern.

In the above works, the pumped-storage hydro unit has to be either pumping or generating at a given time. However, due to the physical limits from pumping/generating turbines, there are usually minimum outputs for the generating mode and minimum consumptions for the pumping mode. These model features imply that, a pumped-storage hydro unit is forced to operate at one of the two limits in some cases if the current model is used in a unit commitment and economic dispatch problem. These conditions would result in inefficient operations. That is, because of the minimum limits of generation and consumption, the pumped-storage hydro unit is either generating or pumping at least at its minimum output or consumption limit, respectively, if it is operating. However, at certain times in the day it may be best to neither pump or generate. In other words, constantly charging or discharging the pumped-storage hydro unit is not always the best strategy for system operation.

In [202], the coordinated hourly scheduling of wind and pumped-storage units is modeled in the problem of day-ahead scheduling of power systems. Three modes, pumping, generating, and idle are modeled for each of the pump storage units. However, without explicitly modeling the transition of

133

the modes, it is not clear how to include some operation features e.g. transition time between modes and min up/down time for each mode. In [202], the transition between modes are assumed to be able to complete within one time interval. Nevertheless, this is not a general case, particularly in the context of real-time markets where the interval may be only five or fifteen minutes.

In order to represent the operational features of pumped-storage hydro in a day-ahead market, we explored the model used for combined cycle gas turbines (CCGTs) in the unit commitment problem and found the configuration based model used for CCGTs [79] and [181] can be extended to better represent a pumped-storage hydro unit in the day-ahead market.

6.3.2 Combined Cycle Gas Turbines

We find the CCU configuration based model described in [79], [48], [189] and [181, Section 5.4] is particularly fit for the operation of a pumped-storage hydro unit. In the configuration based model of a CCU, the configurations which are different combinations of CTs/STs are modeled as individual units. Besides all the operational configurations, there is an "alloff" configuration indicating the off state of the plant. All the configurations including the "alloff" configurations are mutually exclusive indicating that there is only one configuration on at any time of the operation of the plant. Therefore, the complicated operations, such as operation costs, output limits and feasibility of transitions between configurations, can be specifically dealt with.

Similar to CCGTs, a pumped-storage hydro unit can also be modeled

134

with two operational configurations namely pumping and generating. In order to allow the unit to stay idle (neither pumping or generating), an "alloff" configuration can be introduced as with the CCGT. The transition between different modes are modeled using transition variables. Thus the operational features such as the constraints on transition time between modes, min up/down time of each mode can be handled well. In addition, compared to the model in [202], the configuration based pumped-storage hydro model is more scalable. It can be easily extended if necessary to have operational modes considering different components in a pump hydro unit as discussed in [145], which potentially can provide more flexibility to the operation of a pumped-storage hydro unit.

The other CCGT models besides the configuration based model are less suitable for modeling PSH. For example, the aggregate model is not applicable for a pumped-storage hydro unit because the pumping/generating operation features cannot be represented. The other models discussed in [98] are designed to address the operational features of individual turbines in a configuration, e.g., min up/down time of each ST or CT in a 1CT+1ST configuration etc. However, the operation configuration in a pumped-storage hydro unit would be composed from a single unit or a group of identical units operating in the same mode. Therefore, it is not necessary to explicitly distinguish each of the units in a configuration of a pumped-storage hydro model.

6.3.3 Contributions

In order to accurately represent the operation features of a pumped-storage hydro unit in day-ahead market, we extend the configuration based model in [79] with a representation of operation features of a pumped-storage hydro unit to propose a novel configuration based pumped-storage hydro model in this chapter. The contributions are:

- The proposed model can reflect the physical features accurately and enhance the operational flexibility of a pumped-storage hydro unit by introducing an additional "alloff" configuration.

- A numerical example is presented to demonstrate the effectiveness of the proposed pumped-storage hydro model. The impacts of bid prices for pump loads on the pumped-storage hydro owner's profits and system social welfare are discussed in the case study.

- The implementation of the proposed pumped-storage hydro formulation and a computational study in a MISO prototype unit commitment model is ongoing.

6.4 Problem Formulation

The configuration based modeling of pumped-storage hydro unit represents all feasible operation modes of a pumped-storage hydro unit. We assume that, at each pumped-storage hydro unit, either there is only one pumping and one generating turbine or there are multiple identical turbines. Based on this
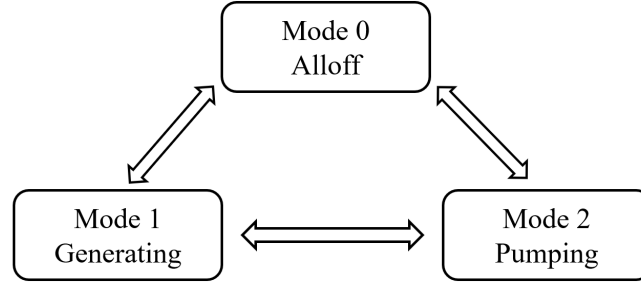
Figure 6.1: Mode transition diagram of a pumped-storage hydro unit in two consecutive periods.

assumption, there are only three operation modes in each of the turbines in a pumped-storage hydro unit and transitions are allowed between each pair of the modes, as shown in Fig. 6.1. The "Mode 0" represents the state when the pumped-storage hydro turbine is offline.

Nomenclature

Sets and indices:

$g \in G_{sh}$ set of pumped-storage hydro units;

$g \in G_{sh,r}$ set of pumped-storage hydro units that share the same

reservoir r;

$g \in G$ set of rest of generating units;

$m \in M_g$ set of configurations, $m = 0$:*all off*,

$m = s$: *storage / pumping*,

$m = h$: *hydro / generating*;

$n \in M_g^{F,m}$ set of configurations that configuration m can feasibly transit to;

$r \in R$ set of reservoirs.

Data [units]:

D_t system demand at period t [\$/MW];

$\underline{P}_{gt}^h$ minimum power output of configuration h at unit g at period t in economic mode [MW];

$\overline{P}_{gt}^h$ maximum power output of configuration h at unit g at period t in economic mode [MW];

$\underline{P}_{gt}^s$ minimum power storage of configuration s at unit g at period t in economic mode [MW];

$\overline{P}_{gt}^s$ maximum power storage of configuration s at unit g at period t in economic mode [MW];

η_g^s pumping efficiency of the pumped-storage hydro unit g [NA];

η_g^h generating efficiency of the pumped-storage hydro unit g [NA];

$E_{r,1}$ initial energy levels of the reservoir r [MW];

$E_{r,T+1}$ final energy levels of the reservoir r [MW];

$\overline{E}_r$ maximum energy levels of the reservoir r [MW].

Variables [units]:

$e_{r,t}$ energy stored in the reservoir r at time t [MW];

u_{gt}^{m} binary variable, commitment variable of unit g configuration

m at period t [NA];

v_{gt}^{mn} binary variable, transition variable between configuration m

and configuration n of generator g at period t [NA];

q_{gt}^{h} continuous variable, amount of energy production of

configuration h at unit g at time period t [MW];

q_{gt}^{s} continuous variable, amount of energy consumed in

configuration s at unit g at time period t [MW];

q_{gt} continuous variable, amount of energy production of other

generating unit g at time period t [MW].

Derived Data [units]:

$H_{gt}^{k,h}$ the piecewise cost of the kth segment of piecewise

approximation of the production cost or bid price of

configuration h at generator g at period t [\$/MW];

$P_{gt}^{k,h}$ the break point of the kth segment of piecewise approximation

of the production cost of configuration h at generator g at

period t [MW].

$C_{g,t}^{s}$ the bid pumping price of unit g at time t [\$/MW].

Auxiliary Variables [units]:

f_{gt}^h continuous variable, energy cost of h configuration at unit of

         configuration at unit of s configuration of unit g at period t

         [$ /hr];

$C(q_{gt})$ cost function of generating unit g [$ /hr].

6.4.1 Objective Function

The objective of the day-ahead unit commitment problem is to minimize the system operating costs. The operation costs related to a pumped-storage hydro unit is the offer costs of the generating mode minus the bid prices of the pumping mode which is reflected as negative costs in (6.1). Note that the offer costs and bid prices from a PSH can be zero. The third term in (6.1) represents the generation costs of the rest of generators in the system.

$$\min_{q,u,v,e} \sum_{g \in G_{sh}} \sum_{t \in T} (f_{gt}^h - C_{gt}^s q_{g,t}^s) + \sum_{g \in G} \sum_{t \in T} C(q_{gt}) \tag{6.1}$$

6.4.2 Piece-wise Costs Function

The operation costs of the generating mode of a pumped-storage hydro unit is modeled as a piece-wise linear function in (6.2). Notice that this is a generalized way to represent the production cost of a generating unit, and that the generation costs from a PSH unit could be zero.

140

$$s.t. : f_{gt}^h \geq H_{gt}^{k,h}(q_{gt}^h - P_{gt}^{k-1,h})$$
$$+ u_{gt}^h \sum_{\theta=1}^{\theta=k-1} H_{gt}^{\theta,h}(P_{gt}^{\theta,h} - P_{gt}^{\theta-1,h}) \qquad (6.2)$$
$$\forall k = 1, ..., K, \forall g \in G_{sh}, \forall t \in T$$

6.4.3 System Energy Balance Constraints

The generation has to be balanced with demand in the system at all time. In (6.3), the total generation in the system including the generation from pumped-storage hydro units on the left should be balanced with the sum of the fixed demand and the pumping demand from the pumped-storage hydro units on the right.

$$\sum_{g \in G} q_{gt} + \sum_{g \in G_{sh}} q_{gt}^h = D_t + \sum_{g \in G_{sh}} q_{gt}^s \ \forall t \in T \qquad (6.3)$$

6.4.4 State and Transition Logic Constraints

Constraints (6.4) guarantee that the unit commitment variables of each mode in a pumped-storage hydro plant described in Fig. 6.1 are mutually exclusive, which is also modeled for CCGTs in [238]:

$$\sum_{m \in M_g} u_{gt}^m = 1 \ \ \forall g \in G_{sh}, \forall t \in T \qquad (6.4)$$

The transition between two modes m, n in one pumped-storage hydro plant g at time t is defined as a binary variable v_{gt}^{mn}. Notice that the start up

and shut down of a mode are modeled as the transition between the mode and the "alloff" mode. These constraints are modeled for CCGTs in [272].

$$u_{gt}^m - u_{g\,t-1}^m = \sum_{n \in M_g^{F,m}} v_{gt}^{nm} - \sum_{n \in M_g^{F,m}} v_{gt}^{mn}$$

$$\forall g \in G_{sh}, \forall m \in M, \forall t \in T \tag{6.5}$$

In addition to the mutually exclusive constraints on commitment variable of each configurations, there should be at most one feasible transition at any time [79].

$$\sum_{m \in M_g} \sum_{n \in M_g^{F,m}} v_{gt}^{mn} \leq 1$$

$$\forall g \in G_{sh}, \forall t \in T \tag{6.6}$$

6.4.5 Box constraints

The amount of generation at each time from the pumped-storage hydro unit is constrained not only by the physical features of the turbine but also by the amount of energy stored in the system as shown in (6.7). However, the right side of the inequality is a product of a binary variable and the minimum of a constant and a continuous variable. The linearization of this constraint is shown in Appendix A. The amount of energy stored in the pumped-storage hydro system is only limited by the features of the turbine as shown in (6.8).

$$\underline{P}_g^h u_{gt}^h \leq q_{g,t}^h \leq u_{gt}^h \min\{\overline{P}_g^h, \eta_g^h e_{r,t}\}$$

$$\forall r \in R \quad \forall g \in G_{sh,r} \quad \forall t \in T \tag{6.7}$$

142

$$\underline{P}^s_g u^s_{gt} \leq q^s_{g,t} \leq u^s_{gt} \overline{P}^s_g \quad \forall g \in G_{sh} \quad \forall t \in T \tag{6.8}$$

6.4.6 Storage Energy Balance and State of Charge Constraints

The energy stored in a reservoir shared by multiple pumped-storage hydro units is balanced at each consecutive hour shown in (6.9). Parameters η^h_g and η^s_g are the efficiencies of generating and pumping indicating energy losses in both modes. The energy stored in the reservoir at the beginning of each day is given by (6.10) and the energy stored in the reservoir at the end of each day is constrained in (6.11). The inequalities in (6.12) constrain the total energy stored in the reservoir at each time interval. These constraints are modeled in a pumped-storage hydro unit based on [66], [118], [213], [67], [56], [288], [196] and [145].

$$e_{r,t+1} = e_{r,t} + \sum_{g \in G_{sh,r}} \eta^s_g q^s_{g,t} - \sum_{g \in G_{sh,r}} \frac{q^h_{g,t}}{\eta^h_g} \quad \forall r \in R \quad \forall t \in T \tag{6.9}$$

$$e_{r,1} = E_{r,1} \quad \forall r \in R \tag{6.10}$$

$$e_{r,T+1} = E_{r,T+1} \quad \forall r \in R \tag{6.11}$$

$$\underline{E_r} \leq e_{r,t} \leq \overline{E_r} \quad \forall r \in R \quad \forall t \in T \tag{6.12}$$

The start up/down time, transition time and the minimum up/down time are not listed here. They can be easily handled by the configuration

143

based model. The security constraints are not included, the details can be found in [79].

6.5   Numerical Results

Table 6.2 shows the units considered in this case study. Two thermal generators with different capacities and different costs are included to represent the generations besides pumped-storage hydro units in the system and to generate prices. The two pumped-storage hydro units in a pumped-storage hydro plant namely PSH1 and PSH2 share a reservoir. The bid prices for pumping load are initially specified as 27$/$MWh$ and there are no generating costs for both units. We will further discuss the impacts of the bidding price to the social welfare of the system in this chapter. For a simple presentation, the marginal generation costs and bid prices are constants over feasible generation and consumption levels and independent of time for all units. Notice that pumping in both units are "block loads" meaning that the pumping load is either at a predetermined level or zero. This is a typical operating feature of the pumped-storage hydro units in the MISO system. The energy efficiency of the pumping and generating processes are identical in both units.

The minimum and maximum energy allowed to be stored in the reservoir along with the state of charge of the reservoir at the beginning and the end time interval are described in Table 6.3. Notice that the state of charge at the end time interval is required to equal that at the beginning time interval, any energy used for generations from the pumped-storage hydro has to be stored

Table 6.2: Unit Parameters

Unit	Cost/Price	$\underline{q}^m$	$\overline{q}^m$	η_g^m
	\$/MWh	MW	MW	
1: PSH1 Pump	27	200	200	0.9
2: PSH1 Gen	0	100	200	0.9
3: PSH2 Pump	27	200	200	0.9
4: PSH2 Gen	0	100	200	0.9
5: Thermal Gen 1	30	0	400	NA
6: Thermal Gen 2	20	0	900	NA

earlier or recharged later within the studied time range.

Table 6.3: Reservoir

	$\underline{E_r}$	$\overline{E_r}$	$E_{r,1}$	$E_{r,T+1}$
	MWh	MWh	MWh	MWh
Reservoir	350	3500	1000	1000

A day ahead unit commitment (UC) and economic dispatch (ED) problem is solved with a 24 hours net-load scenario in the system. Reserve requirements, ramp constraints, and transmission security constraints are ignored in the problem. The energy price at each node in the transmission network or locational marginal price (LMP) is the dual value at the energy balance constraint in (6.3) after the problem been solved. Notice that, since there is no transmission network constraint in this case study, there is a single LMP for the whole system at each time interval.

6.5.1 Bid Price for Pump Load

The bid prices for pump loads submitted by the pumped-storage unit owners represent their willingness to purchase and consume the electricity in the pumping modes. However, the bid prices are calculated based on the owner's information and forecast of the system LMP that would likely to be deviate from a realization. Thus, the bid prices will cause the solution of the UC and ED problem to deviate from maximizing social welfare. The compromised system objective by the pump bid prices will in turn impair the benefits to the pumped-storage hydro unit owners.
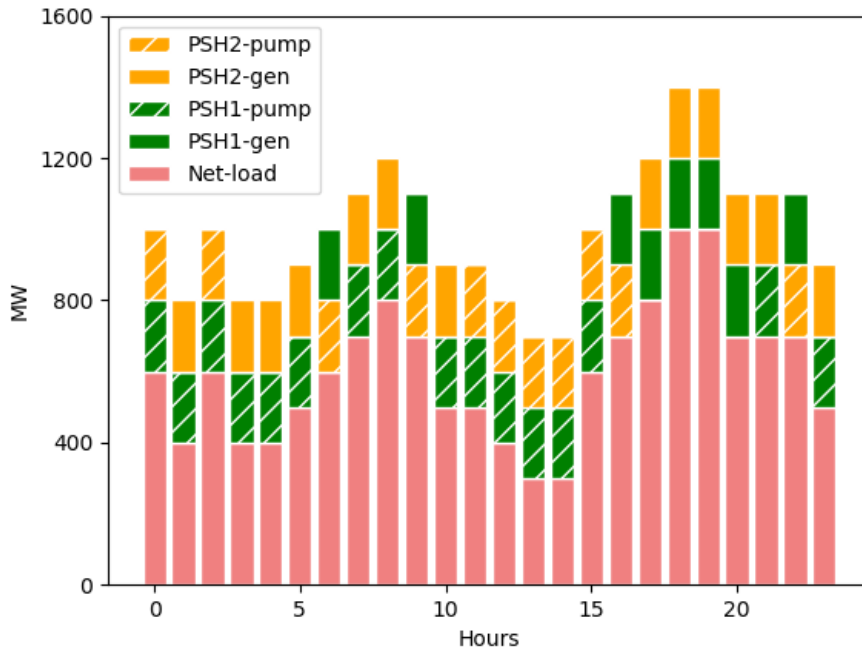
Figure 6.2: Unit Dispatches with Bid Prices for Pump Loads.

Net-load is defined in the section as the system constant load minus the renewable generations not including pumped-storage hydro (PSH). Fig. 6.2 shows the UC and ED solutions of the dispatches of the two pumped-storage units on top of the system net-load when bid prices for pump loads are considered and set to 27$/$MWh$ as shown in Table 6.2.

The net-load is an emulation of the California "Duck Curve" where solar generation boosts in the middle of the day and creates a deep drop in the net-load. The LMP is therefore lower and the PSH units are expected to pump in those hours (11-15). However, we observed that there are several hours (1,3-10,16,21-23) when one PSH unit is pumping and the other PSH unit is generating. Fig. 6.3 shows the outputs of PSH units on top of the state of charge of the reservoir. We can observe that at the hours when the PSH units pump and generate at the same time (particularly hours between 3-10), PSH units gradually deplete the state of charge of the reservoir by their round loop efficiency.

The simultaneous pumping and generating is due to the non-zero bid prices for pumping. In particular, because a positive bid price is submitted and included in the objective of the problem in (6.1) (boxed term), the system encourages PSH units to pump to reduce the objective function. At the same time, the generation and pump loads of the PSH appear at the left and right side of (6.3) (boxed terms). Because the generation cost from the PSH unit is zero, the "free" generation from one PSH unit will balance the pumping load from the other PSH unit as indicated in (6.3). The results shown in this

147
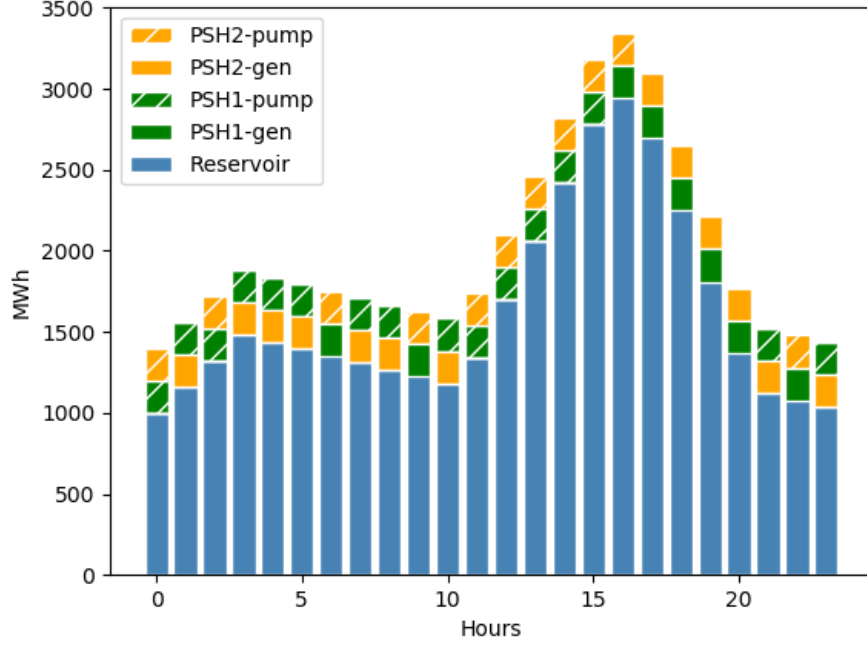
Figure 6.3: Reservoir State of Charges with Bid Prices for Pump Loads.

example is a clear demonstration that a positive pump bid price would damage the social welfare.

$$\min_{q,u,v,e} \sum_{g \in G_{sh}} \sum_{t \in T} f_{gt}^h \boxed{-C_{gt}^s q_{g,t}^s} + \sum_{g \in G} \sum_{t \in T} C(q_{gt}) \tag{6.1}$$

$$\sum_{g \in G} q_{gt} + \sum_{g \in G_{sh}} q_{gt}^h = D_t + \sum_{g \in G_{sh}} q_{gt}^s \ \forall t \in T \tag{6.3}$$

148

6.5.2 Eliminate Bid Price for Pump Loads

Alternatively, we suggest to eliminate the bid price for pump loads from the system objective as shown in (6.1'). Assuming the non-water generation costs for a PSH unit is zero, the objective only contains the generation costs of the rest of the generators besides the PSHs in the system. The price charged to the pump load is the system LMP instead of their self-bid prices.

$$\min_{q,u,v,e} \sum_{g \in G} \sum_{t \in T} C(q_{gt}) \tag{6.1'}$$

With the updated objective, the dispatch solutions are presented in Fig. 6.4. The first change we observe is that the PSH units no longer pump and generate at a same time interval. Pumping from PSH units appears at midnight (hour 0-4) and middle of the day (hour 10-14 and 16) when the net load is low. The PSH units are dispatched to generate at morning peak (hour 8) and evening peak (hour 17-20) when the net load is high. The PSH units don't pump at every time interval when net-load is low because the state of charge in the reservoir at the end of the day is required to return to its initial level.

First, from the system operator point of view, the results in Fig. 6.4 show the effectiveness of pump hydro storage units shaving the peak and filling the sink of the net-load shape. Therefore, the PSH units positively contribute to reduce the system generation costs and to maximize the social welfare. A flatter net-load including the outputs from the PSH units is also good for
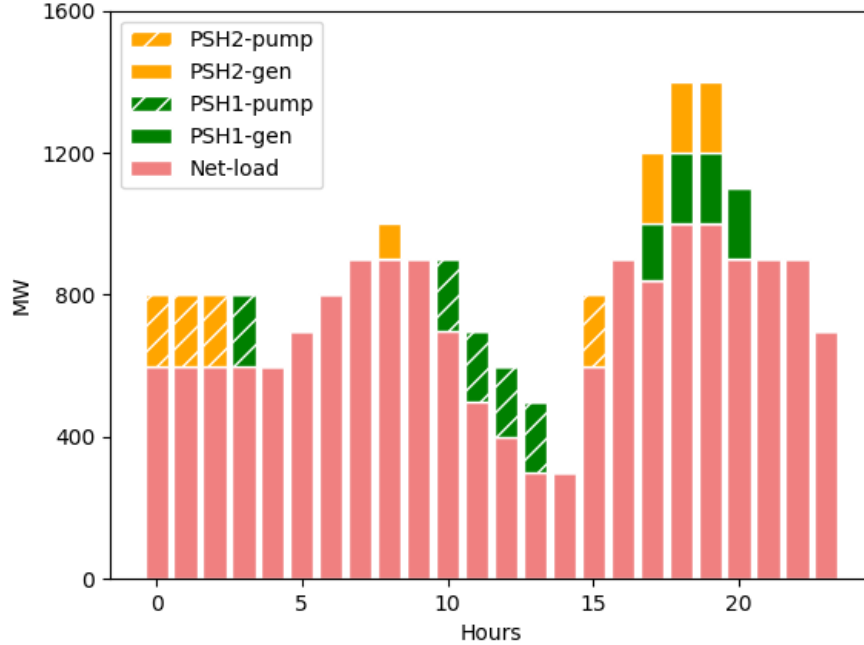
Figure 6.4: Unit Dispatches with Bid Prices for Pump Loads Eliminated.

relieving the system and preventing generation shortage and price spikes.

Second, in Fig. 6.4, it is clearly observed that PSH units pump when the net-load is low corresponding to a lower LMP when pumping. So, the PSH units will be charged less for their pumping load. In contrast, it is also clear that PSH units generate when the net-load is high corresponding to a higher LMP when the hydro generating. The PSH units will be paid more for their generations in those time intervals. After the bid prices for pump loads been removed, the PSH owners should expect higher profits.

In Table 6.4, the PSH owner's profits are further compared to the so-

Table 6.4: PSH Owner Profits and Social Welfare

	With non-zero pump bid price	With zero pump bid price
	$	$
PSH Profits	-32,000	1,160
System Costs	402,048	380,858

lutions where positive bid prices for pump loads are considered. From Table 6.2, the bid price for pump loads in this study is 27$/MWh. It falls into the range between the cost of the two thermal generators and it is a reasonable price that a PSH owner might bid in this system.

The results show that the bid prices for the pump loads can cause wrong incentives in the problem and result in lost profits for PSH owners. The system generation costs represent the social welfare in the UC and ED problem. Therefore, the wrong incentives caused by the bid prices for pump loads lead the problem to a solution that deviates from the maximum social welfare. As shown in Table 6.4, after we eliminate the bid prices for pump loads, both the PSH owners' profits and the social welfare are improved.

The reservoir state of charge is presented in Fig 6.5. It is straightforward to see that the PSH units store energy into the reservoir at the beginning and the middle of the day and charge the reservoir in the evening. The movement of the stored energy in the reservoir is also a demonstration that social welfare is maintained.
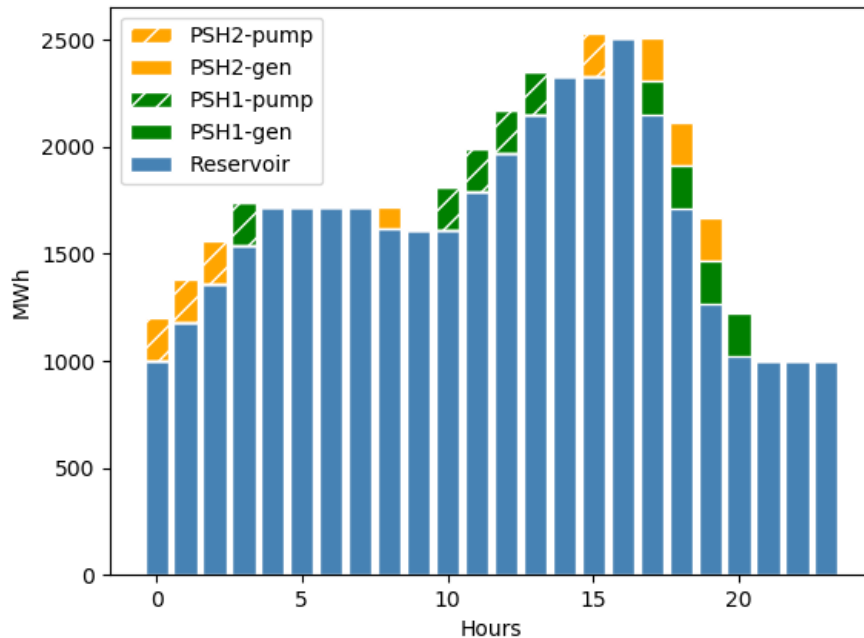
Figure 6.5: Reservoir State of Charges with Bid Prices for Pump Loads Eliminated.

6.5.3 Sensitivity Analysis on the Generation and Pump Efficiencies

In this section, we discuss the effects of efficiency lost at generation and pump modes in a PSHU to the dispatch solutions in the unit commitment problem. The formulation that removes the non-zero bid prices for pump load described in Section 6.5.2 is used in this study. The parameters for the case study remain the same from Table 6.2 except for the efficiency at PSH1 which is highlighted in Table 6.5.

With the changed efficiency at PSH1 in Table 6.5, PSH1 has a lower pumping efficiency and a higher generating efficiency compare to PSH2 while

152

Unit	Cost/Price $/MWh	$\underline{q}^m$ MW	$\overline{q}^m$ MW	η_g^m
1: PSH1 Pump	27	200	200	0.81
2: PSH1 Gen	0	100	200	1
3: PSH2 Pump	27	200	200	0.9
4: PSH2 Gen	0	100	200	0.9

the round loop efficiency for both units are still the same.
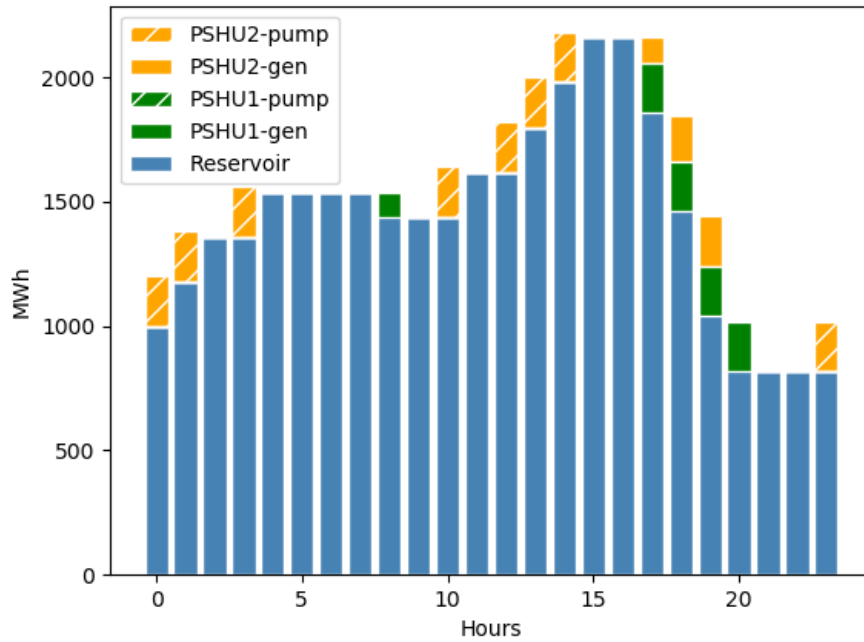
Figure 6.6: Reservoir State of Charges with Sensitivity Analysis on PSH Efficiencies.

Figure 6.6 shows the state of charges of the reservoir in dispatch results.

We observe that PSH1 only generates and all the pump loads are from unit PSH2. The results indicate that the system is using the best of the high efficiencies of pump at PSH1 and generation at PSH2. Therefore, the system objective is reduced to \$378,436. The profits of the PSH units would be increased if both units belong to a single owner for the same reason. However, if the two units belong to two separate owners, then the PSH1 would make more profits by its high efficient generation and PSH2 may lose profits because its high efficient pump even if their round loop efficiencies are the same.

In the proposed formulation, we removed the generation costs and bid prices of a pumped-storage hydro unit in the objective function as discussed in Section 6.5.1 and Section 6.5.2. Then the only cost from a pumped-storage hydro unit in the proposed model is from its efficiency lost presented in the state of charge constraints in (6.9). This accurately reflects the operational characteristics of a pumped-storage unit and serve the purpose of maximizing the social welfare. The sensitivity analysis in this section also shows that the proposed formulation creates incentives for the owners who share a reservoir to install PSH units with a high generation efficiency and a low pump efficiency.

6.6 Summary

In this chapter, a configuration based pumped-storage hydro model in the day-ahead market is presented. Because of the pump "block load" feature and the minimum limit of the generations, the operation of a pump storage hydro unit is difficult to fit into a model that requires the unit to be either

pumping or generating at any given time. Introducing the three configurations model with generating, pumping, and "alloff" configurations can resolve this issue. In addition, the proposed formulation is flexible to model the transition between any pair of configurations if the transition takes more than one time interval or incurs with additional costs.

A numerical study is presented with two identical PSH units in a PSH plant sharing a reservoir. The effectiveness of the pumped-storage hydro units in the proposed model are demonstrated with examples. The bid prices for pump loads are discussed. The disadvantages of including positive bid prices for pump loads and their negative effects on social welfare are presented with quantified simulation results. Sensitivity analysis on the efficiency of a pumped-hydro unit is presented.

The implementation of the proposed formulation in a MISO prototype UC model is ongoing. Future work will be done with case studies in the MISO system. The compactness of the formulation will be further discussed and the computational results will be presented with MISO large case studies.

Chapter 7

Conclusions and Future Work

This dissertation has proposed mixed-integer programming formulations of two power system problems, namely the interdiction problem and the unit commitment problem. We present the conclusion in two sections, each correspond to a part of this dissertation.

7.1 Interdiction Problem

7.1.1 Cascading Outage Analysis (COA)

Comprehensive outage studies in power systems are described before the presentation of an interdiction problem. An enhanced COA model is illustrated in a case study of a test system. The model provides a way to evaluate the short term impacts of an attack, e.g. the amount of short-term load shed. The COA model applies four outage checkers, namely Transient Stability Checker, Frequency Outage Checker, Overload Outage Checker, and Voltage Outage Checker to simulate the system behavior after an initial disturbance, i.e. an attack. The contributions of this work are as follows. First, the cascading outage analysis model is converted to the Python environment and it is easier to connect the COA to other models or other software. Second, the

156

current COA code is fully automated and can directly read initiating events from a database, modify the case study, and run transient and steady state analysis. Third, the frequency checker (as under and over frequency protection relays) is incorporated into the transient analysis. It gives two advantages to the model, namely, actual frequency response is used by relays instead of system wide approximation, and since it is part of the transient analysis, if the protection relay takes any action, the impact of that action on transient analysis is automatically considered.

Nevertheless, the cascading outage analysis still has several limitations. Potential improvements include:

- The cascading outage analysis model uses a set of predetermined parameters and settings for protection devices. In the industry applications, different coordinations and settings among various protection schemes may lead to different system behavior.
- There are some control schemes in power systems, including controlled islanding schemes and automatic tap changers, etc that are not modeled in the cascading outage analysis tool. These sophisticated models could be incorporated and studied to make the simulation results more reflective of reality.

7.1.2 Cyber Attack

Using the developed COA model, different cyber attacks in power sytems have been studied. From the simulation results of cyber attacks tar-

157

geted on grid control centers, we find that the number of transmission lines outaged at a given voltage level in the attacked TDSP is critical as a predictor of algorithmic non-convergence. There exists a threshold at each voltage level such that an algorithmic non-convergence will occur when the attacked TDSP has more branches tripped than the threshold. We also observe that if the system survives from the contingency, then an attack on a TDSP with more branches at the lower voltage levels would cause more load lost.

We simulated of IoT demand increase attacks at different scales including a 1% of load increase attack, a 10% of sudden load increase attack and a 30% of sudden load increase attack. The simulation shows the actions of UFLS and over frequency protection are sufficient to prevent an immediate system failure or cascading failures in the transmission system in short time scales after the attack. Additional actions may be needed at longer time scales after a 30% load increase attack to restore the stable operation of the system, but a system blackout will likely not occur in these situations.

In addition, a "frequency swing attack" is defined as a cycle of load increase and decrease IoT attack that aims to push the frequency swing to violate the frequency protection thresholds in the system. However, the frequency swing attack doesn't show an ability to cause an immediate disconnection of generators. A possible repeated frequency swing attack has been discussed. The impacts of depleting the UFLS resources are discussed. The analysis shows the effectiveness of such attack would be impacted by any additional frequency protection measures in the system.

The cyber attack simulations have certain limitations and future work can be done to extend this work:

- The results from transient simulations can be more precise if a detailed transient data for a large system becomes available.

- The protections considered in this study is a subset of the protections in power systems that would contribute to a cascading outage after a disturbance in the system. However, future work can be done to explore the impacts from other protections that are commonly equipped in the power systems.

- In the study of IoT demand attacks, we considered only an IoT demand attack that is evenly distributed across all the load points in the system. However, in the future work, we will consider IoT demand attacks targeting only a part of the system.

7.1.3   Interdiction Problem with COA Model

Based on the knowledge learned from the comprehensive study of cascading outages and cyber attacks in power systems, an interdiction problem is reformulated to include the COA model to consider the short-term impacts of attacks. The Global Benders Decomposition method with the COA model as the sub-problem is implemented in a 37 bus test system. Because of the cascading effects, it is difficult to find valid Bender's cuts. However, with a good "importance" measurement for elements in the master problem, it is still feasible to find a close to optimal solution.

We discovered some approximate linear correlations between the total disrupted power flows in an attack and the load lost post attack under the simulation with COA model. A similar correlation is observed in the 37 Bus system. This correlation is used for generating Bender's cuts in the GLBD algorithm. Case studies and tests in the 37 Bus system shown the efficiency of the proposed method. The computational effects of the proposed method is discussed.

7.2 Unit Commitment Problem

7.2.1 Combined Cycle Unit Formulation

A mixed-integer programming formulation that represents the transition ramping of CCUs and removes an invalid assumption of single interval transition is summarized from [181]. Configuration-wise ramping constraints are formulated and compared with the plant-wise ramping constraints that were developed in [181]. The transition ramping model is implemented with configuration-component hybrid CC model in a MISO prototype UC tool. Computational results on a MISO system show a moderate increase in computational complexity when transition ramping modeling is considered. The problem sizes of the transition ramping model with different ramping constraints are presented and discussed.

Although the formulation and discussion of the transition ramping model in this dissertation are dedicated to a combined cycle unit, they can be extended and applied to the modeling of units with similar features in the

system. This will be discussed for pumped-storage hydro.

7.2.2 Pumped Storage Hydro Unit

A configuration based pumped storage hydro model in the day-ahead market is presented. Because of the pump "block load" feature and the minimum limit of the generations, the operation of a pump storage hydro unit is difficult to fit into a model that requires the unit to be either pumping or generating at a given time. Introducing the three configurations model with generating, pumping and "alloff" configurations can resolve this issue. In addition, the proposed formulation is flexible to model the transition between any pair of configurations if the transition takes more than one time interval or involves additional costs.

A numerical study is presented with two identical PSH units in a PSH plant sharing a reservoir. The effectiveness of the pumped storage hydro units in the proposed model are demonstrated with examples. The disadvantages of including positive bid prices for pump loads and their negative effects on social welfare are discussed with quantified simulation results. Sensitivity analysis on the efficiency of a pumped-hydro unit is discussed.

The implementation of the proposed formulation in a MISO prototype UC model is ongoing. Future work will be done with case studies in the MISO system. The compactness of the formulation will be further discussed and the computational results will be presented with MISO large case studies.

Appendices

Appendix A

Capacity Constraints at Pumped Storage Hydro Model

We formalize the linerization of the capacity constraint for a pumped storage hydro unit in the following remark.

Remark 1. By definition of efficiency, $\eta_g^h \geq 0$. Note that $e_{g,t} \geq 0$ from (6.12). Then, the capacity constraints described in the right-hand side of (6.7) is equivalent to (A.1) and thereby can be linearized as (A.2).

$$q_{g,t}^h \leq \min\{\overline{P}_g^h u_{gt}^h, \eta_g^h e_{r,t}\} \quad \forall r \in R \quad \forall g \in G_{sh,r} \quad \forall t \in T \qquad \text{(A.1)}$$

$$q_{g,t}^h \leq \overline{P}_g^h u_{gt}^h \quad q_{g,t}^h \leq \eta_g^h e_{r,t} \quad \forall r \in R \quad \forall g \in G_{sh,r} \quad \forall t \in T \qquad \text{(A.2)}$$

Proof of Remark 1

Linearize (A.1) to (A.2) is a standard linearization on a minimum operation and it is straightforward. The proof would show the equivalence between right-hand side of (6.7) and (A.1).

We would show the equivalence of two conditions based on the binary variable u_{gt}^h:

$u_{gt}^h = 1$:

right-hand side of (6.7) = (A.1) $\Rightarrow$

$q_{g,t}^h \leq \min\{\overline{P}_g^h, \eta_g^h e_{r,t}\}$ $\forall r \in R$ $\forall g \in G_{sh,r}$ $\forall t \in T$,

$u_{gt}^h = 0$:

right-hand side of (6.7) $\Rightarrow q_{g,t}^h \leq 0$ $\forall r \in R$ $\forall g \in G_{sh,r}$ $\forall t \in T$,

$(A.1) \Rightarrow q_{g,t}^h \leq \min\{0, \eta_g^h e_{r,t}\}$ $\forall r \in R$ $\forall g \in G_{sh,r}$ $\forall t \in T$,

$\because \eta_g^h \geq 0$ and $e_{r,t} \geq 0$ $\forall r \in R$ $\forall g \in G_{sh,r}$ $\forall t \in T$,

$\Rightarrow \eta_g^h e_{r,t} \geq 0$ $\forall r \in R$ $\forall g \in G_{sh,r}$,

$\Rightarrow \min\{0, \eta_g^h e_{r,t}\} = 0$ $\forall r \in R$ $\forall g \in G_{sh,r}$ $\forall t \in T$,

$\therefore$ right-hand side of (6.7) = $(A.1) \Rightarrow$

$q_{g,t}^h \leq 0$ $\forall r \in R$ $\forall g \in G_{sh,r}$ $\forall t \in T$.

Appendix B

Discussion of the Transition with Zero Transition Time

When the transition time is zero in a CCU plant, there is no transition ramping curves. Transitions between two configurations is shown in Fig. B.1.
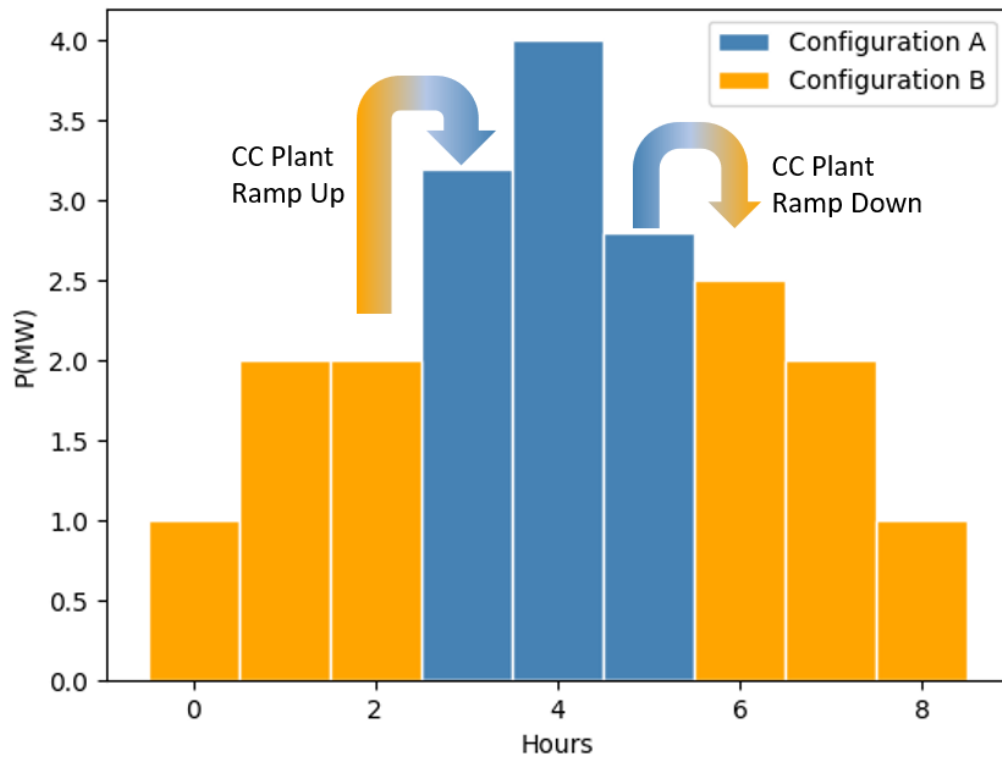
Figure B.1: Illustration of transitions with zero transition time.

For the units with zero transition time, the plant-wise ramping constraints (5.9) and (5.10) are valid with no need for alterations. However, the constants $A(y', y)$ and H^y of those units with zero transition time in configuration-wise ramping constraints (5.11) and (5.12) are changed.

Two conditions, namely CCU plant ramp up from configuration B to A and CCU plant ramp down from configuration A to B shown in Fig. B.1, are considered respectively in the calculation of $A(y', y)$:

$$A(y', y) = I(y', y)\underline{p}^y + (1 - I(y', y))\overline{p}^y \quad \forall y' \in M^{T,y}. \quad \text{(B.1)}$$

where:

$$I(y', y) = \begin{cases} 1, & \text{if } \overline{p}^{y'} < \overline{p}^y, \text{ CCU ramp up} \\ 0, & \text{if } \overline{p}^{y'} > \overline{p}^y, \text{ CCU ramp down} \end{cases} \quad \forall y' \in M^{T,y}.$$

$$H^y = \overline{p}^y \ \forall y. \quad \text{(B.2)}$$

After the substitution, when a transition between configurations occurs, the configuration-wise ramping constraints (5.11) and (5.12) applied on the start up configuration are in two conditions:

- When the CCU ramps up (e.g. configuration A starts up when the plant ramps up in Fig. B.1):

$$p_t^y \leq R_U^y + \underline{p}^y \ \forall t, \forall y. \quad \text{(5.11')}$$

$$p_t^y \geq \underline{p}^y - R_D^y \ \forall t, \forall y. \quad \text{(5.12')}$$

Constraint (5.11') indicates that, due to the ramping constraints, the maximum output of the start up configuration is its lower bound plus

166

the ramp up rate. Constraint (5.12') would limit the output of the start up configuration to be greater than its lower bound minus the ramp down rate. However, since the output of the configuration is always greater than its lower bound, constraint (5.12') would never be active.

- When the CCU ramps down (e.g. configuration B starts up when the plant ramps down in Fig. B.1):

$$p_t^y \leq R_U^y + \overline{p}^y \; \forall t, \forall y. \tag{5.11''}$$

$$p_t^y \geq \overline{p}^y - R_D^y \; \forall t, \forall y. \tag{5.12''}$$

Constraint (5.12'') indicates that, due to the ramping constraints, the minimum output of the start up configuration is its upper bound minus the ramp down rate. Constraint (5.11'') would limit the output of the start up configuration to be less than its upper bound plus the ramp up rate. However, since the output of the configuration is always less than its upper bound, constraint (5.11'') would never be active.

After the substitution, when a transition between configurations occurs, the configuration-wise ramping constraints (5.11) and (5.12) applied on the shut down configuration become:

- Shut down configuration:

$$q_{t-1}^y \geq 0 \; \forall t, \forall y. \tag{5.11''}$$

167

$$q_{t-1}^y \leq \overline{q}^y \ \forall t, \forall y. \tag{5.12"}$$

That is, when a configuration shuts down in a transition, constraints (5.11") and (5.12") would never apply additional limits to the output of the configuration.

Notice that, the transition data required for this calculation and substitution of the constants is available off-line. Therefore, the operation of substituting the constants of the unit with zero transition time will not impact the formulation and computation in the optimization.

Bibliography

[1] A. Cherepanoy. A New Threat for Industry Control Systems. Technical report, ESET, 2017.

[2] ABB. Time over/under voltage relay and protection assemblies model RXEDK 2h and RAEDK user manual. `www.abb.com/product/us/9AAC30405217.aspx`, ABB Inc, 2004.

[3] M. Selim Aktürk, Alper Atamtürk, and Sinan Gürel. A strong conic quadratic reformulation for machine-job assignment with controllable processing times. *Operations Research Letters*, 37(3):187–191, 2009.

[4] Yousef M. Al-Abdullah, Ahmed Salloum, Kory W. Hedman, and Vijay Vittal. Analyzing the Impacts of Constraint Relaxation Practices in Electric Energy Markets. *IEEE Transactions on Power Systems*, 31(4):2566–2577, July 2016.

[5] R Alamian, M Behbahani-Nejad, and A Ghanbarzadeh. A state space model for transient flow simulation in natural gas pipelines. *Journal of Natural Gas Science and Engineering*, 9:51–59, 2012.

[6] David L Alderson, Gerald G Brown, W Matthew Carlyle, and R Kevin Wood. Solving defender-attacker-defender models for infrastructure defense. In R. Kevin Wood and Robert. F. Dell, editors, *Operations*

Research, Computing, and Homeland Defense, pages 28–49. Hanover, MD, 2011.

[7] R Allan and R Billinton. Probabilistic assessment of power systems. *Proc. IEEE*, 88(2):140–162, 2000.

[8] Omar Alrawi, Chaz Lever, Manos Antonakakis, and Fabian Monrose. Sok: Security evaluation of home-based iot deployments. In *SoK: Security Evaluation of Home-Based IoT Deployments*, page 0. IEEE.

[9] Rogelio E Alvarez. *Interdicting electrical power grids*. PhD thesis, Monterey, California. Naval Postgraduate School, 2004.

[10] Sajjad Amini, Fabio Pasqualetti, and Hamed Mohsenian-Rad. Dynamic load altering attacks against power system stability: Attack models and protection schemes. *IEEE Transactions on Smart Grid*, 9(4):2862–2872, 2018.

[11] Sami Ammari and Kwok W. Cheung. Advanced combined-cycle modeling. *2013 IEEE Grenoble Conference PowerTech, POWERTECH 2013*, 2013.

[12] Seungwon An, Qing Li, and T.W. Gedra. Natural gas and electricity optimal power flow. In *2003 IEEE PES Transmission and Distribution Conference and Exposition (IEEE Cat. No.03CH37495)*, volume 1, pages 138–143. IEEE, 2003.

[13] George Anders. Commitment techniques for combined-cycle generating units. Technical report, 2005.

[14] Philip M Anderson and M˷ Mirheydar. A low-order system frequency response model. *IEEE Transactions on Power Systems*, 5(3):720–729, 1990.

[15] Manos Antonakakis, Tim April, Michael Bailey, Matt Bernhard, Elie Bursztein, Jaime Cochran, Zakir Durumeric, J Alex Halderman, Luca Invernizzi, Michalis Kallitsis, et al. Understanding the mirai botnet. In *USENIX Security Symposium*, pages 1092–1110, 2017.

[16] José M. Arroyo. Bilevel programming applied to power system vulnerability analysis under multiple contingencies. *IET Generation, Transmission & Distribution*, 4(2):178, February 2010.

[17] José M. Arroyo and Francisco D. Galiana. On the solution of the bilevel programming formulation of the terrorist threat problem. *IEEE Transactions on Power Systems*, 20(2):789–797, May 2005.

[18] Siu Kui Au and J L Beck. Important sampling in high dimensions. *Structural Safety*, 25(2):139–163, 2003.

[19] Siu Kui Au and J L Beck. Subset simulation and its application to seismic risk based on dynamic analysis. *Journal of Engineering Mechanics*, 129(8):901–917, 2003.

[20] Siu Kui Au and James L Beck. Estimation of small failure probabilities in high dimensions by subset simulation. *Probabilistic Engineering Mechanics*, 16(4):263–277, 2001.

[21] Siu Kui Au, J Ching, and J L Beck. Application of subset simulation methods to reliability benchmark problems. *Structural Safety*, 29(3):183–193, 2007.

[22] Siu Kui Au and Y Wang. *Engineering Risk Assessment with Subset Simulation*. Singapore: John Wiley & Sons, 2014.

[23] Siu Kui Au, Zhi-Hua Wang, and Siu-Ming Lo. Compartment fire risk analysis by advanced Monte Carlo simulation. *Engineering Structures*, 29(9):2381–2390, 2007.

[24] Frédéric Babonneau, Yurii Nesterov, and Jean-Philippe Vial. Design and operations of gas transmission networks. *Operations research*, 60(1):34–47, 2012.

[25] Egon Balas. Disjunctive programming: Properties of the convex hull of feasible points. *Discrete Applied Mathematics*, 89(1-3):3–44, 1998.

[26] Ross Baldick. The generalized unit commitment problem. *IEEE Transactions on Power Systems*, 10(1):465–475, 1995.

[27] Ross Baldick, Thekla Boutsika, Jin Hur, Manho Joung, Yin Wu, and Minqi Zhong. Reducing the vulnerability of electric power grids to

terrorist attacks. Technical report, The University of Texas at Austin, 2009.

[28] Mapundi K Banda and Michael Herty. Multiscale modeling for gas flow in pipe networks. *Mathematical Methods in the Applied Sciences*, 31(8):915–936, 2008.

[29] Mapundi K Banda, Michael Herty, and Axel Klar. Gas flow in pipeline networks. *NHM*, 1(1):41–56, 2006.

[30] Jonathan F. Bard. Short-Term Scheduling of Thermal-Electric Generators Using Lagrangian Relaxation. *Operations Research*, 36(5):756–766, October 1988.

[31] Jonathan F. Bard. Some properties of the bilevel programming problem. *Journal of Optimization Theory and Applications*, 68(2):371–378, February 1991.

[32] Jonathan F. Bard. *Practical bilevel optimization: algorithms and applications*. Springer Science & Business Media, Dordrecht, Netherlands, 1998.

[33] Jonathan F. Bard and James E. Falk. An explicit solution to the multi-level programming problem. *Computers & Operations Research*, 9(1):77–100, 1982.

[34] Jonathan F. Bard and James T. Moore. A branch and bound algorithm for the bilevel programming problem. *SIAM Journal on Scientific and Statistical Computing*, 11(2):281–292, 1990.

[35] Clayton Barrows, Marissa Hummon, Wesley Jones, and Elaine Hale. Time Domain Partitioning of Electricity Production Cost Simulations. page 26, 2014.

[36] John P Barton, David G Infield, et al. Energy storage and its use with intermittent renewable energy. *IEEE transactions on energy conversion*, 19(2):441–448, 2004.

[37] Carlos Batlle and Pablo Rodilla. An Enhanced Screening Curves Method for Considering Thermal Cycling Operation Costs in Generation Expansion Planning. *IEEE Transactions on Power Systems*, 28(4):3683–3691, November 2013.

[38] E. M. L. Beale and J. J. H. Forrest. Global optimization using special ordered sets. *Mathematical Programming*, 10(1):52–69, December 1976.

[39] Jacques F Benders. Partitioning procedures for solving mixed-variables programming problems. *Numerische mathematik*, 4(1):238–252, 1962.

[40] Steven J. Benson, Yinyu Yeb, and Xiong Zhang. Mixed linear and semidefinite programming for combinatorial and quadratic optimization. *Optimization Methods and Software*, 11(1-4):515–544, January 1999.

[41] Dimitri Bertsekas. *Nonlinear Programming*. Athena Scientific, 1999.

174

[42] Dimitri Bertsekas and Nils Sandell. Estimates of the duality gap for large-scale separable nonconvex optimization problems. In *1982 21st IEEE Conference on Decision and Control*, pages 782–785, 1982.

[43] Dimitri P. Bertsekas, Gregory S. Lauer, Nils R. Sandell, and Thomas A. Posbergh. Optimal Short-Term Scheduling of Large-Scale Power Systems. *IEEE Transactions on Automatic Control*, 28(1):1–11, 1983.

[44] Zhaohong Bie, Peng Zhang, Gengfeng Li, Bowen Hua, M Meehan, and Xifan Wang. Reliability Evaluation of Active Distribution Systems Including Microgrids. *Power Systems, IEEE Transactions on*, 27(4):2342–2350, 2012.

[45] R Billinton and A Jonnavithula. Composite system adequacy assessment using sequential Monte Carlo simulation with variance reduction techniques. *Generation, Transmission and Distribution, IEE Proceedings-*, 144(1):1–6, 1997.

[46] Roy Billinton and Wenyuan Li. *Reliability assessment of electrical power systems using Monte Carlo methods*. New York: Plenum, 1994.

[47] C.E. Blair and R.G. Jeroslow. The value function of a mixed integer program: I. *Discrete Mathematics*, 19(2):121–138, 1977.

[48] Bill Blevins. Combined-cycle unit modeling in the nodal design. *ERCOT, Taylor, Texas*, 2007.

[49] Severin Borenstein. Peak-Time Rebates: Money for Nothing?, 2014.

[50] Conrado Borraz-Sanchez. Optimization methods for pipeline transportation of natural gas. 2010.

[51] François Bouffard and Francisco D Galiana. Stochastic Security for Operations Planning With Significant Wind Power Generation. 23(2):306–316, 2008.

[52] Meherwan P Boyce. Handbook for cogeneration and combined cycle power plants. 2004.

[53] Stephen Boyd and Lieven Vandenberghe. *Convex Optimization*. Cambridge University Press, 2004.

[54] Gerald G. Brown, W. Matthew Carlyle, Robert C. Harney, Eric M. Skroch, and R. Kevin Wood. Interdicting a Nuclear-Weapons Project. *Operations Research*, 57(4):866–877, August 2009.

[55] Gerald G. Brown, W. Matthew Carlyle, Javier Salmerón, and R. Kevin Wood. Defending critical infrastructure. *Interfaces*, 36(6):530–544, December 2006.

[56] Paul D Brown, JA Peças Lopes, and Manuel A Matos. Optimization of pumped storage capacity in an isolated power system with large renewable penetration. *IEEE Transactions on Power systems*, 23(2):523–531, 2008.

[57] Charles D Brummitt, Paul D H Hines, Ian Dobson, Cristopher Moore, and Raissa M D'Souza. Transdisciplinary electric power grid science.

Proceedings of the National Academy of Sciences of the United States of America, 110(30):12159, July 2013.

[58] Waqquas A. Bukhsh, Andreas Grothey, Ken I M McKinnon, and Paul A. Trodden. Local solutions of the optimal power flow problem. *IEEE Transactions on Power Systems*, 28(4):4780–4788, 2013.

[59] Sergey V Buldyrev, Roni Parshani, Gerald Paul, H Eugene Stanley, and Shlomo Havlin. Catastrophic cascade of failures in interdependent networks. *Nature*, 464(7291):1025–8, April 2010.

[60] Francesco Cadini, Diana Avram, Nicola Pedroni, and Enrico Zio. Subset Simulation of a reliability model for radioactive waste repository performance assessment. *Reliability Engineering & System Safety*, 100:75–83, 2012.

[61] Michael Cadwalader, Paul Gribik, William Hogan, and Susan Pope. Extended LMP and Financial Transmission Rights. Technical report, Harvard University, 2010.

[62] Michael Caramanis, Elli Ntakou, William W. Hogan, Aranya Chakrabortty, and Jens Schoene. Co-optimization of power and reserves in dynamic T&D power markets with nondispatchable renewable generation and distributed energy resources. *Proceedings of the IEEE*, 104(4):807–836, 2016.

[63] M. Carrion and J.M. Arroyo. A Computationally Efficient Mixed-Integer Linear Formulation for the Thermal Unit Commitment Problem. *IEEE Transactions on Power Systems*, 21(3):1371–1378, August 2006.

[64] L M Carvalho, R A Gonzalez-Fernandez, A M da Silva, M da Rosa, and V Miranda. Simplified Cross-Entropy Based Approach for Generating Capacity Reliability Assessment. *IEEE Trans. Power Syst.*, 28(2):1609–1616, 2013.

[65] Defense Use Case. Analysis of the cyber attack on the ukrainian power grid. *Electricity Information Sharing and Analysis Center (E-ISAC)*, 2016.

[66] Edgardo D Castronuovo and JA Peças Lopes. On the optimization of the daily operation of a wind-hydro power plant. *IEEE Transactions on Power Systems*, 19(3):1599–1606, 2004.

[67] Edgardo D Castronuovo and Joao A Pecas Lopes. Optimal operation and hydro storage sizing of a wind–hydro power plant. *International Journal of Electrical Power & Energy Systems*, 26(10):771–778, 2004.

[68] Hale Cetinay, Saleh Soltan, Fernando A Kuipers, Gil Zussman, and Piet Van Mieghem. Analyzing cascading failures in power grids under the ac and dc power flow models. *SIGMETRICS Performance Evaluation Review*, 45(3):198–203, 2017.

[69] G. W. Chang, G. S. Chuang, and T. K. Lu. A simplified combined-cycle unit model for mixed integer linear programming-based unit commitment. In *2008 IEEE Power and Energy Society General Meeting - Conversion and Delivery of Electrical Energy in the 21st Century*, pages 1–6. IEEE, July 2008.

[70] Hsiao-Dong Chang, Chia-Chi Chu, and Gerry Cauley. Direct stability analysis of electric power systems using energy functions: theory, applications, and perspective. *Proceedings of the IEEE*, 83(11):1497–1529, 1995.

[71] Modassar Chaudry, Nick Jenkins, and Goran Strbac. Multi-time period combined gas and electricity network optimisation. *Electric Power Systems Research*, 78(7):1265–1279, July 2008.

[72] Modassar Chaudry, Jianzhong Wu, and Nick Jenkins. A sequential Monte Carlo model of the combined GB gas and electricity network. *Energy Policy*, 62:473–483, 2013.

[73] Bo Chen, Nishant Pattanaik, Ana Goulart, Karen L Butler-Purry, and Deepa Kundur. Implementing attacks for modbus/tcp protocol in a real-time cyber physical system test bed. In *Communications Quality and Reliability (CQR), 2015 IEEE International Workshop Technical Committee on*, pages 1–6. IEEE, 2015.

[74] Guo Chen, Zhao Yang Dong, David J Hill, and Yu Sheng Xue. Exploring

reliable strategies for defending power systems against targeted attacks. *IEEE Transactions on Power Systems*, 26(3).

[75] Jie Chen, James S Thorp, and Ian Dobson. Cascading dynamics and mitigation assessment in power system disturbances via a hidden failure model. *International Journal of Electrical Power & Energy Systems*, 27(4):318–326, 2005.

[76] Quan Chen and L Mili. Composite Power System Vulnerability Evaluation to Cascading Failures Using Importance Sampling and Antithetic Variates. *IEEE Trans. Power Syst.*, 28(3):2321–2330, 2013.

[77] Richard Li-Yang Chen, Amy Cohn, Neng Fan, and Ali Pinar. Contingency-risk informed power system design. *IEEE Transactions on Power Systems*, 29(5):2087–2096, 2014.

[78] Yonghong Chen, Aaron Casto, Fengyu Wang, Qianfan Wang, Xing Wang, and Jie Wan. Improving large scale day-ahead security constrained unit commitment performance. *IEEE Transactions on Power Systems*, 31(6):4732–4743, 2016.

[79] Yonghong Chen and Fengyu Wang. Mip formulation improvement for large scale security constrained unit commitment with configuration based combined cycle modeling. *Electric Power Systems Research*, 148:147–154, 2017.

[80] Yonghong Chen, Fengyu Wang, and Congcong Wang. Miso enhanced combined cycle. *White paper, MISO*, 2018.

[81] Anton Cherepanov. Win32/industroyer, a new threat for industrial control systems. *White paper, ESET (June 2017)*, 2017.

[82] Michael Chertkov, Vladimir Lebedev, and Scott Backhaus. Cascading of Fluctuations in Interdependent Energy Infrastructures: Gas-Grid Coupling. page 13, November 2014.

[83] Hsiao-Dong Chiang, Felix F Wu, and Pravin P Varaiya. A bcu method for direct analysis of power system transient stability. *IEEE Transactions on Power Systems*, 9(3):1194–1208, 1994.

[84] Eastern Interconnection Planning Collaborative. Gas-Electric System Interface Study Target 3: Natural Gas and Electric System Contingency Analysis. Technical report, 2015.

[85] Benoît Colson, Patrice Marcotte, and Gilles Savard. An overview of bilevel optimization. *Annals of Operations Research*, 153(1):235–256, April 2007.

[86] Cong Liu, M. Shahidehpour, Zuyi Li, and M. Fotuhi-Firuzabad. Component and Mode Models for the Short-Term Scheduling of Combined-Cycle Units. *IEEE Transactions on Power Systems*, 24(2):976–990, May 2009.

[87] Kelly J. Cormican, David P. Morton, and R. Kevin Wood. Stochastic network interdiction. *Operations Research*, 46(2):184–197, April 1998.

[88] Gérard Cornuéjols. Valid inequalities for mixed integer linear programs. *Mathematical Programming*, 112(1):3–44, 2007.

[89] J-M Coron, Brigitte D'Andrea-Novel, and Georges Bastin. A strict Lyapunov function for boundary control of hyperbolic systems of conservation laws. *Automatic Control, IEEE Transactions on*, 52(1):2–11, 2007.

[90] North American Electric Reliability Corporation. Standard TOP-004-0 Transmission Operations. Technical report, 2005.

[91] North American Electric Reliability Corporation. Reliability Concepts-Version 1.0.2. Technical report, 2007.

[92] C. M. Correa-Posada and Pedro Sánchez-Mart\in. Gas network optimization: A comparison of piecewise linear models. *Optimization Online*, 2014.

[93] Carlos M. Correa-Posada and Pedro Sanchez-Martin. Security-Constrained Optimal Power and Natural-Gas Flow. *IEEE Transactions on Power Systems*, 29(4):1780–1787, July 2014.

[94] Carlos M. Correa-Posada and Pedro Sanchez-Martin. Integrated Power and Natural Gas Model for Energy Adequacy in Short-Term Opera-

182

tion. *IEEE Transactions on Power Systems*, 30(6):3347–3355, November 2015.

[95] National Research Council et al. *Terrorism and the electric power delivery system.* National Academies Press, 2012.

[96] A M da Silva, L C de Resende, L A da Fonseca Manso, and R Billinton. Well-being analysis for composite generation and transmission systems. *IEEE Trans. Power Syst.*, 19(4):1763–1770, 2004.

[97] Adrian Dabrowski, Johanna Ullrich, and Edgar R Weippl. Grid shock: Coordinated load-changing attacks on power grids: The non-smart power grid is vulnerable to cyber attacks as well. In *Proceedings of the 33rd Annual Computer Security Applications Conference*, pages 303–314. ACM, 2017.

[98] Chenxi Dai, Yonghong Chen, Fengyu Wang, Jie Wan, and Lei Wu. A configuration-component based hybrid model for combined-cycle units in miso day-ahead market. *IEEE Transactions on Power Systems*, 2018.

[99] Pelin Damc-Kurt, Simge Küçükyavuz, Deepak Rajan, and Alper Atamtürk. A polyhedral study of production ramping. *Mathematical Programming*, 158(1-2):175–205, July 2016.

[100] Cedric De Jonghe, Erik Delarue, Ronnie Belmans, and William D'haeseleer. Determining optimal electricity technology mix with high level of wind power penetration. *Applied Energy*, 88(6):2231–2238, 2011.

[101] Cedric De Jonghe, Benjamin F. Hobbs, and Ronnie Belmans. Optimal Generation Mix With Short-Term Demand Response and Wind Penetration. *IEEE Transactions on Power Systems*, 27(2):830–839, 2012.

[102] Claudio De Persis and Carsten Skovmose Kallesoe. Pressure regulation in nonlinear hydraulic networks by positive and quantized controls. *Control Systems Technology, IEEE Transactions on*, 19(6):1371–1383, 2011.

[103] Daniel De Wolf and Yves Smeers. Mathematical properties of formulations of the gas transmission problem. Technical report, Université libre de Bruxelles, 1994.

[104] Daniel De Wolf and Yves Smeers. The gas transmission problem solved by an extension of the simplex algorithm. *Management Science*, 46(11):1454–1465, November 2000.

[105] Andrés Delgadillo, José Manuel Arroyo, and Natalia Alguacil. Analysis of electric grid interdiction with line switching. *IEEE Transactions on Power Systems*, 25(2):633–641, May 2010.

[106] S. Dempe and J. Dutta. Is bilevel programming a special case of a mathematical program with complementarity constraints? *Mathematical Programming*, 131(1-2):37–48, February 2010.

[107] S. Dempe and S. Franke. On the solution of convex bilevel optimization

problems. *Computational Optimization and Applications*, 63(3):685–703, September 2016.

[108] Stephan Dempe. Discrete Bilevel Optimization Problems. Technical report, 2001.

[109] Stephan Dempe. Annotated bibliography on bilevel programming and mathematical programs with equilibrium constraints. *Optimization*, 52(1):333–359, 2003.

[110] Scott DeNegre. *Interdiction and discrete bilevel linear programming*. PhD thesis, Lehigh University, 2011.

[111] Tamara Denning, Tadayoshi Kohno, and Henry M Levy. Computer security and the modern home. *Communications of the ACM*, 56(1):94–103, 2013.

[112] Mark Dickison, S. Havlin, and H. E. Stanley. Epidemics on interconnected networks. *Physical Review E*, 85(6):066109, June 2012.

[113] Jody Dillon, Daniel J. Burke, Mark J. O'Malley, and Aidan Tuohy. Should unit commitment be endogenously included in wind power transmission planning optimisation models? *IET Renewable Power Generation*, 8(2):132–140, March 2014.

[114] Pia Domschke, Bjorn Geißler, Oliver Kolb, Jens Lang, Alexander Martin, and Antonio Morsi. Combination of nonlinear and linear optimization of

transient gas networks. *INFORMS Journal on Computing*, 23(4):605–617, November 2011.

[115] Y Dong and HR Pota. Fast transient stability assessment using large step-size numerical integration. In *IEE Proceedings C (Generation, Transmission and Distribution)*, volume 138, pages 377–383. IET, 1991.

[116] C A Dorao and M Fernandino. Simulation of transients in natural gas pipelines. *Journal of Natural Gas Science and Engineering*, 3(1):349–355, 2011.

[117] Duke Energy. Peak Time Rebate Pilot Program.

[118] Álvaro Jaramillo Duque, Edgardo D Castronuovo, Ismael Sánchez, and Julio Usaola. Optimal operation of a pumped-storage hydro plant that compensates the imbalances of a wind power producer. *Electric power systems research*, 81(9):1767–1777, 2011.

[119] ENTSO-E. Technical report, ENTSO-E.

[120] EPIS. AURORAxmp Database, Accessed on April 09, 2016.

[121] ERCOT. ERCOT Protocols Section 4: Day-Ahead Operations, 2016.

[122] ERCOT. Underfrequency load shedding 2006 assessment and review, Dec 18, 2016.

[123] ERCOT. Ercot nodal operating guides section 2 system operations and control requirements. `www.ercot.com/content/wcm/current_guides/53525/02_030116.doc`, ERCOT, 2016.

[124] ERCOT. Ercot nodal operating guides section 4 emergency operations. `http://www.ercot.com/content/wcm/libraries/147359/February_1__2018_Nodal_Operating_Guide.pdf`, ERCOT, 2018.

[125] M. J. Bertin et al. *Pisot and Salem Numbers.* user Verlag, Berlin, 1992.

[126] A Fabbri, T G S Roman, J R Abbad, and V H M Quezada. Assessment of the Cost Associated With Wind Generation Prediction Errors in a Liberalized Electricity Market. *Power Systems, IEEE Transactions on*, 20(3):1440–1446, 2005.

[127] James E. Falk. Lagrange Multipliers and Nonconvex Programs. *SIAM Journal on Control*, 7(4):534–545, 1969.

[128] Lei Fan and Yongpei Guan. An Edge-Based Formulation for Combined-Cycle Units. *IEEE Transactions on Power Systems*, 31(3):1809–1819, May 2016.

[129] Lei Fan, Kai Pan, and Yongpei Guan. A strengthened mixed-integer linear programming formulation for combined-cycle units. *European Journal of Operational Research*, 2018.

[130] Diana Fanghänel and Stephan Dempe. Bilevel programming with discrete lower level problems. *Optimization*, 58(8):1029–1047, November 2009.

[131] Federal Energy Regulatory Commission. Order No. 745.

[132] Federal Energy Regulatory Commission and North American Electric Reliability Corporation. Arizona-Southern California Outages on September 8,2011 - Causes and Recommendations. Technical report, 2012.

[133] Feng Pan, Yonghong Chen, David Sun and Ed Rothberg. High-Performance Power-Grid Optimization (HIPPO) for Flexible and Reliable Resource Commitment against Uncertainties, 2016.

[134] FERC. Price Formation in Energy and Ancillary Services Markets Operated by Regional Transmission Organizations and Independent System Operators. Technical report, FERC, 2015.

[135] Earlence Fernandes, Jaeyeon Jung, and Atul Prakash. Security analysis of emerging smart home applications. In *2016 IEEE Symposium on Security and Privacy (SP)*, pages 636–654. IEEE, 2016.

[136] Travis Fisher. 'Demand Response' in Electricity: Economists vs. FERC on (Over)Pricing, 2012.

[137] Christodoulos A. Floudas. *Nonlinear and mixed-integer optimization: fundamentals and applications.* Oxford University Press, New York, 1995.

188

[138] Christodoulos A. Floudas and V. Visweswaran. A global optimization algorithm (GOP) for certain classes of nonconvex NLPs—I. Theory. *Computers & Chemical Engineering*, 14(12):1397–1417, 1990.

[139] Task Force. Final report on the august 14, 2003 blackout in the united states and canada: Causes and recommendations, us-canada power system outage task force, 2004.

[140] José Fortuny-Amat and Bruce McCarl. A representation and economic interpretation of a two-level programming problem. *The Journal of the Operational Research Society*, 32(9):783–792, September 1981.

[141] Abdel-Azia Fouad and Vijay Vittal. *Power system transient stability analysis using the transient energy function method*. Pearson Education, 1991.

[142] Antonio Frangioni and Claudio Gentile. Solving Nonlinear Single-Unit Commitment Problems with Ramping Constraints. *Operations Research*, 54(4):767–775, 2006.

[143] Yong Fu, Zuyi Li, and Lei Wu. Modeling and Solution of the Large-Scale Security-Constrained Unit Commitment. *IEEE Transactions on Power Systems*, 28(4):3524–3533, November 2013.

[144] Lingwen Gan, Na Li, Ufuk Topcu, and Steven H. Low. Exact Convex Relaxation of Optimal Power Flow in Radial Networks. *IEEE Transactions on Automatic Control*, 60(1):72–87, January 2015.

[145] Javier Garcia-Gonzalez, Rocio Moraga Ruiz de la Muela, Luz Matres Santos, and Alicia Mateo Gonzalez. Stochastic joint optimization of wind generation and pumped-storage units in an electricity market. *IEEE Transactions on Power Systems*, 23(2):460–468, 2008.

[146] T.W. Gedra. Natural gas and electricity optimal power flow. In *2003 IEEE PES Transmission and Distribution Conference and Exposition (IEEE Cat. No.03CH37495)*, volume 1, pages 138–143. IEEE, 2003.

[147] Arthur M. Geoffrion. Generalized benders decomposition. *Journal of optimization theory and applications*, 10(4):237–260, 1972.

[148] Arthur M. Geoffrion. Lagrangean relaxation for integer programming. *Approaches to Integer Programming*, 2:82–114, 1974.

[149] J Duncan Glover, Mulukutla S Sarma, and Thomas Overbye. *Power System Analysis & Design, SI Version*. Cengage Learning, 2012.

[150] Jean-Louis Goffin and Jean-Philippe Vial. Convex nondifferentiable optimization: A survey focused on the analytic center cutting plane method. *Optimization Methods and Software*, 17(5):805–867, 2002.

[151] Marta C González, César A Hidalgo, and Albert-László Barabási. Understanding individual human mobility patterns. *Nature*, 453(7196):779–82, June 2008.

[152] R A Gonzalez-Fernandez and A M da Silva. Cross-entropy method for reliability worth assessment of renewable generating systems. In *Proc. 17th Power Syst. Computation Conf., 2011.*

[153] R A Gonzalez-Fernandez and A M da Silva. Reliability Assessment of Time-Dependent Systems via Sequential Cross-Entropy Monte Carlo Simulation. *IEEE Trans. Power Syst.*, 26(4):2381–2389, 2011.

[154] R A Gonzalez-Fernandez, A M da Silva, L C Resende, and M T Schilling. Composite Systems Reliability Evaluation Based on Monte Carlo Simulation and Cross-Entropy Methods. *IEEE Trans. Power Syst.*, 28(4):4598–4606, 2013.

[155] Reinaldo Gonzalez-Fernandez and Armando Leite da Silva. Comparison between Different Cross-Entropy Based Methods Applied to Generating Capacity Reliability. In *Proceedings of 12th PMAPS—Probabilistic Methods Applied to Power Systems*, 2012.

[156] Ajit Gopalakrishnan and Lorenz T Biegler. Economic Nonlinear Model Predictive Control for periodic optimal operation of gas pipeline networks. *Computers & Chemical Engineering*, 52:90–99, 2013.

[157] Michael Grant and Stephen Boyd. CVX: Matlab Software for Disciplined Convex Programming, version 2.1, 2014.

[158] Paul Gribik, William Hogan, and Susan Pope. Market-Clearing Electricity Prices and Energy Uplift. Technical report, Harvard University,

2007.

[159] Sara Grundel, Nils Hornung, Bernhard Klaassen, Peter Benner, and Tanja Clees. Computing Surrogates for Gas Network Simulation using Model Order Reduction. In *Surrogate-Based Modeling and Optimization*, pages 189–212. Springer, 2013.

[160] Sara Grundel, Lennart Jansen, Nils Hornung, Tanja Clees, Caren Tischendorf, and Peter Benner. Model order reduction of differential algebraic equations arising from the simulation of gas transport networks. 2013.

[161] X. Guan, P.B. Luh, H. Yan, and J.A. Amalfi. An optimization-based method for unit commitment. *International Journal of Electrical Power & Energy Systems*, 14(1):9–17, February 1992.

[162] Zeynep H. Gümü and Christodoulos A. Floudas. Global optimization of mixed-integer bilevel programming problems. *Computational Management Science*, 2(3):181–212, July 2005.

[163] Gurobi Optimization Inc. Gurobi optimizer reference manual, 2016.

[164] Jagabondhu Hazra and Avinash K Sinha. Identification of catastrophic failures in power system using pattern recognition and fuzzy estimation. *IEEE Transactions on Power Systems*, 24(1):378–387, 2009.

[165] Kory W. Hedman, Richard P. O'Neill, and Shmuel S. Oren. Analyzing valid inequalities of the generation unit commitment problem. In *2009*

IEEE/PES Power Systems Conference and Exposition, pages 1–6. IEEE, 2009.

[166] M Herty, J Mohring, and V Sachers. A new model for gas flow in pipe networks. *Mathematical Methods in the Applied Sciences*, 33(7):845–855, 2010.

[167] Michael Herty. Coupling conditions for networked systems of Euler equations. *SIAM Journal on Scientific Computing*, 30(3):1596–1612, 2008.

[168] Michael Herty, Alexander Kurganov, and Dmitry Kurochkin. Numerical method for optimal control problems governed by nonlinear hyperbolic systems of pdes. *Communication in Mathematical Sciences*, 2014.

[169] Gerald T Heydt. Computer analysis methods for power systems. 1986.

[170] Gerald Thomas Heydt, Badrul H. Chowdhury, Mariesa L. Crow, Daniel Haughton, Brian D. Kiefer, Fanjun Meng, and Bharadwaj R. Sathyanarayana. Pricing and control in the next generation power distribution system. *IEEE Transactions on Smart Grid*, 3(2):907–914, 2012.

[171] Paul Hines, Eduardo Cotilla-Sanchez, and Seth Blumsack. Do topological models provide good information about electricity infrastructure vulnerability? *Chaos (Woodbury, N.Y.)*, 20(3):033122, September 2010.

[172] Michael Hinze, Rene Pinnau, Michael Ulbrich, and Stefan Ulbrich. Optimization with PDE constraints, volume 23 of Mathematical Modelling: Theory and Applications, 2009.

[173] Benjamin F. Hobbs, Michael H. Rothkopf, Richard P. O'Neill, and Hungpo Chao. *The Next Generation of Electric Power Unit Commitment Models.* 2001.

[174] William Hogan. Demand Response Pricing in Organized Wholesale Markets. Technical report, Harvard University, 2010.

[175] William Hogan. Electricity Market Design and Efficient Pricing: Applications for New England and Beyond. Technical report, Harvard University, 2014.

[176] William Hogan. Demand Response: Getting the Prices Right. Technical report, Harvard University, 2016.

[177] William Hogan and Brendan Ring. On Minimum-Uplift Pricing for Electricity Markets. Technical report, Harvard University, 2003.

[178] William W. Hogan. Electricity Market Design: Optimization and Market Equilibrium, 2016.

[179] Tim Hoheisel, Christian Kanzow, and Alexandra Schwartz. Theoretical and numerical comparison of relaxation methods for mathematical programs with complementarity constraints. *Mathematical Programming*, 137(1-2):257–288, September 2011.

[180] Yunan Hu, Olga I Koroleva, and Miroslav Krstić. Nonlinear control of mine ventilation networks. *Systems & control letters*, 49(4):239–254, 2003.

[181] Bowen Hua. *Unit Commitment: Tight Formulation and Pricing.* PhD thesis, University of Texas at Austin, 2018.

[182] Bowen Hua and Ross Baldick. A Convex Primal Formulation for Convex Hull Pricing, May 2016.

[183] Bowen Hua and Ross Baldick. A Convex Primal Formulation for Convex Hull Pricing. *IEEE Transactions on Power Systems*, 32(5):3814–3823, September, 2017.

[184] Bowen Hua, Zhaohong Bie, Siu Kui Au, Wenyuan Li, and Xifan Wang. Extracting rare failure events in composite system reliability evaluation via subset simulation. *IEEE Transactions on Power Systems*, 30(2):753–762, 2015.

[185] Bowen Hua, Zhaohong Bie, Cong Liu, Gengfeng Li, and Xifan Wang. Eliminating Redundant Line Flow Constraints in Composite System Reliability Evaluation. *IEEE Transactions on Power Systems*, 28(3):3490–3498, August 2013.

[186] Bing Huang, Mohammad Majidi, and Ross Baldick. Case study of power system cyber attack using cascading outage analysis model. *IEEE PES GM, Portland OR*, 2018.

[187] Sy-Ruen Huang and S L Chen. Evaluation and improvement of variance reduction in Monte Carlo production simulation. *Energy Conversion, IEEE Transactions on*, 8(4):610–620, 1993.

[188] Justin Hudson. A Review on the Numerical Solution of the 1D Euler equations. 2006.

[189] Hailong Hui, Chien-Ning Yu, Feng Gao, and Resmi Surendran. Combined cycle resource scheduling in ercot nodal market. In *Power and Energy Society General Meeting, 2011 IEEE*, pages 1–8. IEEE, 2011.

[190] Jin Hur, Man-Ho Joung, and Ross Baldick. Sequential outage checkers for analyzing cascading outages and preventing large blackouts. *Journal of Electrical Engineering and Technology*, 6(5):585–594, 2011.

[191] Arieh Iserles. Stability and dynamics of numerical methods for nonlinear ordinary differential equations. *IMA journal of numerical analysis*, 10(1):1–30, 1990.

[192] ISO-NE. Adressing gas dependence. Technical report, 2012.

[193] Eitan Israeli. *System interdiction and defense.* PhD thesis, Naval Postgraduate School, 1999.

[194] Eitan Israeli and R. Kevin Wood. Shortest-path network interdiction. *Networks*, 40(2):97–111, September 2002.

[195] R.A. Jabr. Rank-constrained semidefinite program for unit commitment. *International Journal of Electrical Power & Energy Systems*, 47:13–20, May 2013.

[196] Ruiwei Jiang, Jianhui Wang, and Yongpei Guan. Robust unit commitment with wind power and pumped storage hydro. *IEEE Transactions on Power Systems*, 27(2):800, 2012.

[197] Xichen Jiang, Jiangmeng Zhang, Brian J. Harding, Jonathan J. Makela, and Alejandro D. Dominguez-Garcia. Spoofing GPS Receiver Clock Offset of Phasor Measurement Units. *IEEE Transactions on Power Systems*, 28(3):3253–3262, August 2013.

[198] Young-Do Jo and Bum Jong Ahn. A method of quantitative risk assessment for transmission pipeline carrying natural gas. *Journal of hazardous materials*, 123(1-3):1–12, August 2005.

[199] C G Justus, W R Hargraves, and Ali Yalcin. Nationwide assessment of potential output from wind-powered generators. *Journal of Applied Meteorology*, 15(7):673–678, 1976.

[200] Carsten Kallesøe, Rafa\l Wisniewski, and Tom Jensen. A Distributed Algorithm for Energy Optimization in Hydraulic Networks. In *Preprints of the 19th World Congress*, pages 11926–11931. IFAC, 2014.

[201] Rolf Kehlhofer, Frank Hannemann, Bert Rukes, and Franz Stirnimann. *Combined-cycle gas & steam turbine power plants*. Pennwell Books,

2009.

[202] Mohammad E Khodayar, Mohammad Shahidehpour, and Lei Wu. Enhancing the dispatchability of variable wind generation by coordination with pumped-storage hydro units in stochastic power systems. *IEEE Transactions on Power Systems*, 28(3).

[203] D S Kirschen, D Jayaweera, D P Nedic, and R N Allan. A probabilistic indicator of system stress. *IEEE Trans. Power Syst.*, 19(3):1650–1657, 2004.

[204] Daniel S Kirschen, Juan Ma, Vera Silva, and Regine Belhomme. Optimizing the flexibility of a portfolio of generating plants to deal with wind generation. *2011 IEEE Power and Energy Society General Meeting*, pages 1–7, July 2011.

[205] Daniel S Kirschen, Angel Rosso, Juan Ma, Student Member, and Luis F Ochoa. Flexibility from the Demand Side. 2012.

[206] Tatsuhiko Kiuchi. An implicit method for transient gas flows in pipe networks. *International Journal of Heat and Fluid Flow*, 15(5):378–383, 1994.

[207] C. R. Knight, E. R. Jervis, and G. R. Herd. The Definition of Terms of Interest in the Study of Reliability. *IRE Transactions on Reliability and Quality Control*, PGRQC-5:34–56, April 1955.

[208] Ben Knueven, Jim Ostrowski, and Jean-Paul Watson. A Novel Matching Formulation for Startup Costs in Unit Commitment. 2017.

[209] Donald K. Knuth. *The T$_E$Xbook*. Addison-Wesley, 1984.

[210] Olga I Koroleva and Miroslav Krstic. Approximate solutions to nonlinear fluid networks with periodic inputs. In *American Control Conference, 2004. Proceedings of the 2004*, volume 3, pages 2284–2289. IEEE, 2004.

[211] Olga I Koroleva and Miroslav Krstic. Averaging analysis of periodically forced fluid networks. *Automatica*, 41(1):129–135, 2005.

[212] Olga I Koroleva, Miroslav Krstić, and Geert W Schmid-Schönbein. Decentralized and adaptive control of nonlinear fluid flow networks. *International Journal of Control*, 79(12):1495–1504, 2006.

[213] Magnus Korpaas, Arne T Holen, and Ragne Hildrum. Operation and sizing of energy storage for wind power plants in a market system. *International Journal of Electrical Power & Energy Systems*, 25(8):599–606, 2003.

[214] Dheepak Krishnamurthy, Wanning Li, and Leigh Tesfatsion. An 8-Zone Test System Based on ISO New England Data: Development and Application. *IEEE Transactions on Power Systems*, 31(1):234–246, 2016.

[215] Miroslav Krstic and Andrey Smyshlyaev. Backstepping boundary control for first-order hyperbolic PDEs and application to systems with

actuator and sensor delays. *Systems & Control Letters*, 57(9):750–758, 2008.

[216] Miroslav Krstic and Andrey Smyshlyaev. *Boundary control of PDEs: A course on backstepping designs*, volume 16. Siam, 2008.

[217] Prabha Kundur, Neal J Balu, and Mark G Lauby. *Power system stability and control*, volume 7. McGraw-hill New York, 1994.

[218] Prabha Kundur, John Paserba, Venkat Ajjarapu, Göran Andersson, Anjan Bose, Claudio Canizares, Nikos Hatziargyriou, David Hill, Alex Stankovic, Carson Taylor, et al. Definition and classification of power system stability ieee/cigre joint task force on stability terms and definitions. *IEEE transactions on Power Systems*, 19(3):1387–1401, 2004.

[219] Alexis Kwasinski. Local energy storage as a decoupling mechanism for interdependent infrastructures. In *2011 IEEE International Systems Conference*, pages 435–441. IEEE, April 2011.

[220] Leslie Lamport. *LaTeX: A document preparation system.* Addison-Wesley, 2nd edition, 1994.

[221] Eamonn Lannoye, Damian Flynn, and Mark O'Malley. The role of power system flexibility in generation planning. In *2011 IEEE Power and Energy Society General Meeting*, pages 1–6. IEEE, July 2011.

[222] Eamonn Lannoye, Student Member Ieee, Damian Flynn, Senior Member Ieee, Mark O Malley, and Fellow Ieee. Power System Flexibility Assessment - State of the Art. 2012.

[223] Eamonn Lannoye, Student Member, Damian Flynn, Senior Member, and Mark O Malley. Evaluation of Power System Flexibility. 27(2):922–931, 2012.

[224] A M Leite Da Silva, R A G Fernandez, and C Singh. Generating Capacity Reliability Evaluation Based on Monte Carlo Simulation and Cross-Entropy Methods. *IEEE Trans. Power Syst.*, 25(1):129–137, 2010.

[225] C. Lemaréchal and A. Renaud. A geometric study of duality gaps, with applications. *Mathematical Programming*, 90(3):399–427, 2001.

[226] Claude Lemaréchal. Lagrangian relaxation. In *Computational combinatorial optimization*, pages 112–156. Springer, 2001.

[227] Gengfeng Li, Zhaohong Bie, Bowen Hua, and Xifan Wang. Reliability evaluation of distribution systems including micro-grids considering demand response and energy storage. In *Universities Power Engineering Conference (UPEC), 2012 47th International*, pages 1–6, 2012.

[228] Ruoyang Li, Qiuwei Wu, and Shmuel S. Oren. Distribution locational marginal pricing for optimal electric vehicle charging management. *IEEE Transactions on Power Systems*, 29(1):203–211, 2014.

[229] Tao Li, Mircea Eremia, and Mohammad Shahidehpour. Interdependency of Natural Gas Network and Power System Security. *IEEE Transactions on Power Systems*, 23(4):1817–1824, November 2008.

[230] Tao Li and Mohammad Shahidehpour. Price-based unit commitment: A case of Lagrangian relaxation versus mixed integer programming. *IEEE Transactions on Power Systems*, 20(4):2015–2025, 2005.

[231] Wenyuan Li. *Risk assessment of power systems: models, methods, and applications.* John Wiley & Sons, 2005.

[232] George Liberopoulos and Panagiotis Andrianesis. Critical Review of Pricing Schemes in Markets with Non-Convex Costs. *Operations Research*, 64(1):17–31, 2016.

[233] George Liberopoulos and Panagiotis Andrianesis. Critical Review of Pricing Schemes in Markets with Non-Convex Costs. *Operations Research*, 64(1):17–31, 2016.

[234] D Lieber, A Nemirovskii, and R Y Rubinstein. A fast Monte Carlo method for evaluating reliability indexes. *Reliability, IEEE Transactions on*, 48(3):256–261, 1999.

[235] Churlzu Lim and J Cole Smith. Algorithms for discrete and continuous multicommodity flow network interdiction problems. *IIE Transactions*, 39(1):15–26, 2007.

[236] Cong Liu, Changhyeok Lee, and Mohammad Shahidehpour. Look Ahead Robust Scheduling of Wind-Thermal System With Considering Natural Gas Congestion. *IEEE Transactions on Power Systems*, 30(1):544–545, January 2015.

[237] Cong Liu, Mohammad Shahidehpour, Yong Fu, and Zuyi Li. Security-constrained unit commitment with natural gas transmission constraints. *IEEE Transactions on Power Systems*, 24(3):1523–1536, August 2009.

[238] Cong Liu, Mohammad Shahidehpour, Zuyi Li, and Mahmoud Fotuhi-Firuzabad. Component and mode models for the short-term scheduling of combined-cycle units. *IEEE Transactions on Power systems*, 24(2):976–990, 2009.

[239] Cong Liu, Mohammad Shahidehpour, and Jianhui Wang. Coordinated scheduling of electricity and natural gas infrastructures with a transient model for natural gas flow. *Chaos (Woodbury, N.Y.)*, 21(2):025102, June 2011.

[240] Xuan Liu, Zuyi Li, Zhikang Shuai, and Yunfeng Wen. Cyber attacks against the economic operation of power systems: a fast solution. *IEEE Transactions on Smart Grid*, 8(2):1023–1025, 2017.

[241] Yao Liu, Peng Ning, and Michael K. Reiter. False data injection attacks against state estimation in electric power grids. In *Proceedings of the 16th ACM Conference on Computer and Communications Security*, CCS '09, pages 21–32, New York, NY, USA, 2009. ACM.

[242] Miguel Sousa Lobo, Lieven Vandenberghe, Stephen Boyd, and Hervé Lebret. Applications of second-order cone programming. *Linear Algebra and its Applications*, 284(1-3):193–228, 1998.

[243] London Economics. Estimating Value of Lost Load—Final report to OFGEM. Technical report, London Economics, 2011.

[244] Bo Lu and Mohammad Shahidehpour. Short-term scheduling of combined cycle units. *IEEE Transactions on Power Systems*, 19(3):1616–1625, 2004.

[245] D.L Lukes and D.L Russell. A global theory for linear-quadratic differential games. *Journal of Mathematical Analysis and Applications*, 33(1):96–123, January 1971.

[246] F Mittelbach M Goosens and A Samarin. *The LATEXCompanion*. Addison-Wesley, 1994.

[247] Juan Ma, Vera Silva, Regine Belhomme, Daniel S. Kirschen, and Luis F. Ochoa. Evaluating and planning flexibility in sustainable power systems. In *IEEE Transactions on Sustainable Energy*, volume 4, pages 200–209. IEEE, 2013.

[248] Tao Ma, Hongxing Yang, Lin Lu, and Jinqing Peng. Technical feasibility study on a standalone hybrid solar-wind system with pumped hydro storage for a remote island in hong kong. *Renewable energy*, 69:7–15, 2014.

[249] Tao Ma, Hongxing Yang, Lin Lu, and Jinqing Peng. Pumped storage-based standalone photovoltaic power generation system: Modeling and techno-economic optimization. *Applied energy*, 137:649–659, 2015.

[250] Jan Machowski, Janusz Bialek, and James Richard Bumby. *Power system dynamics and stability*. John Wiley & Sons, 1997.

[251] Saeed D Manshadi and Mohammad E Khodayar. Resilient operation of multiple energy carrier microgrids. *IEEE Transactions on Smart Grid*, 6(5):2283–2292, 2015.

[252] GA Maria, C Tang, and J Kim. Hybrid transient stability analysis (power systems). *IEEE Transactions on Power Systems*, 5(2):384–393, 1990.

[253] Alexander Martin, Markus Möller, and Susanne Moritz. Mixed integer models for the stationary case of gas network optimization. *Mathematical Programming*, 105(2-3):563–582, November 2005.

[254] Alberto Martinez-Mares and Claudio R. Fuerte-Esquivel. A Unified Gas and Power Flow Analysis in Natural Gas and Electricity Coupled Networks. *IEEE Transactions on Power Systems*, 27(4):2156–2166, November 2012.

[255] Andreu Mas-Colell, Michael Dennis Whinston, and Jerry R Green. *Microeconomic Theory*. Oxford University Press, 1995.

[256] Drago Matko, Gerhard Geiger, and Withold Gregoritza. Verification of various pipeline models. *Mathematics and computers in simulation*, 53(4):303–308, 2000.

[257] Alan W. McMasters and Thomas M. Mustin. Optimal interdiction of a supply network. *Naval Research Logistics Quarterly*, 17(3):261–268, September 1970.

[258] A C G Melo, G C Oliveira, M Morozowski, and M V F Pereira. A hybrid algorithm for Monte Carlo/enumeration based composite reliability evaluation. In *Probabilistic Methods Applied to Electric Power Systems, 1991, Third International Conference on*, pages 70–74.

[259] A C G Melo, M V F Pereira, and A M da Silva. Frequency and duration calculations in composite generation and transmission reliability evaluation. *Power Systems, IEEE Transactions on*, 7(2):469–476, 1992.

[260] Lamine Mili, Qun Qiu, and Arun G Phadke. Risk assessment of catastrophic failures in electric power systems. *International Journal of Critical Infrastructures*, 1(1):38–63, 2004.

[261] V Miranda, L de Magalhaes Carvalho, M A da Rosa, A M Leite Da Silva, and C Singh. Improving Power System Reliability Calculation Efficiency With EPSO Variants. *IEEE Trans. Power Syst.*, 24(4):1772–1779, 2009.

[262] MISO. Convex Hull Workshop 3. Technical report, 2010.

[263] Sidhant Misra, Michael W Fisher, Scott Backhaus, Russell Bent, Michael Chertkov, and Feng Pan. Optimal compression in natural gas networks: a geometric programming approach. *arXiv preprint arXiv:1312.2668*, 2013.

[264] Alexander Mitsos. Global solution of nonlinear mixed-integer bilevel programs. *Journal of Global Optimization*, 47(4):557–582, October 2009.

[265] Alexander Mitsos, Panayiotis Lemonidis, and Paul I. Barton. Global solution of bilevel programs with a nonconvex inner program. *Journal of Global Optimization*, 42(4):475–513, December 2007.

[266] Jerry L Modisette, Jason P Modisette, and Others. Transient and Succession-of-Steady-States Pipeline Flow Models. *Pipeline Simulation Interest Group*, 2001.

[267] Saeed Mohajeryami, Milad Doostan, and Peter Schwarz. The impact of Customer Baseline Load (CBL) calculation methods on Peak Time Rebate program offered to residential customers. *Electric Power Systems Research*, 137:59–65, August 2016.

[268] Amir-Hamed Mohsenian-Rad and Alberto Leon-Garcia. Distributed internet-based load altering attacks against smart power grids. *IEEE Transactions on Smart Grid*, 2(4):667–674, 2011.

[269] J. T. Moore and J. F. Bard. The mixed integer linear bilevel programming problem. *Operations Research*, 38(5):911–921, 1990.

[270] M.S. Morais and J.W. Marangon Lima. Combined natural gas and electricity network pricing. *Electric Power Systems Research*, 77(5-6):712–719, April 2007.

[271] German Morales-España, Jesus M. Latorre, and Andres Ramos. Tight and Compact MILP Formulation of Start-Up and Shut-Down Ramping in Unit Commitment. *IEEE Transactions on Power Systems*, 28(2):1288–1296, May 2013.

[272] Germán Morales-España, Carlos M Correa-Posada, and Andres Ramos. Tight and compact mip formulation of configuration-based combined-cycle units. *IEEE Transactions on Power Systems*, 31(2):1350–1359, 2016.

[273] Germán Morales-España, Jesus M. Latorre, and Andres Ramos. Tight and compact MILP formulation for the thermal unit commitment problem. *IEEE Transactions on Power Systems*, 28(4):4897–4908, 2013.

[274] Susanne Moritz. *A mixed integer approach for the transient case of gas network optimization*. PhD thesis, TU Darmstadt, 2007.

[275] David P. Morton, Feng Pan, and Kevin J. Saeger. Models for nuclear smuggling interdiction. *IIE Transactions*, 39(1):3–14, January 2007.

[276] Alexis L Motto, José M Arroyo, and Francisco D Galiana. A mixed-integer lp procedure for the analysis of electric grid security under disruptive threat. *IEEE Transactions on Power Systems*, 20(3):1357–1365, 2005.

[277] John A. Muckstadt and Sherri A. Koenig. An Application of Lagrangian Relaxation to Scheduling in Power-Generation Systems. *Operations Research*, 25(3):387–403, June 1977.

[278] J. Munoz, N. Jimenez-Redondo, J. Perez-Ruiz, and J. Barquin. Natural gas network modeling for power systems reliability studies. In *2003 IEEE Bologna Power Tech Conference Proceedings,*, volume 4, pages 20–27. IEEE.

[279] Alan T. Murray, Timothy C. Matisziw, and Tony H. Grubesic. Critical network infrastructure analysis: interdiction and system flow. *Journal of Geographical Systems*, 9(2):103–117, January 2007.

[280] N. Judson. Interdependence of the Electricity Generation System and the Natural Gas System and Implications for Energy Security. Technical report, 2013.

[281] India National Load Dispatch Centre. Preliminary report on grid disturbance in NEW grid on 31st July 2012. Technical report, 2012.

[282] Muhammad Naveed, Xiao-yong Zhou, Soteris Demetriou, XiaoFeng Wang, and Carl A Gunter. Inside job: Understanding and mitigating the threat

of external device mis-binding on android. In *NDSS*, 2014.

[283] George Nemhauser and Laurence Wolsey. *Integer and combinatorial optimization*. Wiley-Interscience, 1999.

[284] NERC. Cyber risk preparedness assessment table-top exercise 2012 report, 2012.

[285] NERC. Nerc standard bal-002-1a. `https://www.nerc.com/files/bal-002-1a.pdf`, NERC, 2012.

[286] Jean Medard T Ngnotchouye, Michael Herty, Sonja Steffensen, and Mapundi K Banda. Relaxation approaches to the optimal control of the Euler equations. *Computational & Applied Mathematics*, 30(2):399–425, 2011.

[287] Dung T. Nguyen, Yilin Shen, and My T. Thai. Detecting Critical Nodes in Interdependent Power Networks for Vulnerability Assessment. *IEEE Transactions on Smart Grid*, 4(1):151–159, March 2013.

[288] Ernan Ni, Peter B Luh, and Stephen Rourke. Optimal integrated generation bidding and scheduling with risk management under a deregulated power market. *IEEE Transactions on Power Systems*, 19(1):600–609, 2004.

[289] Marco Nicolosi. Wind power integration and power system flexibilityAn empirical analysis of extreme events in Germany under the new negative price regime. *Energy Policy*, 38(11):7257–7268, November 2010.

[290] Northwest Power and Conservation Council. 6th Northwest Conservation and Electric Power Plan.

[291] A. Nouri-Borujerdi. Transient modeling of gas flow in pipelines following catastrophic failure. *Mathematical and Computer Modelling*, 54(11-12):3037–3045, December 2011.

[292] C. I. Nweke, F. Leanez, G. R. Drayton, and M. Kolhe. Benefits of chronological optimization in capacity planning for electricity markets. In *2012 IEEE International Conference on Power System Technology (POWERCON)*, pages 1–6. IEEE, October 2012.

[293] Richard P O'Neill, Paul M Sotkiewicz, Benjamin F Hobbs, Michael H Rothkopf, and William R Stewart. Efficient market-clearing prices in markets with nonconvexities. *European Journal of Operational Research*, 164(1):269–285, 2005.

[294] Australian Energy Market Operator. Black system, south australia, 28 september 2016. *Report of the Australian Energy Market Operator Limited (AEMO)*, 2017.

[295] Miguel Ortega-vazquez. The Value of Operational Flexibility in Power Systems with Significant Wind Power Generation Franc. pages 1–5, 2011.

[296] André Ortner and Daniel Huppmann. Modeling competitive equilibrium prices for energy and balancing capacity in electricity markets involving

non-convexities, 2016.

[297] A. Osiadacz. Optimal numerical method for simulating dynamic flow of gas in pipelines. *International Journal for Numerical Methods in Fluids*, 3(2):125–135, March 1983.

[298] Andrzej J Osiadacz. *Simulation and analysis of gas networks*. Gulf Publishing Company, Houston, 1987.

[299] James Ostrowski, Miguel F. Anjos, and Anthony Vannelli. Tight Mixed Integer Linear Programming Formulations for the Unit Commitment Problem. *IEEE Transactions on Power Systems*, 27(1):39–46, 2012.

[300] Annual Energy Outlook. With projects to 2050. *Washington, DC: US Energy Information Administration*, 2017.

[301] Thomas J Overbye. Fostering intuitive minds for power system design. *IEEE Power and Energy Magazine*, 99(4):42–49, 2003.

[302] N.P. Padhy. Unit CommitmentA Bibliographical Survey. *IEEE Transactions on Power Systems*, 19(2):1196–1205, May 2004.

[303] Bryan Palmintier and Mort Webster. Impact of unit commitment constraints on generation expansion planning with renewables. In *2011 IEEE Power and Energy Society General Meeting*, pages 1–7. IEEE, 2011.

[304] Bryan S. Palmintier. *Incorporating Operational Flexibility into Electric Generation Planning - Impacts and Methods for System Design and Policy Analysis*. PhD thesis, Massachusetts Institute of Technology, 2013.

[305] Bryan S. Palmintier and Mort D. Webster. Heterogeneous unit clustering for efficient operational flexibility modeling. *IEEE Transactions on Power Systems*, 29(3):1089–1098, 2014.

[306] Bryan S. Palmintier and Mort D. Webster. Impact of Operational Flexibility on Electricity Generation Planning With Renewable and Carbon Targets. *IEEE Transactions on Sustainable Energy*, 7(2):672–684, 2016.

[307] Kai Pan and Yongpei Guan. A Polyhedral Study of the Integrated Minimum-Up/-Down Time and Ramping Polytope. Technical report, University of Florida, 2015.

[308] M F Pellissetti and G I Schuëller. Scalable uncertainty and reliability analysis by integration of advanced Monte Carlo simulation and generic finite element solvers. *Computers & Structures*, 87(13):930–947, 2009.

[309] M V F Pereira and N J Balu. Composite generation/transmission reliability evaluation. *Proc. IEEE*, 80(4):470–491, 1992.

[310] M Perninge, F Lindskog, and L Soder. Importance Sampling of Injected Powers for Electric Power System Security Analysis. *IEEE Trans. Power Syst.*, 27(1):3–11, 2012.

[311] PG&E. PG&E Peak Time Rebate Program (PTR).

[312] D Phillips and Fp Jenkin. A mathematical model for determining generating plant mix. *Third PSCC, Rome*, 1969.

[313] Kok-Kwang Phoon. *Reliability-based design in geotechnical engineering: computations and applications.* Singapore: Taylor & Francis, 2008.

[314] J H Pickels and I H Russell. Importance sampling for power system security assessment. In *Probabilistic Methods Applied to Electric Power Systems, 1991, Third International Conference on*, pages 47–52.

[315] Jim Pierobon. Two FERC settlements illustrate attempts to game' demand response programs, 2013.

[316] N M Pindoriya, P Jirutitijaroen, D Srinivasan, and C Singh. Composite Reliability Evaluation Using Monte Carlo Simulation and Least Squares Support Vector Classifier. *IEEE Trans. Power Syst.*, 26(4):2483–2490, 2011.

[317] PJM. PJM Manual 11: Energy and Ancillary Services Market Operations, 2015.

[318] PJM Energy Market Uplift Senior Task Force. MISO Make-Whole Payment Overview, 2014.

[319] Karmen Poljanšek, Flavio Bono, and Eugenio Gutiérrez. Seismic risk assessment of interdependent critical infrastructure systems: The case

of European gas and electricity networks. *Earthquake Engineering & Structural Dynamics*, 41(1):61–79, January 2012.

[320] PowerWorld.

[321] Ana Quelhas, Esteban Gil, James D. McCalley, and Sarah M. Ryan. A Multiperiod Generalized Network Flow Model of the U.S. Integrated Energy System: Part IModel Description. *IEEE Transactions on Power Systems*, 22(2):829–836, May 2007.

[322] Ana Quelhas and James D. McCalley. A Multiperiod Generalized Network Flow Model of the U.S. Integrated Energy System: Part IISimulation Results. *IEEE Transactions on Power Systems*, 22(2):837–844, May 2007.

[323] Deepak Rajan and Samer Takriti. Minimum up/down polytopes of the unit commitment problem with start-up costs. Technical report, IBM Research Division, 2005.

[324] S.M. Rinaldi, J.P. Peerenboom, and T.K. Kelly. Identifying, understanding, and analyzing critical infrastructure interdependencies. *IEEE Control Systems Magazine*, 21(6):11–25, 2001.

[325] Brendan Ring. *Dispatch based pricing in decentralised power systems.* PhD thesis, University of Canterbury, 1995.

[326] R.M.Lee, M.J. Assante. Analysis of the Cyber Attack on the Ukraine Power Grid. Technical report, E-ISAC and SANS, 2016.

[327] Christian P Robert and George Casella. *Monte Carlo statistical methods*, volume 319. New York: Springer, 2004.

[328] Eyal Ronen, Adi Shamir, Achi-Or Weingarten, and Colin OFlynn. Iot goes nuclear: Creating a zigbee chain reaction. In *Security and Privacy (SP), 2017 IEEE Symposium on*, pages 195–212. IEEE, 2017.

[329] B Rothfarb, H Frank, D M Rosenbaum, K Steiglitz, and D J Kleitman. Optimal design of offshore natural-gas pipeline systems. *Operations research*, 18(6):992–1020, 1970.

[330] Royal Academy of Engineering. The cost of generating electricity, 2004.

[331] Reuven Y Rubinstein. Optimization of computer simulation models with rare events. *European Journal of Operational Research*, 99(1):89–112, 1997.

[332] Reuven Y Rubinstein. *Simulation and the Monte Carlo method*. New York: Wiley, 2008.

[333] Carlos Ruiz, Antonio J. Conejo, and Steven A. Gabriel. Pricing non-convexities in an electricity pool. *IEEE Transactions on Power Systems*, 27(3):1334–1342, 2012.

[334] Ernest K Ryu and Stephen P Boyd. Adaptive Importance Sampling via Stochastic Convex Programming. *arXiv preprint arXiv:1412.4845*, 2014.

[335] Vinay Sachidananda, Jinghui Toh, Shachar Siboni, Asaf Shabtai, and Yuval Elovici. Poster: Towards exposing internet of things: A roadmap. In *Proceedings of the 2016 ACM SIGSAC Conference on Computer and Communications Security*, pages 1820–1822. ACM, 2016.

[336] G. K. Saharidis and M. G. Ierapetritou. Resolution method for mixed integer bi-level linear problems based on decomposition technique. *Journal of Global Optimization*, 44(1):29–51, March 2008.

[337] Mukhtar H. Sahir and Arshad H. Qureshi. Specific concerns of Pakistan in the context of energy security issues and geopolitics of the region. *Energy Policy*, 35(4):2031–2037, April 2007.

[338] Javier Salmeron, Kevin Wood, and Ross Baldick. Analysis of electric grid security under terrorist threat. *IEEE Transactions on power systems*, 19(2):905–912, 2004.

[339] Javier Salmeron, Kevin Wood, and Ross Baldick. Worst-case interdiction analysis of large-scale electric power grids. *IEEE Transactions on power systems*, 24(1):96–104, 2009.

[340] Javier Salmeron and R. Kevin Wood. The value of recovery transformers in protecting an electric transmission grid against attack. *IEEE Transactions on Power Systems*, 30(5):2396–2403, September 2015.

[341] Javier Salmeron, R Kevin Wood, and Ross Baldick. Optimizing electric grid design under asymmetric threat (ii). 2004.

[342] N Samaan and C Singh. Assessment of the annual frequency and duration indices in composite system reliability using genetic algorithms. In *Power Engineering Society General Meeting, 2003, IEEE*, volume 2, pages 692–697.

[343] Robert B Schainker. Executive overview: energy storage options for a sustainable energy future. In *Power Engineering Society General Meeting, 2004. IEEE*, pages 2309–2314. IEEE, 2004.

[344] Wolf Peter Schill, Michael Pahle, and Christian Gambardella. Start-up costs of thermal power plants in markets with increasing shares of variable renewable generation. *Nature Energy*, 2(6), 2017.

[345] Dane A. Schiro, Tongxin Zheng, Feng Zhao, and Eugene Litvinov. Convex Hull Pricing in Electricity Markets: Formulation, Analysis, and Implementation Challenges. *IEEE Transactions on Power Systems*, 2015.

[346] K. Schneider, C.C. Liu, and J.P. Paul. Assessment of Interactions Between Power and Telecommunications Infrastructures. *IEEE Transactions on Power Systems*, 21(3):1123–1130, August 2006.

[347] Susan M Schoenung and Clayton Burns. Utility energy storage applications studies. *IEEE transactions on Energy Conversion*, 11(3):658–665, 1996.

[348] G I Schuëller and H J Pradlwarter. Benchmark study on reliability estimation in higher dimensions of structural systems–an overview. *Struc-

tural Safety, 29(3):167–182, 2007.

[349] M. Shahidehpour, Y. Fu, and T. Wiedman. Impact of Natural Gas Infrastructure on Electric Power Systems. *Proceedings of the IEEE*, 93(5):1042–1056, May 2005.

[350] Lawrence F Shampine and Mark W Reichelt. The matlab ode suite. *SIAM journal on scientific computing*, 18(1):1–22, 1997.

[351] G.B. Sheble and G.N. Fahd. Unit commitment literature synopsis. *IEEE Transactions on Power Systems*, 9(1):128–135, 1994.

[352] Hanif D. Sherali and Warren P. Adams. A Hierarchy of Relaxations between the Continuous and Convex Hull Representations for Zero-One Programming Problems. *SIAM Journal on Discrete Mathematics*, 3(3):411–430, August 1990.

[353] Aonghus Shortt, Juha Kiviluoma, and Mark O'Malley. Accommodating Variability in Generation Planning. *IEEE Transactions on Power Systems*, 28(1):158–169, 2013.

[354] John Siciliano. Ferc sets rules to protect grid from malware spread through laptops, October,2017.

[355] Siemens. Siprotec 5 distance protection and line differen- tial protection and overcurrent protection for 3-pole tripping 7sa84, 7sd84, 7sa86, 7sd86, 7sl86, 7sj86 technical data, 2012.

[356] Siemens. Siprotec 5 distance protection and line differential protection and overcurrent protection for 3-pole tripping 7sa84, 7sd84, 7sa86, 7sd86, 7sl86, 7sj86 technical data, Siemens AG, 2012.

[357] Filippo Simini, Marta C González, Amos Maritan, and Albert-László Barabási. A universal model for mobility and migration patterns. *Nature*, 484(7392):96–100, April 2012.

[358] Filippo Simini, Amos Maritan, and Zoltán Néda. Human mobility in a continuum approach. *PloS one*, 8(3):e60069, January 2013.

[359] R. Sioshansi, R. O'Neill, and S.S. Oren. Economic Consequences of Alternative Solution Methods for Centralized Unit Commitment in Day-Ahead Electricity Markets. *IEEE Transactions on Power Systems*, 23(2):344–352, 2008.

[360] Ramteen Sioshansi, Shmuel Oren, and Richard O'Neill. Three-part auctions versus self-commitment in day-ahead electricity markets. *Utilities Policy*, 18(4):165–173, 2010.

[361] Saleh Soltan, Prateek Mittal, and H Vincent Poor. Blackiot: Iot botnet of high wattage devices can disrupt the power grid. In *27th {USENIX} Security Symposium ({USENIX} Security 18)*, pages 15–32, 2018.

[362] P.M. Sotkiewicz and J.M. Vignolo. Nodal Pricing for Distribution Networks: Efficient Pricing for Efficiency Enhancing DG. *IEEE Transactions on Power Systems*, 21(2):1013–1014, May 2006.

[363] Southern California Edison. Demand Bidding Program.

[364] Michael Spivak. *The joy of TEX*. American Mathematical Society, Providence, R.I., 2nd edition, 1990.

[365] Friedrich Steinhäusler, P Furthner, W Heidegger, S Rydell, and L Zaitseva. Security risks to the oil and gas industry: Terrorist capabilities. *Strategic Insights*, 7(1):1–44, 2008.

[366] Can Sun, Zhaohong Bie, Gengfeng Li, and Bowen Hua. Analysis of wind power integration capacity in wind-hydro-thermal hybrid power system. In *Innovative Smart Grid Technologies (ISGT Europe), 2012 3rd IEEE PES International Conference and Exhibition on*, pages 1–8, 2012.

[367] Supreme Court of the United States. Federal Energy Regulatory Commission v. Electric Power Supply Association et al., Certiorari to the United States Court Of Appeals for the District of Columbia Circuit, 2016.

[368] Richard D Tabors and Seabron Adamson. Measurement of Energy Market Inefficiencies in the Coordination of Natural Gas & Power. In *System Sciences (HICSS), 2014 47th Hawaii International Conference on*, pages 2335–2343. IEEE, 2014.

[369] Maryamsadat Tahavori, John Leth, Carsten Kallesøe, and Rafael Wisniewski. Optimal control of nonlinear hydraulic networks in the presence of disturbance. *Nonlinear Dynamics*, 75(3):539–548, 2014.

[370] Maria Tamayo, Yu Xiaofeng, Xing Wang, and Jianfeng Zhang. Configuration based Combined Cycle model in market resource commitment. In *2013 IEEE Power & Energy Society General Meeting*, pages 1–5. IEEE, 2013.

[371] Chee-Wooi Ten, Chen-Ching Liu, and Govindarasu Manimaran. Vulnerability assessment of cybersecurity for scada systems. *IEEE Transactions on Power Systems*, 23(4):1836–1846, 2008.

[372] A R D Thorley and C H Tiley. Unsteady and transient flow of compressible fluids in pipelinesa review of theoretical and some experimental studies. *International journal of heat and fluid flow*, 8(1):3–15, 1987.

[373] Daniel P Thunnissen, Siu Kui Au, and Eee R Swenka. Uncertainty quantification in the preliminary design of a spacecraft attitude control system. *AIAA Journal of Aerospace Computing, Information, and Communication*, 4:902–917, 2007.

[374] Daniel P Thunnissen, Siu Kui Au, and Ggg T Tsuyuki. Uncertainty Quantification in Estimating Critical Spacecraft Component Temperatures. *AIAA Journal of Thermophysics and Heat Transfer*, 21(2):422–430, 2007.

[375] Andreas Ulbig, Student Member, and Göran Andersson. On Operational Flexibility in Power Systems. 2012.

[376] U.S.-Canada Power System Outage Task Force. Final Report on the August 14, 2003 Blackout in the United States and Canada: Causes and Recommendations. Technical report, 2004.

[377] U.S.-Canada Power System Outage Task Force. August 14th Blackout: Causes and Recommendations, 2014.

[378] US Energy Information Administration. Updated capital cost estimates for electricity generation plants, 2010.

[379] US Energy Information Administration. Annual Energy Outlook 2015, 2015.

[380] Halit Üster and ebnem Dilaverolu. Optimization for design and operation of natural gas transmission networks. *Applied Energy*, 133:56–69, November 2014.

[381] Marianna Vaiman, Keith Bell, Yousu Chen, Badrul Chowdhury, Ian Dobson, Paul Hines, Milorad Papic, Stephen Miller, and Pei Zhang. Risk assessment of cascading outages: Methodologies and challenges. *IEEE Transactions on Power Systems*, 27(2):631, 2012.

[382] Alf J. van der Poorten. Some problems of recurrent interest. Technical Report 81-0037, School of Mathematics and Physics, Macquarie University, North Ryde, Australia 2113, August 1981.

[383] G. van Rossum. Python tutorial, technical report cs-r9526, centrum voor wiskunde en informatica (cwi). Technical report, 1995.

[384] Mathieu Van Vyve. Linear prices for non-convex electricity markets: models and algorithms. Technical report, 2011.

[385] F F C Veliz, C L Tancredo Borges, and A M Rei. A Comparison of Load Models for Composite Reliability Evaluation by Nonsequential Monte Carlo Simulation. *IEEE Trans. Power Syst.*, 25(2):649–656, 2010.

[386] L. Vicente, G. Savard, and J. Judice. Discrete linear bilevel programming problem. *Journal of Optimization Theory and Applications*, 89(3):597–614, June 1996.

[387] Luís N. Vicente and Paul H. Calamai. Bilevel and multilevel programming: A bibliography review. *Journal of Global Optimization*, 5(3):291–306, October 1994.

[388] Juan Pablo Vielma. Mixed Integer Linear Programming Formulation Techniques. *SIAM Review*, 57(1):3–57, January 2015.

[389] V Visweswaran, C A Floudas, M G Ierapetritou, and E N Pistikopoulos. A decomposition-based global optimization approach for solving bilevel linear and quadratic programs. In *State of the art in global optimization*, pages 139–162. Springer, 1996.

[390] Heinrich von Stackelberg. *Market structure and equilibrium*. Springer, Berlin, Germany, 2011.

[391] Congcong Wang, Peter B. Luh, Paul Gribik, Tengshun Peng, and Li Zhang. Commitment Cost Allocation of Fast-Start Units for Approximate Extended Locational Marginal Prices. *IEEE Transactions on Power Systems*, 2016.

[392] Congcong Wang, Tengshun Peng, Peter B. Luh, Paul Gribik, and Li Zhang. The subgradient simplex cutting plane method for extended locational marginal prices. *IEEE Transactions on Power Systems*, 28(3):2758–2767, 2013.

[393] Gui Wang, Uday V. Shanbhag, Tongxin Zheng, Eugene Litvinov, and Sean Meyn. An Extreme-Point Subdifferential Method for Convex Hull Pricing in Energy and Reserve Markets—Part I: Algorithm Structure. *IEEE Transactions on Power Systems*, 28(3):2111–2120, 2013.

[394] Gui Wang, Uday V. Shanbhag, Tongxin Zheng, Eugene Litvinov, and Sean Meyn. An Extreme-Point Subdifferential Method for Convex Hull Pricing in Energy and Reserve Markets—Part II: Convergence Analysis and Numerical Performance. *IEEE Transactions on Power Systems*, 28(3):2121–2127, 2013.

[395] Lingfeng Wang and C Singh. Population-Based Intelligent Search in Reliability Evaluation of Generation Systems With Wind Power Penetration. *IEEE Trans. Power Syst.*, 23(3):1336–1345, 2008.

[396] Yezhou Wang and Ross Baldick. Cascading outage analysis using sequential outage checkers. 2012.

[397] Yezhou Wang and Ross Baldick. Case study of an improved cascading outage analysis model using outage checkers. In *Power and Energy Society General Meeting (PES), 2013 IEEE*, pages 1–5. IEEE, 2013.

[398] Yezhou Wang and Ross Baldick. Interdiction analysis of electric grids combining cascading outage and medium-term impacts. *IEEE Transactions on Power Systems*, 29(5):2160–2168, 2014.

[399] Yu Wang, Zijun Cao, and Siu Kui Au. Practical reliability analysis of slope stability by advanced Monte Carlo simulations in a spreadsheet. *Canadian Geotechnical Journal*, 48(1):162–172, 2010.

[400] Zhi-Hua Wang, Elie Bou-Zeid, Siu Kui Au, and James A Smith. Analyzing the sensitivity of WRF's single-layer urban canopy model to parameter uncertainty using advanced Monte Carlo simulation. *Journal of Applied Meteorology and Climatology*, 50(9):1795–1814, 2011.

[401] W Wangdee and R Billinton. Reliability-performance-index probability distribution analysis of bulk electricity systems. *Electrical and Computer Engineering, Canadian Journal of*, 30(4):189–193, 2005.

[402] W Wangdee and R Billinton. Bulk electric system well-being analysis using sequential Monte Carlo simulation. *IEEE Trans. Power Syst.*, 21(1):188–193, 2006.

[403] Alan Washburn and R. Kevin Wood. Two-person zero-sum games for network interdiction. *Operations Research*, 43(2):243–251, April 1995.

[404] Energy Information Administration; 2019. Washington, DC: US Department of Energy. EIA - Electricity Data.

[405] H. Wei and X. Bai. Semi-definite programming-based method for security-constrained unit commitment with operational and optimal power flow constraints. *IET Generation, Transmission & Distribution*, 3(2):182–197, February 2009.

[406] U.-P. Wen and Y.-H. Yang. Algorithms for solving the mixed integer two-level linear programming problem. *Computers & Operations Research*, 17(2):133–142, January 1990.

[407] Ue-Pyng Wen and Shuh-Tzy Hsu. Linear bi-level programming problems – a review. *The Journal of the Operational Research Society*, 42(2):125–133, February 1991.

[408] Young-Min Wi, Ji-Hui Kim, Sung-Kwan Joo, Jong-Bae Park, and Jae-Chul Oh. Customer baseline load (CBL) calculation using exponential smoothing model with weather adjustment. In *2009 Transmission & Distribution Conference & Exposition: Asia and Pacific*, pages 1–4. IEEE, October 2009.

[409] Wolfram Wiesemann, Angelos Tsoukalas, Polyxeni-Margarita Kleniati, and Berç Rustem. Pessimistic bilevel optimization. *SIAM Journal on Optimization*, 23(1):353–380, February 2013.

[410] Frank Wolak. Residential Customer Response to Real-Time Pricing: The Anaheim Critical-Peak Pricing Experiment. 2006.

[411] Richard Wollmer. Removing arcs from a network. *Operations Research*, 12(6):934–940, December 1964.

[412] Laurence A Wolsey. *Integer programming*. Wiley, New York, 1998.

[413] Pl Wong and R Larson. Optimization of natural-gas pipeline systems via dynamic programming. *Automatic Control, IEEE Transactions on*, 13(5):475–481, 1968.

[414] R. Kevin Wood. Deterministic network interdiction. *Mathematical and Computer Modelling*, 17(2):1–18, January 1993.

[415] R. Kevin Wood. Bilevel network interdiction models: Formulations and solutions. *Wiley Encyclopedia of Operations Research and Management Science*, 2011.

[416] Suming Wu, Roger Z Rios-Mercado, E Andrew Boyd, and L Ridgway Scott. Model relaxations for the fuel cost minimization of steady-state gas pipeline networks. *Mathematical and Computer Modelling*, 31(2):197–220, 2000.

[417] E Benjamin Wylie and Victor Lyle Streeter. Fluid transients. *New York, McGraw-Hill International Book Co., 1978. 401 p.*, 1, 1978.

[418] Pan Xu and Lizhi Wang. An exact algorithm for the bilevel mixed integer linear programming problem under three simplifying assumptions. *Computers & Operations Research*, 41:309–318, January 2014.

[419] Yingxiang Yang, C Herrera-Yagüe, N Eagle, and Marta C González. A Multi-Scale Multi-City Study of Commuting Patterns Incorporating Digital Traces. *Submitted to PNAS*, 2014.

[420] Maziar Yazdani Damavandi, Iman Kiaei, Mohamad Kazem Sheikh-El-Eslami, and Hossein Seifi. New approach to gas network modeling in unit commitment. *Energy*, 36(10):6243–6250, October 2011.

[421] Wang Yezhou. *Security of Electric Power Systems: Cascading Outage Analysis, Interdiction Model and Resilience to Natural Disasters*. PhD thesis, UT Austin, 2015.

[422] Rafael Zárate-Miñano, Thierry Van Cutsem, Federico Milano, and Antonio J Conejo. Securing transient stability using time-domain simulations within an optimal power flow. *IEEE Transactions on Power Systems*, 25(1):243–253, 2010.

[423] Victor M Zavala. Stochastic optimal control model for natural gas networks. *Computers & Chemical Engineering*, 64:103–113, 2014.

[424] Bo Zeng. Easier than we thought—a practical scheme to compute pessimistic bilevel optimization problem. Technical report, University of Pittsburgh, 2015.

[425] Bo Zeng and Yu An. Solving bilevel mixed integer program by reformulations and decomposition. Technical report, University of South Florida, 2014.

[426] Bo Zeng and Long Zhao. Solving two-stage robust optimization problems using a column-and-constraint generation method. *Operations Research Letters*, 41(5):457–461, September 2013.

[427] Qiaozhu Zhai, Xiaohong Guan, Jinghui Cheng, and Hongyu Wu. Fast Identification of Inactive Security Constraints in SCUC Problems. *IEEE Transactions on Power Systems*, 25(4):1946–1954, 2010.

[428] Jiazi Zhang and Lalitha Sankar. Physical system consequences of unobservable state-and-topology cyber-physical attacks. *IEEE Transactions on Smart Grid*, 7(4), 2016.

[429] Tong Zhang, Ross Baldick, and Thomas Deetjen. Optimized generation capacity expansion using a further improved screening curve method. *Electric Power Systems Research*, 124:47–54, 2015.

[430] Xi Zhang, Dong Liu, Choujun Zhan, and K Tse Chi. Effects of cyber coupling on cascading failures in power systems. *IEEE Journal on Emerging and Selected Topics in Circuits and Systems*, 7(2):228–238, 2017.

[431] Long Zhao and Bo Zeng. Vulnerability analysis of power grids with line switching. *IEEE Transactions on Power Systems*, 28(3):2727–2736,

August 2013.

[432] Junyang Zhou and Michael A Adewumi. Simulation of transients in natural gas pipelines using hybrid TVD schemes. *International journal for numerical methods in fluids*, 32(4):407–437, 2000.

[433] Yunan Zhu, Jinbao Jian, Jiekang Wu, and Linfeng Yang. Global Optimization of Non-Convex Hydro-Thermal Coordination Based on Semidefinite Programming. *IEEE Transactions on Power Systems*, 28(4):3720–3728, November 2013.

[434] E Zio and N Pedroni. Estimation of the functional failure probability of a thermal–hydraulic passive system by Subset Simulation. *Nuclear Engineering and Design*, 239(3):580–599, 2009.

[435] George Kingsley Zipf. The P1 P2/D Hypothesis: On the Intercity Movement of Persons. *American Sociological Review*, 11(6):pp. 677–686, 1946.

[436] Konstantin M Zuev, James L Beck, Siu Kui Au, and Lambros S Katafygiotis. Bayesian post-processor and other enhancements of Subset Simulation for estimating failure probabilities in high dimensions. *Computers & Structures*, 92:283–296, 2012.